## Disclaimer

The information contained in this document is derived from a summer field camp for undergraduates in Geophysical Engineering at the Colorado School of Mines. The primary purpose of this camp is to teach students the hands-on use of a wide variety of geophysical methods. Secondarily, this camp focused on the issues associated with aquifer recharge dynamics in the Upper Arkansas Valley. However, the processing and interpretation of data gathered in the basin was done, mostly on a first-time basis, by students inexperienced in these activities. Therefore, the results should be regarded appropriately. Neither the Department of Geophysics nor the Colorado School of Mines guarantees the validity of the information presented in this document.

## Acknowledgements

## Abstract

The Geophysical Engineering Department at the Colorado School of Mines requires each student to participate in a summer field session upon completion of their junior year.  For the third consecutive year, the summer field session of 2007 took place in Chaffee County, Colorado from May 13th to the 26th before returning to Golden, Colorado until June 8th.

Thirteen students from the Colorado School of Mines along with three additional students from Boise State University used a variety of geophysical methods in an attempt to characterize the subsurface geology of the Upper Arkansas River Valley (UARV), which is the northern-most extension of the Rio Grande Rift.  More specifically, they hoped to describe the depth and location of the water table in the valley.   After a three day overview of the geology of the area, the students made use of the geophysical techniques that they had learned throughout their studies at the Colorado School of Mines and Boise State University.

Due to the lack of deep geophysical data, very little is known about the geology in the deep subsurface of the UARV.  Methods such as deep seismic, gravity, and magnetics were used to acquire deep data along County Road 251-1 and County Road 250 just north of Salida.  In this area the students attempted to characterize faulting structures and bedding layers.

Another site was established just north of Buena Vista along County Road 385 where the students utilized methods such as direct current resistivity, electromagnetics, ground penetrating radar, and shallow seismic to image the near-subsurface, hoping to gain information pertaining to the water table.  Of particular interest was an agricultural ditch that flowed through the area.  The students attempted to determine the effect that the agricultural ditch had on the recharge of the water table.

Following a two week period of data acquisition in Chaffee County, the students then returned to the Colorado School of Mines for an additional two weeks of data processing and interpretation. They drew conclusions and made interpretations of the processed data from both the north site, in which the near-surface methods were performed, and the south site, in which the deep subsurface methods were performed.  Interpretations of the water table and the geologic structure of the UARV were made and it became evident that, in order to fully understand the subsurface geology and groundwater flow of the valley, there was still work to be done in the UARV.  The students determined objectives and designed an acquisition plan for the field camp 2008.

Geophysics Field Camp 2007 Data Processing Teams:
*Project Manager:* Thomas Cullison
*Assistant Project Manager:* Dan Liechty
*Report Chiefs:* Brian Hart & Earl Marshall
*Presentation Chief:* Shannon Simons

| | |
|---|---|
| **Deep Seismic** | Josh Nichols |
| | Aubry Bingham |
| | Derek Grimm |
| | Zach Pember |
| | Tom O'theim |
| **Shallow Seismic** | Nathaniel Cockrell |
| | Mpho Ramaselaga |
| **EM-57** | Adrian Weaver |
| | Gary Scherer |
| **EM-31** | Zach Pember |
| **DC** | Haider Alabdulaal |
| **VSP** | Shannon Simons |
| **GPR** | Josh Nichols |
| | Aubry Bingham |
| **GIS** | Adrian Weaver |
| | Nathaniel Cockrell |
| | Thomas Cullison |
| **Gravity** | Dan Liechty |
| | Earl Marshall |
| | Thomas Cullison |
| **Magnetics** | Mpho Ramaselaga |
| | Derek Grimm |
| **Geology** | Thomas Cullison |
| | Brian Hart |
| **Integration** | Brian Hart |
| | Adrian Weaver |
| | Derek Grimm |
| **2008 Planning** | Adrian Weaver |
| | Brian Hart |
| | Tom O'theim |
| | Gary Scherer |
| | Thomas Cullison |

Table of Contents:

# Chapter 1: Introduction

## *Background Information*

All students majoring in Geophysical Engineering from the Colorado School of Mines are required to participate in a summer field session. During this endeavor, students gain practical experience and develop a familiarity with the various geophysical methods that have been introduced during the junior year at the Colorado School of Mines. These methods have been an integral part of the students' preceding coursework and field session provides a valuable opportunity to refine the skills acquired throughout the year. The junior class of 2007 went to Chaffee County, Colorado from May 13 through May 26, with the goal of continuing the subsurface investigation previously established by past junior classes in 2005 and 2006. The students spent approximately two weeks gathering data in the field around Buena Vista and Salida and an additional two weeks performing data processing and interpretation of the data gathered in the field. At the end of field camp on June 9, the students gave a presentation of their experience in its entirety with the hopes of advancing the understanding of the Upper Arkansas River Valley.

The first several days of field camp were devoted to the geology and stratigraphy of the area. Dr. Bob Raynolds, a geological consultant with the Denver Museum of Nature and Science, was instrumental in providing the students with an extensive overview of the area's structural geological aspects. He also helped the students to explore for themselves the finer details of the existing outcrops and how these outcrops tie into the geology of the area as a whole. The culmination of Dr. Raynolds's stay involved a presentation by four groups of students, each with their own interpretation as to the subsurface structural makeup of the Upper Arkansas River Valley along a particular cross-sectional line. The students analyzed each of the interpretations and created a final cross section that combined the strengths of each. The remaining time was spent using the various geophysical methods to prove or disprove the various hypotheses of the structural geology as well as seek out the water table and cultivate our knowledge of the groundwater situation. The field camp schedule was configured so that each student would get the opportunity to experience every geophysical method throughout the two week field work portion of camp. This rotation allowed each student to learn the importance of each method and gain insight as to how methods are integrated and complement each other.

In addition, several lectures were assimilated into the field camp flow. Fred Henderson, a geological consultant to Chaffee County, gave a lecture concerning the specific geology of the Mt. Princeton area and utilized known hydrological information to explain the progression of that site's particular geology. Jordan Dimick, a graduating master's student from the Colorado School of Mines, presented the students with the results of his master's thesis regarding the overall hydrology of the area. Fred Berkman, a consultant with the Colorado Geological Survey, offered possible theories as to how the subsurface groundwater flows by using known constraints gathered from several different geothermal wells within the vicinity of the area of study. Finally, Hans Ecke, and associate with GX Technologies, Inc., enlightened the students with the future of seismic data acquisition.

## Problem and Objectives

Chaffee County, encompassing the area of study, contains the Arkansas River, a major tributary of the Mississippi River. The Arkansas River possesses a fairly high discharge rate and provides water for many communities across Colorado, Kansas, Oklahoma, and Arkansas [1]. However, according to the Prior Appropriation Doctrine, the outlying communities of the Upper Arkansas River Valley, including the communities of Buena Vista, Salida, and Poncha Springs, are not allowed to utilize the river as a water source [2]. Their only alternative is groundwater. In addition, current census estimates of the growth rate of this area state that by 2030 the population will have increased by 70%. As the population grows, potable water comes into increasingly higher demand. The resulting implications provide an unsettling picture. The previous two field camp experiences in Chaffee County have been spent characterizing two distinct parts of the Valley's structural geology. Thus, there are several models for explaining the groundwater situation in the Valley. Yet, the same questions concerning groundwater flow, recharge and discharge, and the effect of the Upper Arkansas River Valley's drainage ditches on the groundwater still exist. The construction of more complete models is necessary for a more in-depth analysis of the groundwater situation to be made. A more accurate geological picture is hardly the contribution of one class since each proceeding class builds on and uses the results of the preceding years' work.

The purpose of this report is to present the observed data gathered in Chaffee County as well as make interpretation of this data in order to formulate a more comprehensive groundwater model of the Upper Arkansas River Valley. To accomplish this objective, the students applied their knowledge of geophysics garnered from their previous coursework and made use of several geophysical methods in an attempt to accurately image the subsurface and assess the groundwater situation. The methods included deep seismic and gravity to provide a description of the structural geology. The deep methods helped to characterize the geology, layering, and faulting, which could be indicative as to the behavior of groundwater flow. In addition, the students employed near surface seismic, direct current resistivity, electromagnetics, and ground penetrating radar to characterize near surface structure. Another important objective was to determine the how much, if any, water in the water table can be attributed to leakage through the agricultural ditches. The leakage of water through agricultural ditches into the water table is an important water source to the community of Buena Vista. The possibility of developmental growth to the west of the ditches may diminish the amount of water flowing through the ditches and, therefore, have a direct effect on the water table. The near surface methods were used to provide information about the depth to the water table and subsurface flow patterns.

# Chapter 2: Geology of the Upper Arkansas River Valley

## *Introduction*

The Upper Arkansas River Valley (UARV) is the upper extension of the Rio Grande Rift. Due to the lack of deep geophysical data, the UARV is one of the least understood basins in the Rio Grande Rift.  The Upper Arkansas River Valley lies within an asymmetrical half-graben structure that tilts towards the west.  Only theories exist as to the geology of the interior of the basin as it has not yet been quantitatively characterized.  This half-graben structure in the UARV was created by continental rifting, and it is the northern most half-graben structure that lies along the Rio Grande Rift [1].  The western axis of the UARV is flanked by steeply dipping normal faults as evidenced by the facetted spurs along the eastern flank of the Sawatch Range.  Smaller mountains of the Mosquito Range border the eastern axis of the UARV.  Most of the exposed geology within the valley consists of alluvial, glacial, or fluvial deposits.  However, near the eastern side of the valley, there are some locations where the Precambrian basement rock can be seen in outcrops on the surface. (See Appendix A for geological maps of the UARV)

The mountain peaks in the Sawatch Range that lie along the western flank of the UARV (i.e. the Collegiate Peaks) are composed mostly of metamorphosed Precambrian rock or intrusive igneous plutons that are roughly late Eocene in age.  (See Appendix A for geological maps of the UARV).

Containing the less prominent mountain peaks that flank the eastern side of the UARV, the Mosquito Range is composed of metamorphosed Precambrian rock overlain in some areas by Paleozoic sedimentary rocks.  These sedimentary rocks, consisting of Manitou Dolomite, Harding Quartzite, and Leadville Limestone, are increasingly eroded from the west side to the east side of the valley.  In places, they are overlain by the late Eocene to Oligocene volcanic tuffs, or basaltic lava flows [2].

## *Geologic History*

The rifting of the UARV began roughly 27 million years ago following the development of a volcanic providence in the area which followed the Laramide Orogeny [3]. Evidence of the volcanism includes the Mt. Princeton batholith and other plutons which have been exposed due to erosion.  Furthermore, there are volcanic flows in the UARV area.  The volcanic tuffs that overlay portions of the Mosquito Range have similar chemical composition to the Mt. Princeton batholith.  Both the Princeton batholith and the volcanic tuffs predate the onset of rifting in the UARV area.  The basalt flows on the eastern side of the UARV (e.g. Tenderfoot Mountain) predate the onset of rifting in the valley as well [2].

As the UARV began rifting, the valley floor began to subside and erosion began to fill in the rifting valley. The oldest of these rifting deposits, which are Miocene in age [4], are composed of alluvial deposits of alternating conglomerates, sandstones, and silty mudstones.  These deposits

are collectively known as the Dry Union Formation.  Alluvial deposits continued to fill the valley following the Miocene, and they continue to fill the valley today.  During the Pleistocene, the glacial activity that took place on the western side of the valley left glacial deposits which overlay the alluvium deposits in some areas of the valley [4].  Following the Pleistocene, a period of downcutting began within the valley due to several changes in the local base level.  This downcutting still continues today, and it has caused both the formation of terraces and the deposition of fluvial deposits within the valley.

## *Cross Section*

The northern extension of the Rio Grande rift reaches into an area of the Rocky Mountains that were uplifted during the Laramide Orogeny.  Given the steep faulting the occurred during the Laramide Orogeny, it is possible that the major rift faults with in the UARV half-graben are the result of the subsidence of Laramide thrust blocks.  Therefore, the major normal faults in the UARV half-graben may be Laramide thrust faults that have been reactivated and are moving in the reverse direction.

Given the geology that was observed at exposed outcrops in the UARV area, the processed seismic data from the 2006 Geophysics Field Camp, and the assumed remnant deep larmide faulting in the area, a hypothetical cross section of the line shown in Figure 1 was produced.  The cross section is shown in Figure 2.B.2.
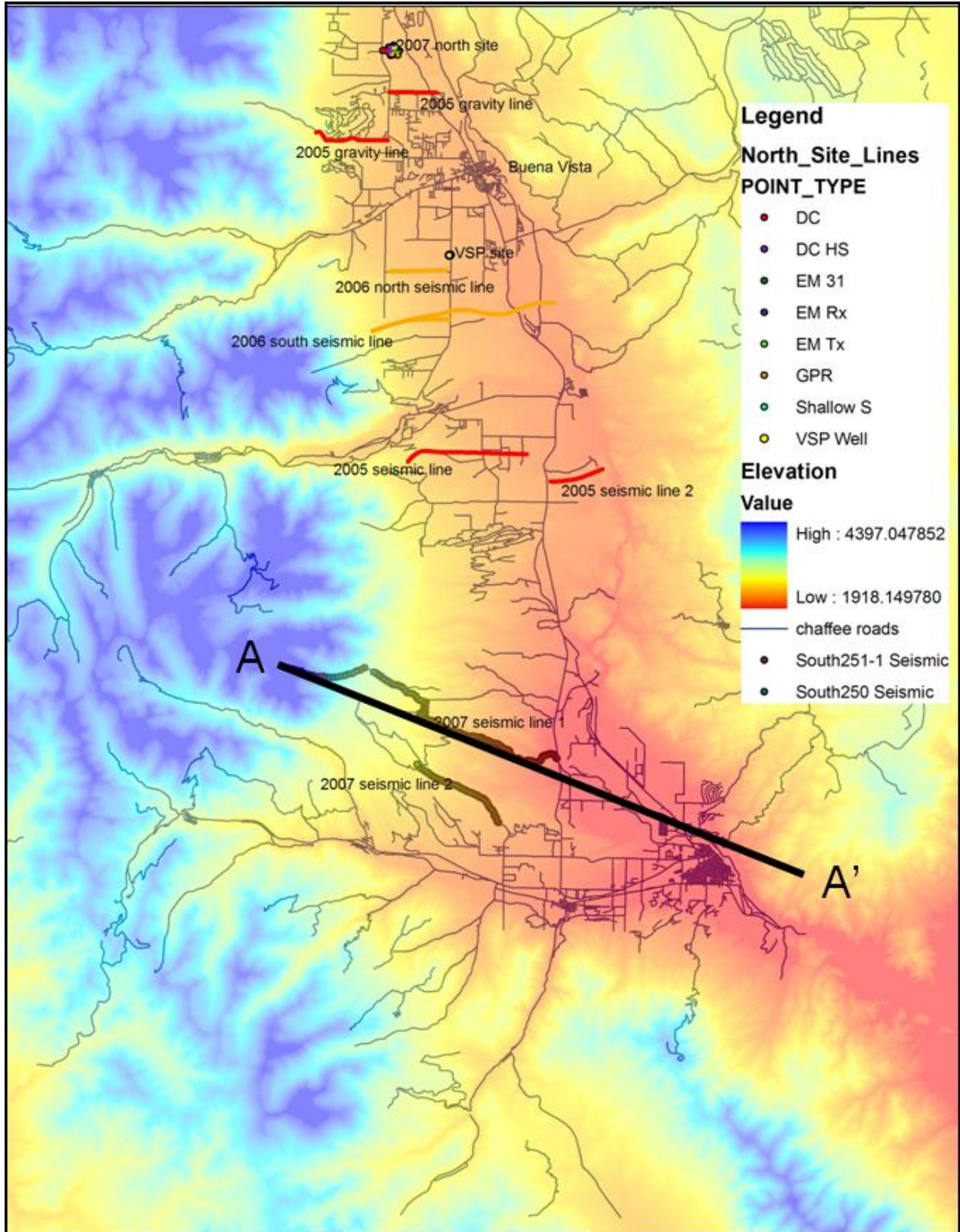
Figure 2.B.1: This shows an elevation color contour map of the Upper Arkansas River Valley. The line draw from A to A' travels through the south site area.  A hypothetical cross section was created fro the line drawn from A to A'.

**Figure 2.B.2:** This shows a hypothetical cross section of the line A to A' shown in Figure 2.B.1.

# Chapter 3: Surveying

## *Introduction*

An integral part of any scientific field investigation is the process of surveying. Surveying is the practice by which one makes measurements of several factors such as latitude and longitude coordinates, elevation, and total distance between measurements. Several instruments and methods are used for this process. The instrument and method depend on the type of surveying investigation being done, the accuracy desired, and time and budget constraints. For example, a particular survey may be looking for only a rough idea of spatial distance and surveying must be conducted quickly and inexpensively. The method which might be used for this type of survey would be *Pace and Chain.* Alternatively, a scientist may take much time making measurements and might consider the accuracy of surveying to be equally important. *Differential Global Positioning System (Differential GPS)* would be a recommended method by which to conduct survey for this study.

Surveying has important implications as the survey's results must be delivered based on survey location and elevation. Data processing for several geophysical methods depends on several of these factors. For instance, gravity reduction has an important correction to be made, the free-air correction, which is dependent on elevation. In addition, any interpretation of data made with the survey's results must be managed according to location. Otherwise, the interpretation of the results may be considered worthless as the results could have been gathered from any arbitrary location. This issue is analogous to the importance of including the unit with a measurement. And, like this analogy, if the survey locations are not clearly given with the survey's results, then the results are inherently meaningless.

## *Differential GPS*

Differential Global Positioning System (Differential GPS) is a surveying method designed for the operator seeking high accuracy. However, it is also among the more expensive surveying methods. It uses a group of satellites to relay information about latitude and longitude coordinates, elevation, any many other factors which might by important to a particular survey. A base station is set up with a disk-shaped antenna to transmit and receive information via satellites to a roving station employing the same type of antenna. If the base station has been set up correctly, the roving station may receive values with an accuracy of a few centimeters.

Differential GPS was the method of choice for the South Site, which contained the geophysical methods of deep seismic, gravity, and magnetics. A survey line was constructed on Chaffee County Road 251-1 for use of all three geophysical methods. Flags were spaced evenly along this road to represent source and receiver stations or measurement locations every 30 meters. Measurements were taken with the differential GPS at each flag location along this road as well as CR 250 for the second deep seismic line. Latitude and longitude as well as elevation values were collected for the purpose of delineating location to each geophysical survey's results, which is important for data reduction.

As stated before, if the base station is set up correctly, the accuracy of differential GPS is within a few centimeters [1].  For almost any particular survey, this accuracy is extremely high.  However, if the base station is set up incorrectly, a systematic error will most likely be seen in each measurement collected which would be the result of human error.  In addition, differential GPS is dependent on communication with a set of satellites.  Inclement weather or heavy cloud cover can affect these lines of communication and might decrease the accuracy of the measurement.

## Handheld GPS

Hand-Held GPS (or just GPS) is much like its Differential counterpart.  It too communicates with a collection of satellites and conducts measurements of the same surveying factors.  GPS is, as its name suggests, held in the operator's hand. As a result, GPS is very portable and convenient and may travel with the operator easily to any survey location where a measurement is necessary.

GPS was the surveying method selected to use at the North Site, along with Total Distance Measurement (TDM) which will be discussed in greater detail in the next section.  It was employed for the investigations using electromagnetics and, to some extent, DC-Resistivity.  Each survey station for the EM-57 survey was brought into the fold using GPS including the corners of this particular survey's transmitter loop.  In addition, the DC-Resistivity lines had their stations' spatial measurements made by GPS.

Unlike its Differential counterpart, GPS is not nearly as accurate.  Typical accuracy values range from 3 to 12 meters, with a best case scenario of 3m [2].  Also, GPS is much more affected by changing/inclement weather conditions than Differential.  Due to GPS's lack of exactness, its use was restricted to the North Site where the results made from the various surveys may be considered more qualitative and less quantitative than the surveys conducted at the South Site.

## Total Distance Measurement (TDM)

TDM is a surveying device in the same vein as the old-fashioned surveying instruments, but with an onboard computer which utilizes a laser to calculate distances and angles from a known reference point which can be converted to latitude/longitude, and elevation.  The laser connects with a prism held by the second operator.  Like Differential GPS, a reference point and coordinate system must be applied for making any measurements using the TDM.  In terms of mobility, the TDM is somewhat laborious to use and requires two distinct operators.  Also, the use of a TDM instrument is on the more expensive side of surveying techniques.

TDM was used at both the North Site and the VSP site.  At the North Site, the TDM made spatial measurements for a couple DC-Resistivity line as well as the Ground Penetrating Radar (GPR) lines.  At the VSP site, the TDM was the primary surveying instrument and captured measurements for the critical coordinates of the survey.

TDM, when used correctly, has a very high accuracy, on the order of a centimeter [3]. Thus, error in its data is usually human error. For example, a reference point and a reference coordinate system must be chosen for TDM operation. If these are not applied correctly to each and every data point following them, a systematic human error will occur. In addition, the prism held by the second operator must be oriented orthogonally to the laser from the onboard computer. If it is not oriented precisely, an alternative error will take place.

## Pace and Chain

The surveying technique of Pace and Chain is the least expensive one yet and only slightly less mobile than the Hand-Held GPS. It requires a measuring tape which an operator uses to measure off particular distances from a reference point. It does not perform any other calculations other than spatial distance and is therefore completely inadequate for taking measurements of latitude/longitude and elevation. Thus, it is the method of choice for one who wishes to gain a rough idea of distance regarding a particular survey and is not concerned with a high degree of accuracy.

Pace and Chain was used extensively at the South Site for preliminary surveying locations. For the first few days of the geophysical portion of field camp, crews were sent out with a measuring tape or two and were asked to "flag" a particular survey line using the Pace and Chain method. That is, each crew measured out station distance and placed a flag at each station using a measuring tape taking values from a starting point. This was done for the deep seismic and the gravity lines, the latter of which was also drawn on by magnetics.

Unlike the previously discussed surveying techniques, Pace and Chain is a very cost-effective method and fairly mobile, technically, requiring only one operator. However, its lack of precision and accuracy can be similar to Hand-Held GPS dependent of the terrain on which an operator uses the technique. On flat terrain, its accuracy can be fairly good given that the measuring tape is taut and that any associated human and instrument error is negligible. Conversely, the type of terrain that the students of the 2007 field camp worked on was not particularly conducive to accurate measurements taken with this method as the mountain roads were, at times, rough and incorporated curves and switchbacks.

## GIS

Geographical Information Systems (GIS) is a set of computer software components whose primary purpose is to display information referenced by spatial location as a means to study the relationships between different types of data [4]. It was first developed in 1964 by Roger Tomlinson, an employee of the Canadian federal Department of Energy, Mines, and Resources, as a way to gather, examine, and manipulate data collected by the Canadian Land Inventory (CLI) [5]. GIS is an effective way to display several diverse types of data and uncover how these types affect one another over a spatial grid.

The students made great use of this system to display survey lines and grids complete with station locations and other pieces of information regarding each data station. In addition, they included features such as topography, county roads, rivers and streams, drainage ditches, and other important features concerning the groundwater and hydrological situation in Chaffee

County. By displaying a particular type of information on each layer of the software and combining these layers into one 2-D representation, the students created a map of the study area which will help to explain the interaction between map components and how each ties into the "big picture".

## Conclusion

The process of surveying provides location references for every piece of data collected during the 2007 field camp experience. With these location references, the students may not only effectively process the data as some surveying factors are requisite to this process, but may also perform data interpretation with a sense of where the results occur.

Knowing where the data was collected and how it pertains to the interpretation enables the students to derive relationships between the results of two or more different areas. Additionally, it may help the students to understand how the geophysical phenomena of one location might bring about changes in another so that they may insightfully discover the underlying structural geology and groundwater situation in Chaffee County.

# Chapter 4: South Site Geophysical Surveys

## *Introduction*

Colorado School of Mines is having a cooperative geophysical field camp with Boise State University in order to map the subsurface of the Upper Arkansas Valley.  In order to allow the Colorado School of Mines to perform their geophysical exploration techniques, Chaffee County has offered exclusive use of county roads 250 and 251-1.  The techniques that were performed included deep seismic, magnetics and gravity surveys.  Gravity was used to map any large scale changes in the density of the subsurface, allowing for an interpretation of the basement rock. Magnetics was used to measure the changes in the magnetic properties of the subsurface to help map fault lines, and deep seismic was used to create a complete map of acoustic impedances of the subsurface.  Combining these three techniques has allowed for the Colorado School of Mines and Boise State University to create a comprehensive analysis of the subsurface of the southern half of the Upper Arkansas Basin.  This analysis was combined with data acquired from the past two years of exploration through CSM field camps along with data acquired north of Buena Vista using various shallow exploration techniques.

## *Deep Seismic*

### Background

The seismic method is based on the response of a medium to mechanical waves through measurements of the elastic properties of the medium.  This response is measured by devices known as geophones, which work by measuring how much the medium moves when a mechanical wave is passed into it. Vibroseis trucks act as the source of the wave.  The trucks stop at predetermined locations, called shot points, and lower a large metal pad to the ground. By using the pad to vibrate the ground, a better coupling is achieved.  This vibration provides the wave the geophones would detect, either directly or through reflections and refractions of the wave in the subsurface.

Reflections and refractions occur when there is a change in the acoustic impedance of the subsurface.  Acoustic impedance is the product of the density of the rock and the velocity of the wave.  Whenever there is large and sudden change in acoustic impedance (like at the contact between two different rock units), part of the wave's energy is reflected back and some is transmitted through the boundary to reflect off lower layers.

Refractions occur when a wave strikes an impedance boundary at a specific angle—the critical angle—and travels along the boundary instead of reflecting back.  As the wave travels along the interface it triggers a new wave called a head wave.  This wave is transmitted back to the surface, much like a reflection, and is recorded by the geophones there.

## Survey Design

Two deep seismic surveys were conducted to better understand the subsurface structure of the Upper Arkansas River Valley.  The surveys were east-west trending 2D profiles on county roads 251-1 and 250. These surveys are located south of previous years' surveys. The orientation of the two seismic lines places them perpendicular to the dip of faults expressed on the surface. This allows for the most information to be obtained regarding the layering, folding, and faulting of the region. Once the data from these two lines are combined with previous years' works, a more complete geologic understanding of the subsurface of the valley can be obtained.

For the acquisition of the data, the vibroseis trucks drive along the road following a line of between 50 to 70 geophone strings.  Each geophone string stretches 30 meters and contains 6 geophones.  Between the trucks and the geophones there are 60 meters where no geophones are active.  This is because any geophones in this 60 meter stretch could contain so much noise that it would decrease the overall quality of the data.  Each string of geophones is connected to a Sercel acquisition box, which is in turn connected to the acquisition station.  The job of the Sercel boxes is to take the data acquired by each of the six geophones attached to it and stack, or sum the data in order to improve the signal-to-noise ratio.  The acquisition station collects each of these gathered records and records them for each shot, creating shot gathers.  The data in these shot gathers are then ready to process in ProMAX.

## Processing

The first step in processing the data is to look at each shot gather individually for noisy traces and reversed polarities. Noisy traces are often the result of wind noise on the geophones or planting geophones poorly.  These traces should be removed in order to increase the signal to noise ratio. A polarity reversal can occur when the wiring inside the geophone strings is reversed and should be corrected so the data stacks constructively.

d 4.B.1:  This shot gather shows a noisy trace, shown in blue, and several traces with polarity reversals, shown in red, which must be corrected.

The signal is filtered, to remove frequencies that do not contain information about the subsurface.  Ideally the signal produced by the seismic source would be a delta function, or an infinitesimally short pulse of infinite amplitude.  Since it is not physically possible to produce such a pulse, the signal is deconvolved.  Deconvolution compares the original signal to how the signal behaves at a boundary, then determines the response of a delta function intersecting the same structure.
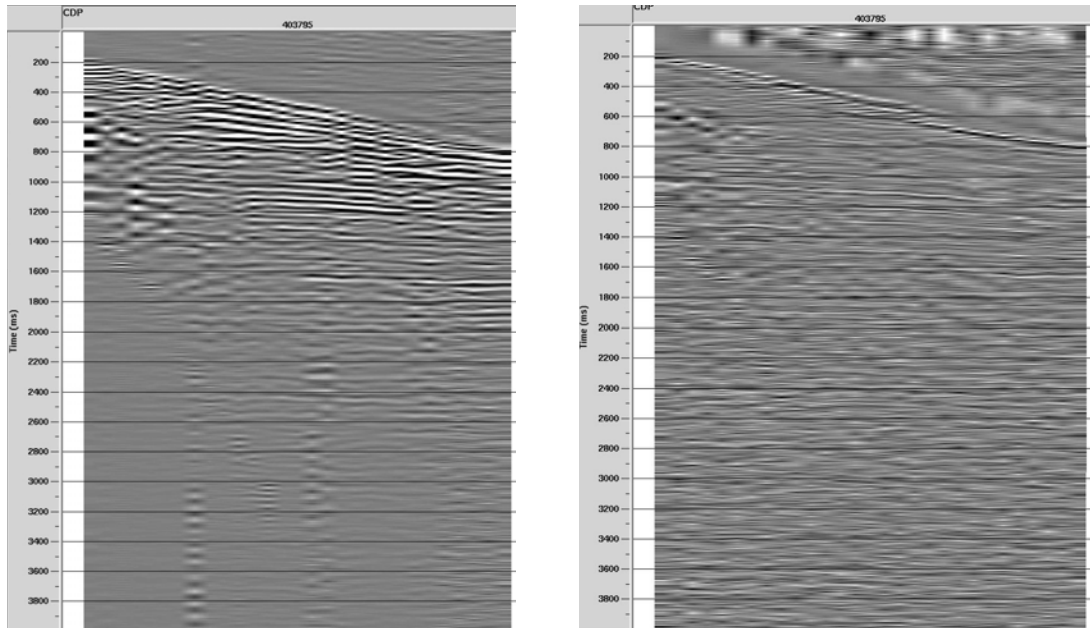
Figure 4.B.2:  The left of the figure shows a shot gather before deconvolution is applied. The right shows the same shot gather after deconvolution which has a greatly improved signal-to-noise ratio.

Using the geometries inserted in the headers of each trace, the traces are realigned taking into account topography and effects of weathering at the surface.  This is typically done in three steps, each improving the accuracy of the image.  The first is elevation statics.  Elevation statics creates a flat surface above the topography of the survey and fills in the gaps with a constant medium.  The traces are then shifted as though the source and receivers were at the surface of the new datum.  This is a quick and inexpensive way to increase the coherence of the reflections.  More expensive, and usually more accurate to reality is refraction statics.  Refraction statics corrects the time position of traces based on a common refractor, usually the first high amplitude, to minimize error.  For this the first break of each shot gather is picked.  Then the traces are shifted to fit a straight line. Elevation statics and refraction statics were tested on the 251-1 and the elevation statics created a much cleaner stack, so refraction statics was not used for either survey in the interest of efficiency.  The third correction, residual statics is applied after normal moveout correction.
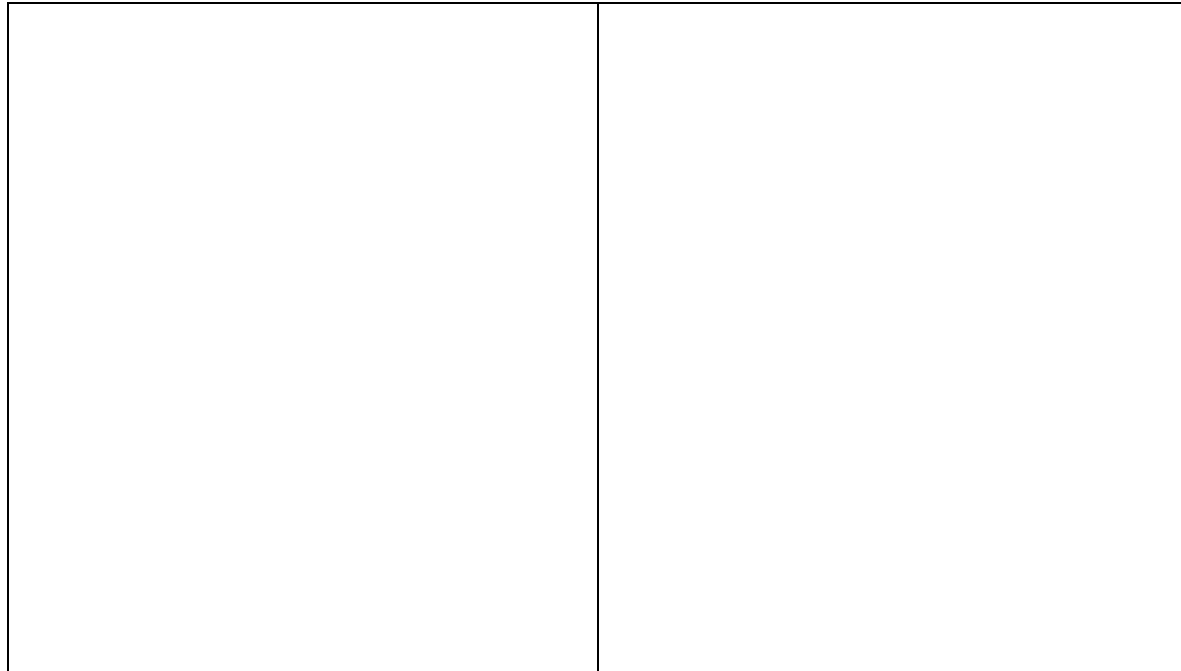
Figure 4.B.3:  The left of the figure shows the stacked data from road 251-1 with elevation statics applied. The right shows the same data with refraction statics applied. With this data the elevation statics were much more effective than the refraction statics at improving the signal-to-noise ratio.

The data is then sorted by CDP, or common depth point, so all the data concerning one location in space is grouped together.  By stacking CDPs and that are close to each other the signal-to-noise ratio is increased and reflections become more prominent in the gather.  The CDP gathers are sorted by offsets.  In this view reflections appear hyperbolic because it takes more time for the signal to travel to and back from the reflector on the longer offsets.  This effect is called normal moveout.  The velocity analysis tool in ProMAX displays the CDP gather and a semblance plot of velocities side by side.  By selecting the correct RMS velocity, the reflection can be flattened.  When the CDP gather is stacked this creates a point instead of a smear. Applying the correct velocities to the gather is important for many reasons.  The normal moveout correction allows the CDP gather to be stacked into a single trace increasing the signal-to-noise ratio. Now each trace more accurately corresponds to the subsurface structure.  Once the whole survey has been corrected for normal moveout, it can be pasted together creating a cross section of the subsurface.  Additionally, picked RMS velocities can be decoupled into interval velocities which provide information about material properties in the subsurface.

Figure 4.B.4:  This figure shows an example semblance plot and CDP gather
which were use to calculate RMS and interval velocities.  The correction for
normal moveout can be observed in the reflector at 1400 ms.

The stacked image, showing the underground structure can still be improved by applying
residual statics correction.  Residual statics is a correction for small scale discrepancies in
position.  In contrast to refraction statics, which corrects statics for an entire shot, residual statics
corrects source and receiver locations based on the velocity model and surface conditions.
Residual statics produced a noticeable difference in the data from 251-1; however, there was
little change in the data from 250 when residual statics were applied.  One reason residual statics
may not make as great a difference is if the initial statics was not an effective correction.  In the
case of county road 250 this could mean reprocessing after applying refraction statics.  The
residual statics correction creates a final stacked image of the data in time.
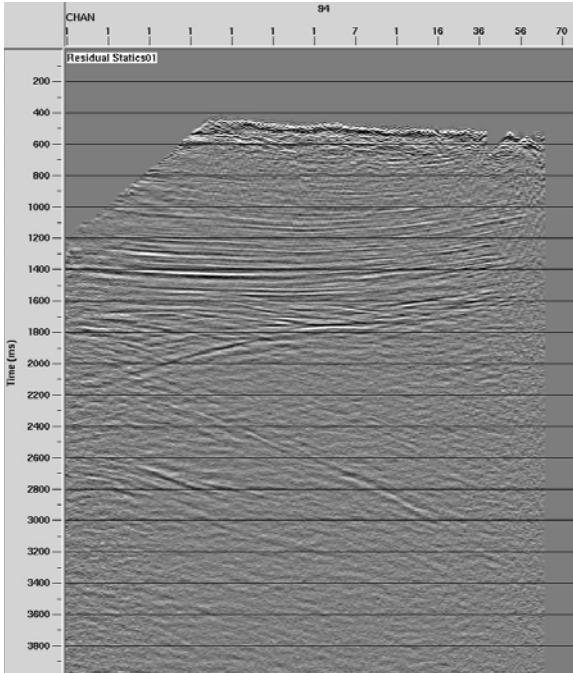
Figure 4.B.5:  The stack on the left shows the data from county road 251-1 after residual statics are applied. The stack on the right shows the data from 250 with residual statics applied.

The stack is a combination of all the waves in all directions, in time.  While this provides much information, some of the information is not spatially correct.  Using the interval velocities the image can be migrated. Migration is a process that places reflections, and diffractions where they are in real time or space.  In this case we performed a post stack time migration.  The migrated image is how the subsurface would look if it were viewed moving down the section at a constant speed.

Figure 4.B.5:  The left image is of the final time migration of road 251-1. The right image is of the final time migration of 250.

By iterating the processing steps starting from the velocity analysis and going through the post stack migration, the accuracy of the image can be greatly improved.  After the time migration both the unmigrated and migrated stack were converted from sections in time, to sections in depth using the interval velocities.
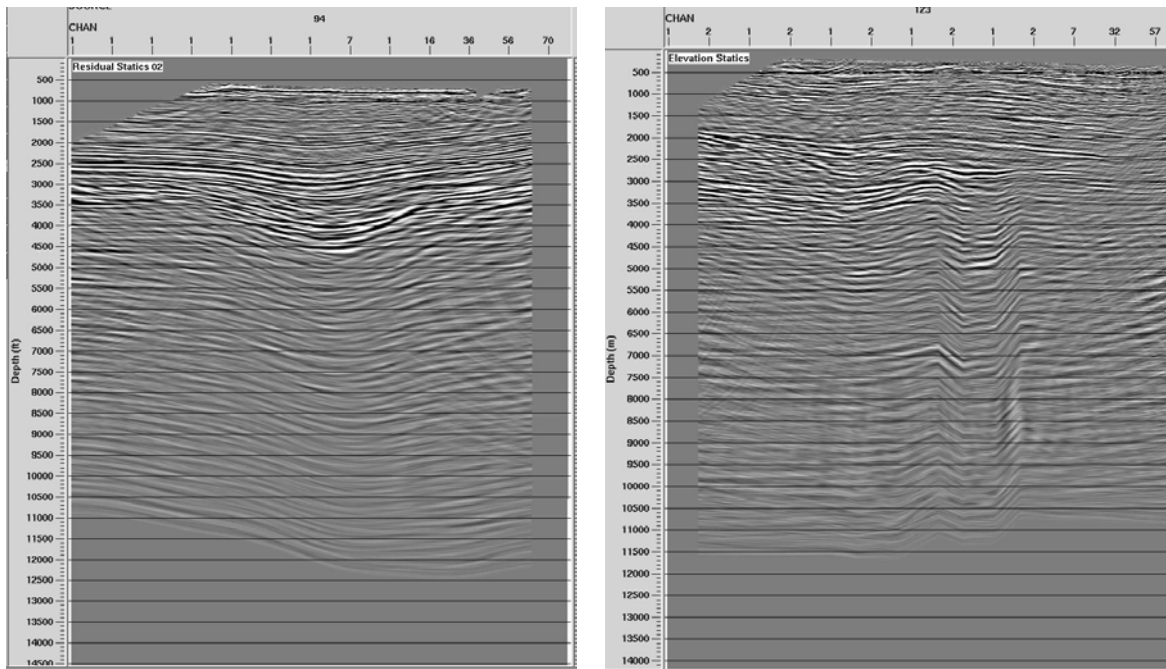


Figure 4.B.6: The image on the left shows the depth section of road 251-1. The right shows the same for road 250.

## Interpretation

Interpretations of the reflections seen in both seismic lines were made, and similarities were seen in both (See figure 4.B.7.) The uppermost layer in each section is the Dry Union Formation because it can be seen in outcrop along the lines. The Dry Union is interpreted to be the extent of the continuous horizontal layers.  The layers of the Dry Union appear to thicken towards the western edge of the basin indicating that deposition occurred during an active rifting period. The lowest strong reflection is interpreted as being the uppermost boundary of the basement. Between the Dry Union and the basement, a layer is seen that pinches out as it moves further east. Due to the high increase in velocity seen at this transition from Dry Union to this layer, it is interpreted to be either a lava flow or Paleozoic sediments similar to those seen in the hills east of the survey site.  The lava flow interpretation is reinforced by the fact that there are places in the valley where the lava is seen being pinched out between the Dry Union and the basement rock.  Also, throughout the valley one can see the Paleozoic sediments between the basement rock and the Dry Union.  On CR251-1 a fault is apparent on the eastern side which appears to cut though the lower stratigraphic package indicating that it occurred before the final deposition of the Upper Dry Union Formation.  In the lower portion of the top left image in Figure 4.B.7 are two coherent dipping reflections.  These reflections do not appear in the migrated images which indicate that they occur outside the survey line.  These reflections may be indications of dipping fault surfaces on both east and west of the ends of the survey line along CR251-1.
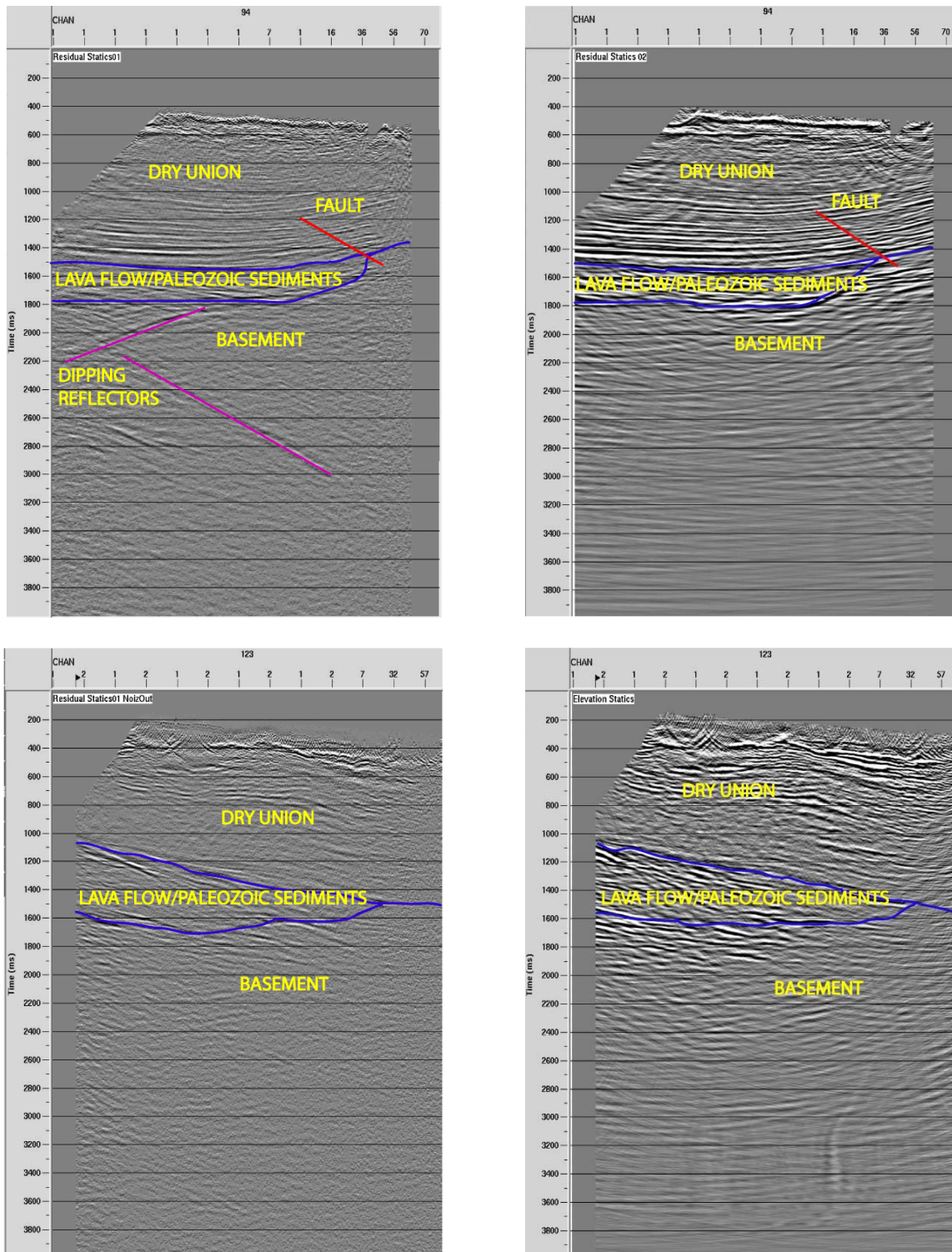
Figure 4.B.7: Top Left: Interpretation of the stacked data from county road 251-1.  Top Right: Migrated data from county road 251-1. Bottom Left: Stacked data from county road 250. Bottom Right: Migrated data from county road 250.

## Error Analysis

One source of error in the data was incorrect geometries. This could be due to inaccuracy in obtaining station information. With the differential GPS, some stations were skipped, and locations and elevations had to be interpolated from surrounding stations.

Another main source of error was noise. The seismic line on CR251-1 ran through a valley and had little noise in the data except for at the end closest to highway 285. This noise could have been due to the nearby highway, but was most likely due to incorrect geometries. In this section of the line the geometries were dissimilar to the other geometries along the line, and so the first 16 CDPs were simply cut out to improve the data. There was also a large amount of noise seen on the seismic line which ran up a ridge on CR250. Every shot in this line showed large amounts of groundroll and air blast noise. This noise was taken out in processing after deconvolution was performed.

This survey could have been improved by extending the survey line on either CR251-1 or CR250, most notably by extending them further up the roads toward the western flank of the valley.

## Conclusion

The data obtained in both surveys created similar and interesting subsurface images. With knowledge of the geology in the valley, an interpretation of the reflections gives a "cross-section" of this side of the valley. This with other data provides important structural information about the southern end of the valley. It can be seen in multiple data sets including seismic that the faulting dynamics of the valley are growing increasingly complicated as the surveys approach the transition zone.

## *Gravity Survey*

### Introduction: Mapping the Arkansas Rift-Valley Basin with Gravity

The purpose of a relative gravity survey across the basin is to directly map the structure of the subsurface. Gravity is the attractive force between two or more bodies of mass. The force is proportional to the mass of the object, and decreases with distance as seen in the $1/R^2$ term of Equation 4.C.1. In the case of the Upper Arkansas Rift-Valley Basin, we are seeing the direct effect of the dense basement rock that makes up the deep subsurface basement floor. Due to its high density, the basement rock that is being extended and faulted stands out as the body that the gravimeter detects.

$$g = -\frac{GM}{R^2}$$

Equation
(4.C.1)

A small mass on a highly sensitive spring inside the gravimeter is being attracted by the dense basement rock and indicates very small scale changes in gravity as the survey moves East to West along the gravity profile.  Based upon variations in gravity, subsurface geometries can be predicted showing the basement rock's distance from the surface at different points along the profile.  As the basement rock dives deeper from the surface, the gravity reading decreases, whereas when the basement rock rises close to the surface the gravity reading increases.  Where sharp changes in gravity are present, forward modeling can be used to detect possible faulting in the subsurface.

Gravity results from data and modeling can be cross correlated with data from the deep seismic survey, either confirming or disproving our modeled structures and our preliminary hypothetical cross sections of the Upper Arkansas Rift-Valley Basin.

## Data Reduction and Corrections

### Counter Reading Correction

The observed gravity value from the Lacoste-Romberg relative gravimeter, needs an instrument conversion correction.  Each relative gravimeter is unique and requires a slight conversion from measured gravity to true relative gravity.  The observed gravity data values were converted to mGals using the dial reading on the gravimeter, **A**, and a table with lists of values including the nearest integer smaller than the reading, **B**, the value in mGal, **C**, and the factor for Interval, **F**.  The correct relative gravity value is given by Equation 4.C.2, and all other corrections are done off of this calibrated value.

Gravity = C + F * (A-B)                                                    Equation (4.C.2)

### Tidal/Drift Correction

Gravity readings are directly affected by both the sun and the moon; similar to the sun and moons' effect on ocean tides.  As the earth rotates with respect to the sun, the gravitational attraction between the sun and any given point on earth changes in both direction and amplitude.  As the moon rotates around the Earth, it also provides a fluctuating gravitational attraction between itself and any given point on the Earth.

This effect causes slowly changing, small scale gravity fluctuations at all points on Earth, which is detected by the gravimeter throughout a given survey and must be corrected for.  This Tidal effect can be modeled as linear on a time scale of approximately 1.5 hours.  After this period, the correction curve becomes non-linear, and attempted corrections are skewed.

Instrument drift is also a small factor in the change of gravity value observed on the gravimeter.  This is the basic concept that over time, gravity readings from the gravimeter itself will drift due to physical effects on the mechanical components within the instrument from wear and aging of

the highly sensitive parts. The drift effect can be paired with the tidal effect, and both can be corrected for using Equation 4.C.3. Where t is the reading time of observation between sub-base stations, $g_b$ and $g_e$ at times $t_b$ and $t_e$ respectively. Reading $g_1$ is the very first, main base station reading.

$$\Delta \text{Gravity tidal/drift} = g_b + (t - t_b)\frac{(g_e - g_b)}{(t_e - t_b)} - g_1 \qquad\qquad \text{Equation}\ (4.C.3)$$

By doubling back to gravity base stations every hour, the change in reading allows the calculation of tidal effects for every point after the base station in that given amount of time. In an ideal survey, it is important to re-measure the main base station to tie in all sub base stations, giving a well approximated tidal/drift correction curve.

Due to the length of the gravity line and terrain covered on Chaffee County 251-1, it was impractical to tie every loop back to the main base station. For this reason, a series of 15 sub-base stations were used to reduce the backtracking done on the line. A linear tidal/drift correction was done for each individual sub-base station loop and the alpine survey to the peak of Mt. Shavano. This data was taken over the course of 5 different days. Once all loops were completed, each with its own base station, Tom Cullison and Dan Liechty performed a base station survey to tie all sub-base stations together. This final base station tie-in allows for the entire line to be corrected to appear as if it had been taken in a single day.

By correcting for tidal/drift effects in this base station survey and using the tidal/drift corrected gravity values from the sub-base station loops, each individual loop and its sub-base station were tied to the main base station. These processes aligned all loops and removed discontinuity from tidal/drift effects from day to day.

During the alpine gravity survey conducted by Earl Marshal, Dan Liechty, and Josh Nichols to the peak of Mt. Shavano, it was not possible to execute full loops, doubling measurements on spread out base stations due to the physically demanding logistics of the climb. There was not enough time to double back to spread out base stations on foot, and the energy required to climb the mountain in such a fashion would not have allowed for the survey to reach the peak. For this reason, every 1 to 1.5 hours, the gravity crew doubled back to the immediately previous gravity station 200 meters down the mountain to re-measure the station and then continue westward up the mountain again and repeating the measurement where the double back started. Initially the tide/drift correction was to be made using a first order derivative of the three repeated base stations, but after examining the data, it was decided that this was an unacceptable method. To make the tide correction, Micro-G generously provided tide corrections at a central latitude, longitude, and elevation to the alpine survey, covering the time span of the survey. From this data, the tide effect was corrected out of the alpine gravity survey.

**Latitude**

When measuring gravity, the instrument is measuring a sum of all accelerations the sensor is experiencing. Accelerations from the tides (taken care of in the Tide/Drift Correction) and the

earth's rotation are the only accelerations strong enough for a correction to be necessary.  As the earth rotates about its axis, it maintains a relatively constant angular velocity.  This means that the points on the earth furthest from the axis of rotation (the equator) will have a higher linear velocity than points near the axis (the poles.)  This means that at the poles there is virtually no centrifugal acceleration, whereas it is a maximum at the equator.  This acceleration works against the force of gravity and decreases the measured gravity at the equator.  Equation 4.C.2 shows the latitude correction equation where φ is latitude in degrees.

$$\Delta\,\text{Gravity Latitude} = 978032.68\,\frac{1+0.00193185138639\sin^2\varphi}{\sqrt{1-0.00669437999013\sin^2\varphi}} \qquad \text{Equation (4.C.4)}$$

In this survey, the line ran roughly east to west, thus having very little variation in latitude.  The variations that do exist in the line have been corrected out but are of such a small magnitude that they would have been unnoticeable within the error of the instrument.


**Free-Air**

Elevation of the survey points ranged from under 8,000 feet at the US285/CR251-1 intersection to 14,229 ft at the summit of Mt. Shavano.  The gravity reading is affected by elevation as defined in the $1/R^2$ term of Equation 4.C.1.  Thus, to achieve an accurate free-air correction, it is imperative to have an extremely precise measurement of elevation.  For the majority of the line, the elevation was measured using the differential GPS as described in Section 3B.  This system, when operating under optimal conditions can pinpoint the elevation to within a centimeter.  However, under tree cover and heavy clouds the accuracy decreases, which can be seen in the data.  For these same reasons, differential GPS was abandoned above flag 1651.  A handheld GPS was used to mark flags 1650-1646.  These elevations points turned out to be unusable due to inherent error in the handheld GPS system.  Elevations were taken from a digital elevation model to be used for these points, this however is still not adequate for reliable data since the DEM has a resolution of 30 meters.  Flag 1645 marked the beginning of the alpine gravity section.  Elevation for points 1645-1627 were taken using 3 independent handheld GPS, a manually calibrate barometric altimeter, and a GPS calibrated altimeter.  From these data sets averages were taken and a confidence interval of +/- 5 meters was achieved.  The data from the GPS could not be reprocessed since each data point is independent of time of day or other external conditions.  On the contrary, the altimeters error is due almost entirely to changes in barometric pressure.  With the exception of severe weather, these changes generally happen slowly throughout the day, allowing linear calibration of the altimeter readings points on the route with precise elevation markings on the USGS quadrangles.  These points include both the beginning (flag 1644) and the summit (flag 1627) along with two points en route.  From these calibrated results, a comparison was done finding that the maximum deviation in any of the five data sets was less than 7 meters.  This error was further decreased by weighting the barometric altimeters higher in the average due to greater confidence.

Using the elevation for the line calculated in the various ways described above, an elevation (free-air) correction was performed.  The free-air gradient is used to reduce the data to a constant elevation datum, in most cases sea level, and the gradient is assumed to be constant at the earth's

surface. This assumption is accurate only with small changes in elevation with respect to the earth's radius, but it is a good approximation within the error of the instrument of this survey. Equations 4.C.5 and 4.C.6 shows the formula used to apply the free air correction, where $h$ is the elevation above sea level in meters.

$$\frac{dg}{dh} = \frac{2gh}{R} - \frac{3gh^2}{R^2} = -0.3086$$

Equation (4.C.5)

$$\Delta \text{ Gravity Free Air} = \frac{dg}{dh} h = -0.3086h$$

Equation (4.C.6)

## Simple Bouguer

After the free-air correction has been applied, the data has been changed to assume that there is no mass between the sea level datum and the elevation of the measurement point. The Simple Bouguer Correction is implemented in order to fill that void space with rock of appropriate density. The two major assumptions of this correction are that the area between the measurement elevation and sea level can be represented by an infinite slab, and that that slab has a reasonable density distribution (Chapin, 1996.) The simple Bouguer Correction can be applied using Equation 4.C.7, where $\rho$ is the density of the slab and $h$ is the elevation above sea level in meters.

$$\Delta \text{ Gravity Bouguer} = -0.04193\rho h$$

Equation (4.C.7)

## Terrain

Once an infinite slab has been produced in the Bouguer Correction, the effects of terrain undulation must be accounted for. This is especially important in mountainous regions such as the Upper Arkansas Valley due to high relief within close proximity to the survey. In most cases the terrain effect will decrease the measured gravity due both to mass missing in the valleys, and excess mass above the survey point in the surrounding mountains.

The terrain correction is produced using a digital elevation model (DEM) of the surrounding terrain. In an effort to conserve processing power, most terrain correction algorithms use a high resolution DEM for the terrain in the local grid, (within a couple kilometers) and a low resolution DEM for areas outside the local grid. It has been found that in the most precise surveys that terrain within a 200 kilometer radius must be taken into account. In this study, only the terrain within Chaffee County will be taken into account. The accuracy provided within this 20-50 kilometer radius of terrain correction is reasonable considering the error of the instrument. Any terrain outside of this radius will only provide differences on the order of a few μGals, and average to be well below the resolution of the instrument.

To perform the terrain correction HammerXYZ, a DOS based program, was used. The program depends on a single large DEM file which is a compilation of both the high resolution local terrain grid, and the low resolution regional terrain grid. A second input file is then used to input all of the survey point locations. The program calculates and sums the effect of each pixel

in the grid on each survey point.  It is easy to see that when a DEM using millions of elevation points and a survey with over 150 survey points are used, the processing can run for days.

## Absolute Gravity Base Station Tie In

The gravity profile was created using relative gravity values recorded on a relative gravimeter. For interpretation purposes, this "floating" relative gravity profile is sufficient for picking faults, geometries and depths to the basement rock for the 2007 Field Camp.  However, in order to tie in to previous years gravity data, and draw connections between previous surveys, a conversion to absolute gravity values is helpful.  By converting to absolute gravity a broad understanding of the basement structure throughout the valley can be achieved using gravity profiles further to the north from previous years.

In 2006, CSM calculated the absolute gravity value at a base station on county road 250 by looping that station several times with a station near the post office of a known absolute gravity value.  By looping base station 2000 from the this years survey with the absolute station on county road 250 three times, an absolute gravity value at station 2000 was calculated and then translated to all other points on the gravity line from this years survey.

## Interpretation

The final data from the gravity line on Chaffee County Road 251-1 is shown in Figure 4.C.1 overlain on an interpreted geologic cross section.  Due to extended processing time on the terrain correction there was not time to complete a forward model to fit a possible structure to the data. It is because of this that there is no vertical scale on the cross section.  Although vertical scale is absent, the dramatic changes in the gravity profile are indicative of faults with significant offset. As can be seen in Figure 4.C.1 the faulting is probably very steep and many of the faults show dip in the opposite direction as expected.  Based on the basement elevations indicated by the gravity profile, and the tectonic regime of the area it is only possible for the three faults in the eastern portion of the cross section to be normal faults dipping to the west.  These normal faults are only possible extension zones and faults dipping the other direction would be possible if an indication of a compressional event, which is very unlikely.
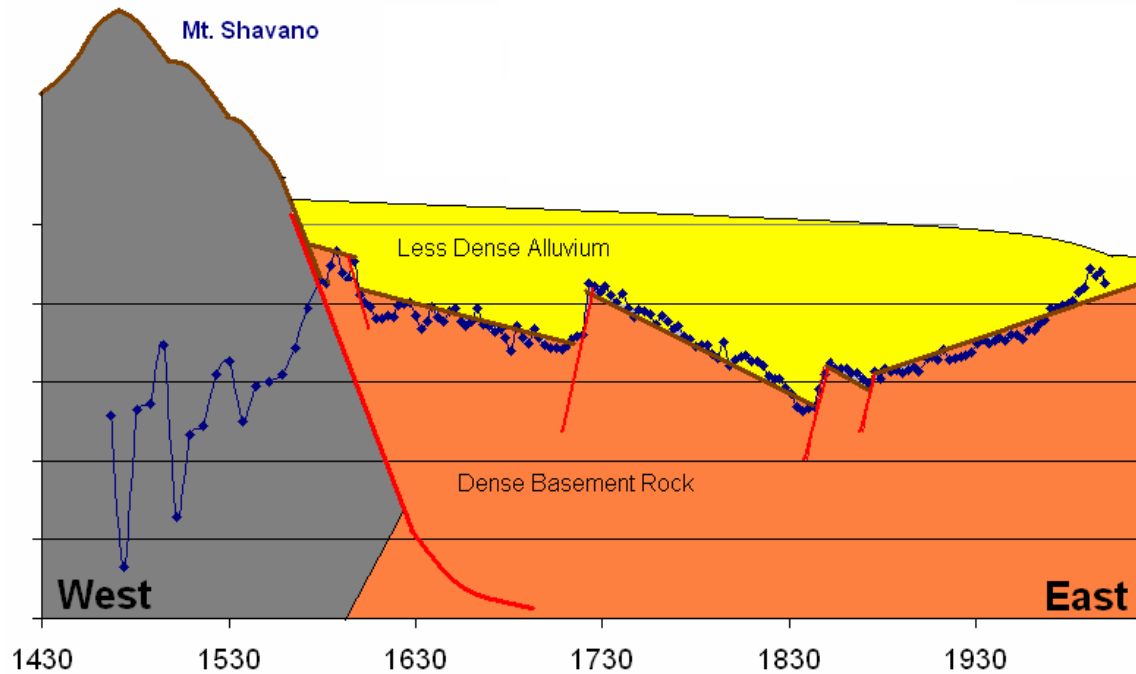
Figure 4.C.1:   Interpreted Cross Section drawn on top of the corrected gravity profile. Notice that under corrected terrain data from the western portion of the line has been left on the plot although it is still ultimately incorrect.  This includes all of the points in the grey section.

The reversal in the faulting direction is hypothesized to be attributed to the line's proximity to the transfer zone near Poncha Pass.  This transfer zone is a poorly understood geologic feature where the high angle normal faulting switches from the west side of the basin in the Upper Arkansas Valley to the east side in the San Louis Valley.  It is only logical that the faulting become more frequent and complex near the transfer zone and the gravity data from this line may be representative of that complexity.

It is worth noting that the gravity data is looking at a contact that is in places multiple kilometers below the surface.  For this reason it is imperative to understand that the faults drawn in figure 4.C.1 are indicating only the major faults, and that there may be a complex system of small scale faulting between these major faults.  This hard to image network of smaller faults may prove to have a large role in the water movement and storage capabilities within the southern portion of the basin.

**Error Analysis**

Among the sources of error in gravity data acquisition and modeling were inaccurate reported elevations from the differential GPS and hand held GPS instruments.  After a rough plot of the corrected gravity data (pre-terrain correction) there was found to be a series of jumps and discontinuities in the gravity profile, too sharp to be indicating true gravity anomalies in the subsurface or deep basement.

Upon first speculation, these jumps in the gravity profile were attributed to possible error in the alignment of the individual loops discussed above in the Tidal/Drift Correction section. However, it was found that none of the discontinuities along the trend occurred at the junction of individual loops, but rather isolated inside individual loops. All jumps in the profile have been linked to highly probable error in elevations reported by both differential and hand held GPS. In Figure 4.C.2 below, the Gravity Profile Error Analysis points out specific instances of reported elevation change on the order of 10 meters over a 30meter distance such as stations 1968, 1967, and 1966. This section of the road in reality is very flat only gradually climbing. An elevation gain of 10 meters over a 30 meter distance in this section of road is completely fallible. These erroneous elevations have been recalculated by averaging the elevations of the two points on either side of the station in question. The smoothing effect on the data can be seen below in Figure 4.C.2

The gravity values circled in green on the West end of the profile seen in Figure 4.C.2 below are inaccurate due to error in elevation reported by hand held GPS. Stations 1650-1646 were recorded by a hand held GPS unit because of difficulty in acquiring satellites with the differential GPS at these locations under dense tree cover. As seen, there is a drop in gravity values at these points along the profile that is directly related to inaccurately reported elevations for these stations. The identification of elevation as the error is made evident in that these anomalous stations were all recorded by hand held GPS and only these stations are affected. This was a very constant section of steep road with the same grade. By changing the elevations of these points to increase in a constant grade from 1651 to station to 1644, we were able to correct for the drastic drop in gravity values and see a continuous trend in the gravity profile as was expected seen in Figure 4.C.2 below.

It should be understood that the free air correction has the strongest effect on the true gravity values acquired, changing the gravity by approximately 0.3 mGal for every meter gained or lost in elevation. When the elevation is off by a few meters, the gravity profile will change dramatically. Other corrections such as tidal/drift and latitude, rarely affect the profile within the detection of the human eye, and are often less influential than human error in taking the measurement. This is indicated by error in human reproducibility of readings at the same location in short time intervals, discussed further below.
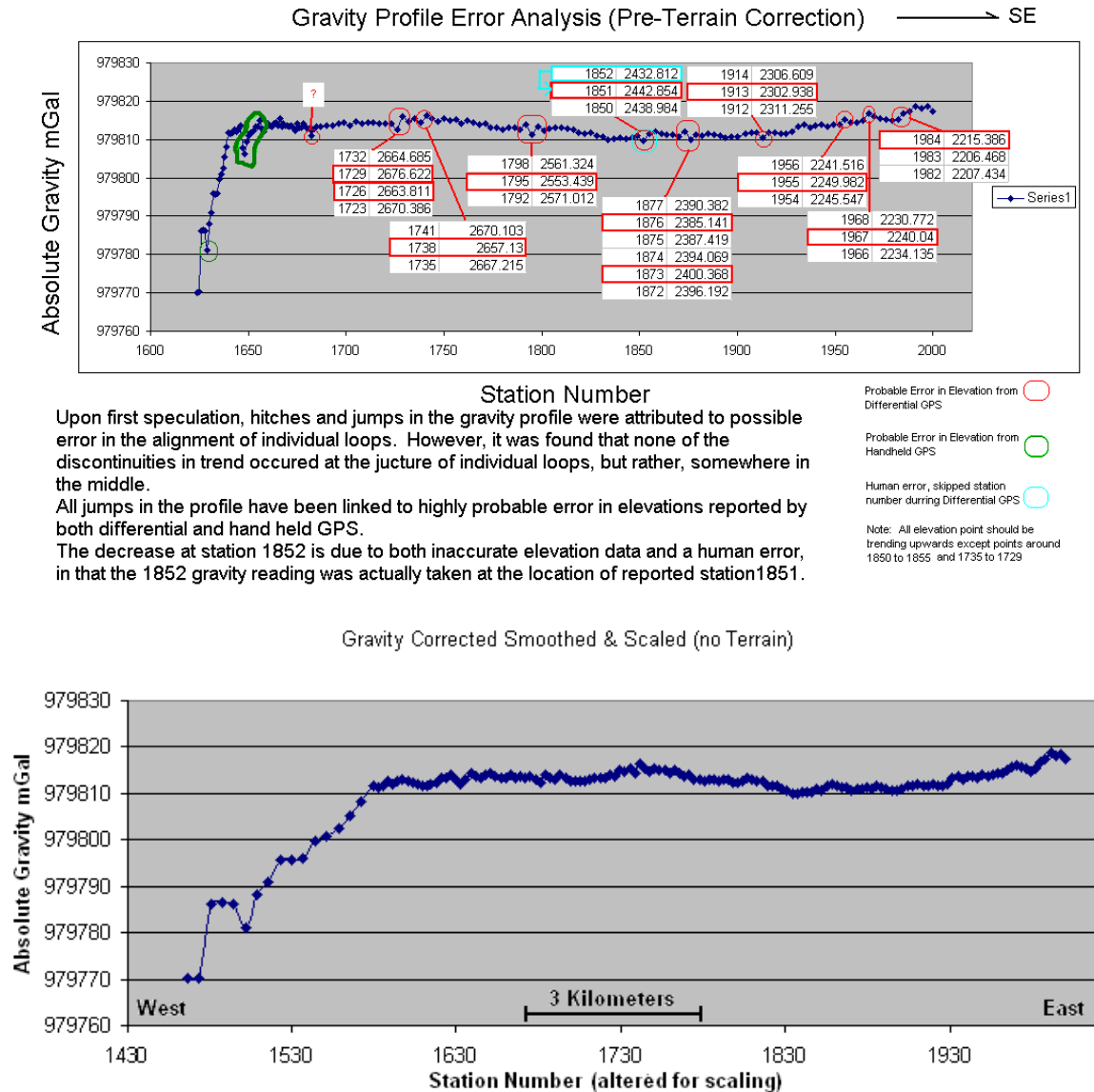
Figure 4.C.2:  Top: Display of errant points in the elevation data and their effect on the corrected data. Bottom:  Corrected data after smoothing of errant elevation data points. Data in both plots is before the terrain correction.


One specific error was identified as a mislabeled station during the differential GPS survey. Station 1857 was never reported in the differential GPS notebook.  Station 1858 was recorded and matched with the GPS identification number, and then skipped down to 1856 matched with a GPS identification number as the next flagged station.  However, it is reported by the survey crew that no station was skipped.  This indicates that the last stations recorded that day from 1856 to 1851 are each erroneously shifted one station eastward in location, affecting gravity stations 1855 and 1852.  They have been shifted back to the west in the gravity corrections to account for the correct elevation and latitude values for Free-Air, Latitude, Simple Bouguer, and Terrain Corrections.

In the alpine survey, the last three readings taken with the gravimeter where recorded while the gravimeter temperature rose as high as 58 degrees Celsius due to loss of charge in the battery. The temperature of the Lacoste-Romberg Relative Gravimeter is kept at a constant 53.3 degrees Celsius at all times, to prevent warping and damage to the highly sensitive spring holding the mass.  This temperature change only occurred in the last three readings of the survey, which include the measurement at the peak of
Mt. Shavano, station 1624, sub-base station 1627 on the way back, and base station 1645. Because of the use of tide corrections from Micro-G, the last two base station readings were not needed, and the peak  Mt. Shavano doesn't effect our gravity profile noticeably due to it's location far west of the faceted spur and its low rise in temperature for that reading (around 54.1 degrees Celsius).  Thus, it is believe these three measurements in the alpine survey do not negatively effect data for the gravity profile.

The terrain correction compounded error on the upper portion of the line.  This was due to lack of DEM data due west of the line.  The radius of correction of the final few points was truncated at about 10km on the west side.  This is an area where it is essential to have this DEM data because the terrain in the area is 4,000-6,000 feet lower than the summit of Mt. Shavano. Overall this lack of DEM data resulted in an under correction of the western most portion of the line.  This under correction decreases in magnitude significantly as you get past east of station 1645 due to the lower elevations and further distance from the western edge of the DEM.  This under compensation for the terrain effects must be corrected before the furthest west section of the line can be interpreted.  Due to processing power and time restraints this reprocessing of the terrain model could not be completed before the report deadline.

Lastly, the effect of human error when taking a measurement on the Lacoste-Romberg Relative Gravimeter is always present.  The average amount of human error in taking a measurement can be determined by examining the reproducibility of measurements by the same person, at the same location over very short periods of time as to reduce the effect of tide and instrument drift. At station 1645 during the base station tie in survey, there were two measurements taken 6 minutes apart.  The first reading was converted to 2777.630 mGal with tide correction, and the second reading was converted to 2777.714 with tide correction.  This is a difference of 0.084 mGal in human error from one reading to the next.  At station 1624, peak Mt. Shavano, two readings were taken two minutes apart.  The first reading was converted to 2491.745 mGal with tide correction, and the second reading was converted to 2491.623 mGal with tide correction. This is a difference of 0.122 mGal from the first reading to the second.  By averaging these two differences, the average human error in measurement reproducibility comes out to be 0.103 mGal, an order of magnitude larger than corrections for tidal/drift, and latitude effects.

## *Magnetics*

The magnetic method is based on the interaction between the Earth's natural magnetic field and the material property of rocks called magnetic susceptibility, which describes how much magnetization a material will experience when placed into a magnetic field.  This method is useful when mapping contacts between highly magnetic and magnetically resistant bodies.  For this reason, it was used along the Deep Seismic and Gravity lines on County Road 251-1 in an attempt to locate the fault separating the magnetic igneous intrusion from the resistive sediments filling the rest of the rift basin.

## Survey Design

Two sets of magnetometers were employed in this survey: a roving magnetometer and a base station. The roving unit was a Geometrics G-858/G Cesium Magnetometer/Gradiometer (Figure 4.D.1) setup as a gradiometer. The basic principles of magnetic surveys still hold for gradient surveys, however two measurements are taken instead of the one used in standard magnetic surveys. These measurements are separated by one meter and are oriented in the direction of the desired gradient. These measurements are differenced in order to determine how much the magnetic field is changing over the one meter separation.



Figure 4.D.1: Geometrics G-858/G Cesium Magnetometer/Gradiometer setup for use in a traditional magnetic survey (photo courtesy of Geometrics website, accessed June 4, 2007)



Figure 4.D.2: Geometrics G-856 Portable Magnetometer (photo courtesy of Geometrics website, accessed June 7, 2007)

The base station was a Geometrics G-856 Portable Magnetometer (Figure 4.D.2). Its purpose was to take continuous measurements at a single location for the duration of the survey so a correction for the diurnal variation could be made. Diurnal variation is the change in the magnetic field of the Earth due to various factors (such as solar wind) throughout the course of the day. Once this data is obtained from the base station, it can be subtracted from the data from the rover's data so an idea of how the subsurface would interact with a static magnetic field can be obtained. Figure 4.D.3 is a graph of the diurnal variation recorded from our base station over an eight hour period.

Figure 4.D.3: Base station data showing magnetic fluctuation with time over approximately an 8 hour period.

## Error Analysis

Possible sources of error are cattle guards, culverts, passing vehicles, and human error when marking positions with flags. Cattle guards, culverts, and vehicles, composed of metal and close to the surface, create a strong response in the data, as can be seen from the data in Figures 4.D.4 and 4.D.5. Several problems also occurred due to missing flags or flags that went into the woods instead of following the road and were thus missed by the operators. This last problem was especially troublesome during data processing, as it was difficult to piece together the lines due to flags and mark ids not being entirely lined up.

## Conclusions

The magnetic line was slated to follow the gravity line along County Road 251-1, however it fell short of crossing the surface expression of the fault due to weather conditions. The data was expected to show a relative increase in magnetic strength as the fault was approached, due to uplifted basement rock. However, this does not seem to occur, probably because the fault was not crossed. The line in which the profile was run was magnetically quiet except for an occasional spike which correlates with the numerous cattle guards crossed (Figure 4.D.4 and 4.D.5).
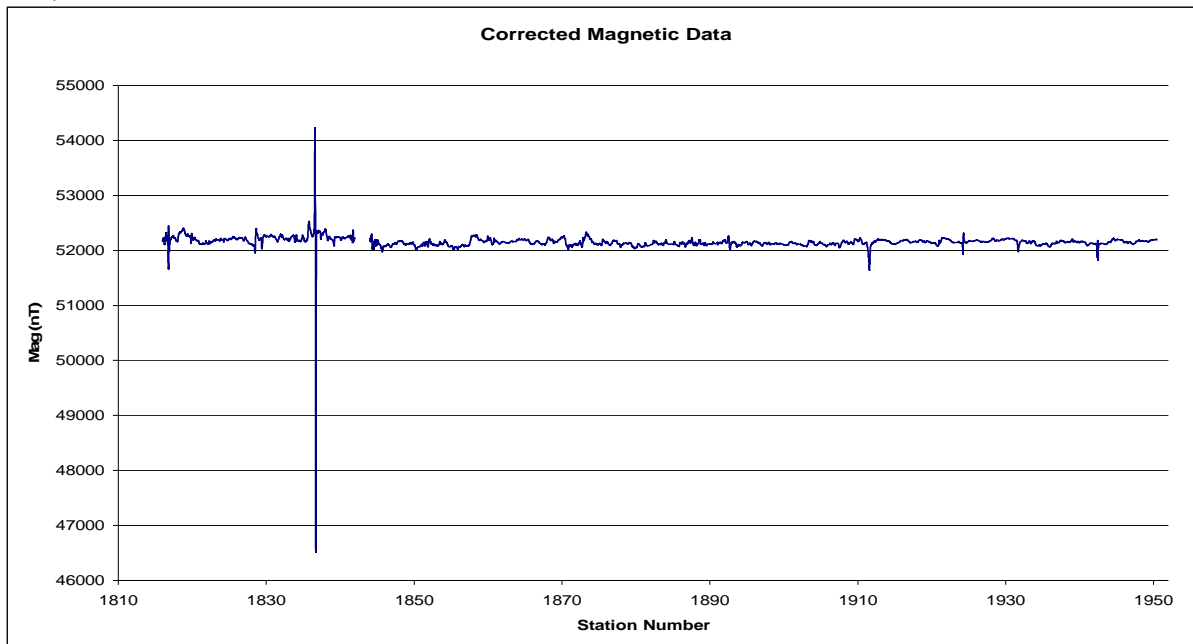


Figure 4.D.4: Magnetic profile between stations 1930 and 1810. The magnetic spike around 1937 is due to a cattle guard grill.
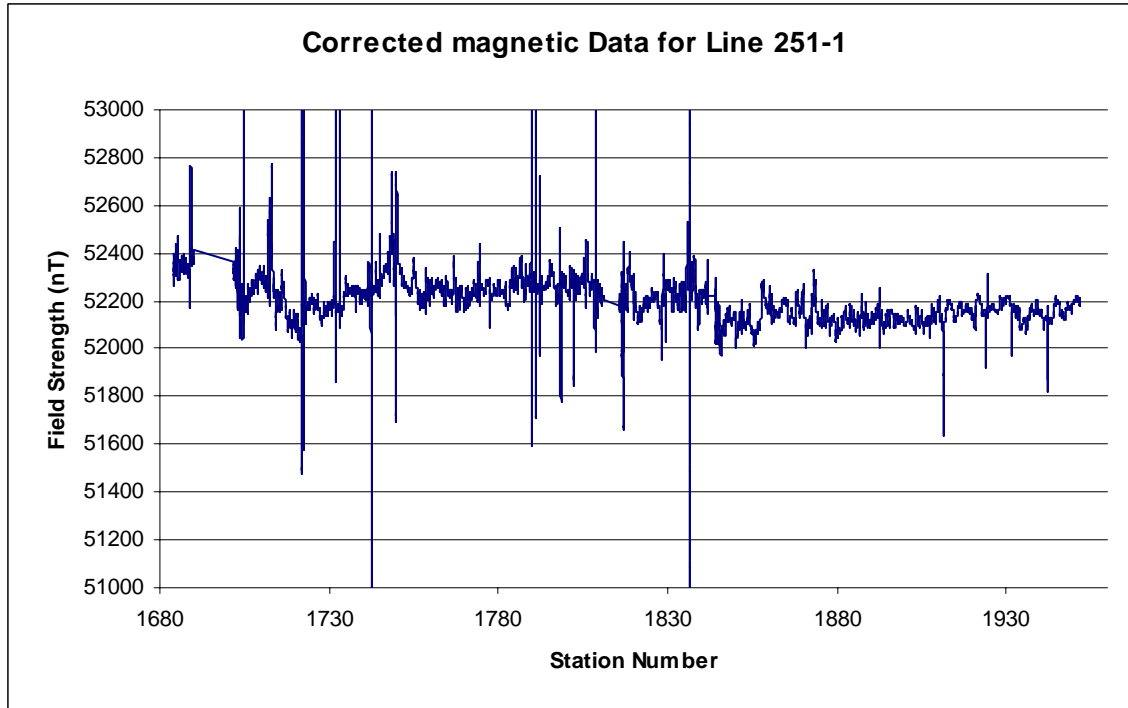
Figure 4.D.5: A complete magnetic profile line (stations 1684 to 1952). The profile shows several spikes which are coincident with either metallic cattle grill or some other foreign metal. Generally the magnetic susceptibility is quiet and does not indicate any significant geological structural change.

When the diurnal corrected magnetic data was compared to the corrected gravity data, several interesting similarities were observed (Figure 4.D.6). These similarities lend credence to the interpretation of the gravity data.

Figure 4.D.6: Correlated Magnetic and Gravity data (gravity is on top, magnetic on bottom)

## *Interpretations and Conclusions from the South Site Data*

The 2007 south line, located along county roads 251-1 and 250 and the ridge of Mt. Shavano, was surveyed using seismic, magnetic, and gravity methods.  Cross correlating theses three surveys has yielded encouraging, reproducible similarities in subsurface basement geometries.

Comparison of the magnetic and gravity surveys reveals what is interpreted to be strong definitive correlations in small stepping fault structures traveling west towards the faceted spur of Mt. Shavano.

The effect of dense causative bodies on a gravity profile tends to be broad and ambiguously defined.  By examining the gravity profile by itself, it is difficult to draw concrete conclusions as to where small scale changes in basement depth and faulting occur.  However, when correlated with magnetic data, which in this survey reveals much sharper discontinuities in basement depth, the gravity profile can be interpreted on smaller scales, and similar geometries between the two reinforce accurate interpretation.

In Figure 4.F.1 below, small scale correlations between the gravity (top line) and magnetic (bottom line) profiles are identified and indicated by orange boxes section by section.  These isolated sections indicate possible changes in angle of dipping beds and small scale faults from stations 1950 to 1720.  The similarities drawn are still somewhat open to interpretation, but strong discontinuities indicated by sharply curved lines in both profiles are well defined and convincingly indicative of faulted basement with considerable throw.

Figure 4.F.1:  This image correlates the gravity data (top) to the magnetic data (bottom.)  Notice that the while the two data sets are scaled to fit directly above one another, the magnetic data seems to be skewed to the east (right).

Comparison of the gravity and seismic profiles reveals much broader and concrete correlations of the basement geometry.  Due to logistic difficulties, the seismic line along county road 251-1 only reached up to station 1832.  The migrated seismic model from station 1992 to 1832 can be seen in Figure 4.F.2 below outlined in red.  The orange line follows the reflector of the basement to Dry Union unconformity.  This unconformity matches almost perfectly with the gravity data above it, which directly maps the dipping geometry of the basement rock.

Figure 4.F.3 below shows the un-migrated seismic data from county road 251-1.  In this figure the basement to Dry Union unconformity can be seen again, and below it is identified a strong linear dipping reflection highlighted in orange.  This reflection is interpreted to shift geometrically up and to the west (left) of the basement reflector after migration modeling is performed.  This is confirmed in that the migrated seismic profile doesn't contain this dipping reflector.

By shifting this un-migrated reflector up and to the left of the unconformity boxed in red in Figure 4.F.2 below, it matches strongly with the dipping gravity profile which is boxed in green.  This dipping reflection is attributed to the dipping unconformity between the basement and Dry Union located between stations1830 and 1730.
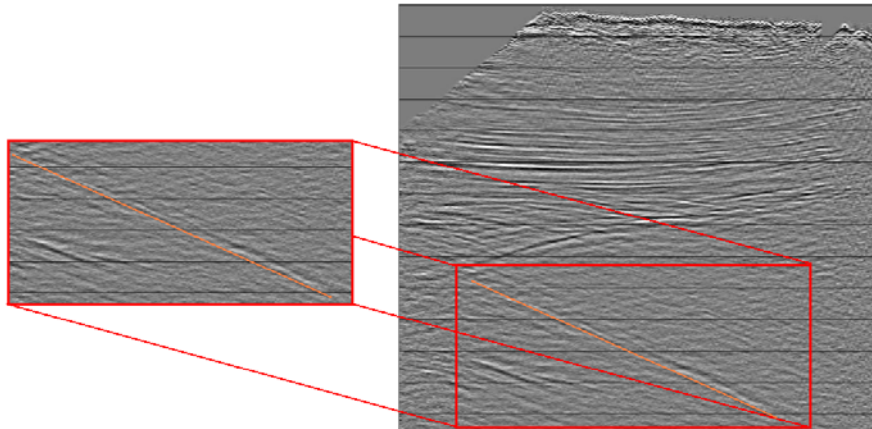


Figure 4.F.2:  Reflection that migrates out of the stack from CR 251-1.  This reflection is correlated to surfaces off of the image in Figure 4.F.3 below.

Figure 4.F.3 Comparison of gravity data to the seismic line on CR251-1.

Ideally, the constructed cross sections from 2005, 2006, and this year's 2007 line would correlate, revealing very similar structures that can be mapped continuously throughout the Upper Arkansas River Valley Rift Basin from north to south.  Interpretations from years 2005 and 2006 located further to the north reveal similar geometries and faulting patterns, whereas the 2007 interpretation deviates in a chaotic fashion.  This change of subsurface geometry has been attributed to the 2007 line's geographic location in the south end of the valley.

It is important to understand that the Upper Arkansas River Valley maintains steeply east dipping faceted spurs off the Collegiate Peaks on the west end of the valley, while the Sangre de Christos to the south have steeply west dipping faceted spurs on the east side of the San Luis Valley.  This geologic conundrum has perplexed geologists for years, and the transition zone between these opposing geologic phenomena is still poorly understood by the geologic community today.  However, it is widely accepted that there is a transition in fault geometry between the Southern end of the Collegiate Peaks and the northern end of the Sangre de Christos, linking the two systems together.

The 2007 line is located very near the southern most end of the Upper Arkansas Valley on what is conceivably the edge of a transition zone into the San Luis Valley.  It should be also noted that the faceted spur diving into the basement off the edge of Mt. Shavano has a strike oriented to the north-east, whereas the faceted spurs to the north, including the 2005 and 2006 lines, are striking just west of north.  This drastic change in strike, occurring only a few kilometers to the north-east of the 2007 line, may account for the chaotic faulting along the 2007 cross section, and also suggests a close proximity of the transition zone. This combined with the likelihood that the 2007 line is approaching or located on the transition zone of the faulting systems, reinforces the reason for chaotic faulting on the 2007 line and its deviation from the geometry of the 2005 and 2006 lines.

Based on the strong correlations between the seismic, magnetic, and gravity profiles, it is believed that the quality of data collected and models created accurately reflect the geometries of

the basement rock along the 2007 south line profile. A one to one scale of the Revised Hypothetical Cross Section of the Upper Arkansas Valley is displayed in Figure 4.F.4 below.
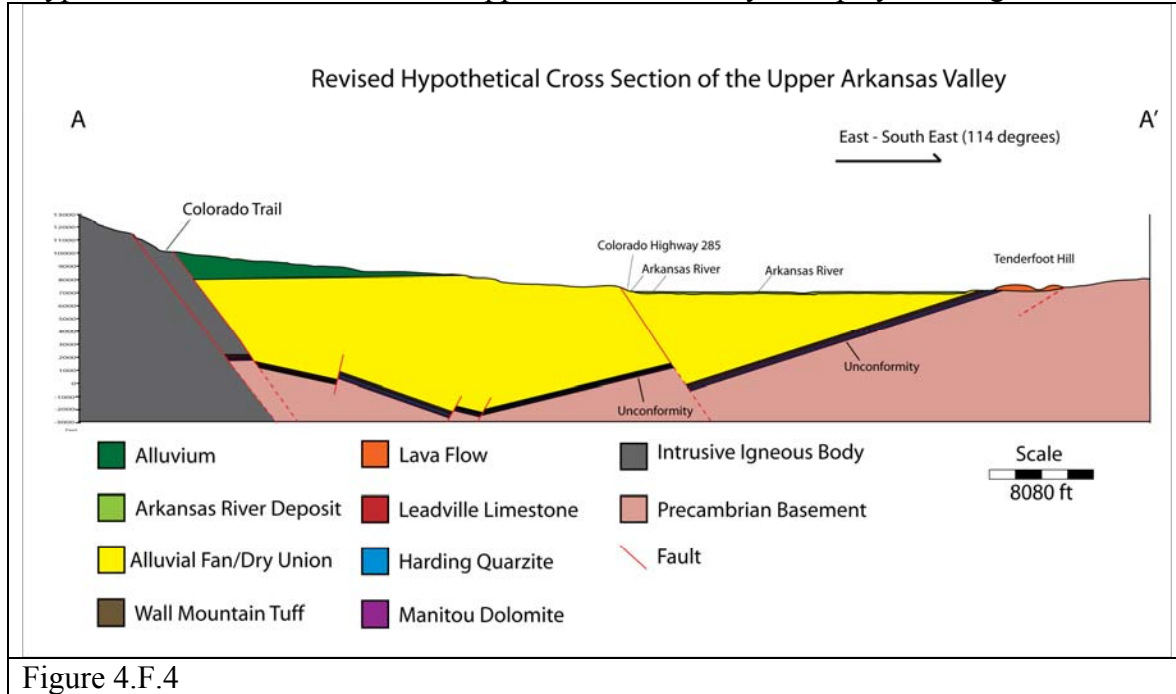


Figure 4.F.4

# Chapter 5: North Site Geophysical Surveys

## *Introduction*

There are several irrigation ditches in the Upper Arkansas Valley.  It is thought that these ditches may leak, supplying the valley with groundwater.  During the drought of 2002 the irrigation ditches were shut off and groundwater levels fell significantly.   Several surveys were conducted in the vicinity of one of these irrigation ditches with the goal of characterizing how the ditches contribute to the water table.

A survey area was chosen North of Buena Vista on the property of Frosty Roe.  The survey area consisted of several large fields, an irrigation ditch, and some small forested areas.  A combination of electrical, electromagnetic, and seismic surveys were preformed over the survey area.  Two shallow hammer seismic surveys were conducted to determine the geometry of the subsurface.  Multiple DC resistivity, ground penetrating radar (GPR), and frequency domain electromagnetic lines were collected.  A large time domain Electromagnetic survey was conducted.  Also, vertical seismic profile (VSP) data was collected in a USGS well a little ways south of Buena Vista.

## *DC Resistivity*

### Introduction:

Our main goal from this academic exercise is an image of the subsurface. However, an image is not enough since we are focusing on water resource. The water table could be mapped using different geophysical surveys. Nevertheless, seismic along with gravity can only show the shape of the aquifer even though water has different physical and chemical properties. Thus, a DC resistivity survey should be applied to solve this problem, taking in the fact that aquifer rocks often have a contrast in conductivity compared to non-aquifer rocks. Therefore, the DC resistivity method will play a vital role in locating the water table and correlating other results from hammer seismic and electromagnetic survey.

### Basic Concepts of the DC Resistivity Method:

DC resistivity is an active geophysical method because it uses two current electrodes (A and B) that supply a direct current into the ground. An active geophysical method uses a source and a receiver to collect the data while a passive method uses receiver to collect data using a natural source. While injecting the current using electrode A and B, voltage was measured across the M and N electrodes. Apparent resistivity was then calculated, which is a measure of the materials resistance to the current flow, using the potential difference and the supplied current (See Equation 5.B.1.

$$\rho_a = \frac{2\pi V}{I \varepsilon_0} \left( \frac{1}{\dfrac{1}{r_{am}} - \dfrac{1}{r_{an}} - \dfrac{1}{r_{bm}} - \dfrac{1}{r_{bn}}} \right)$$
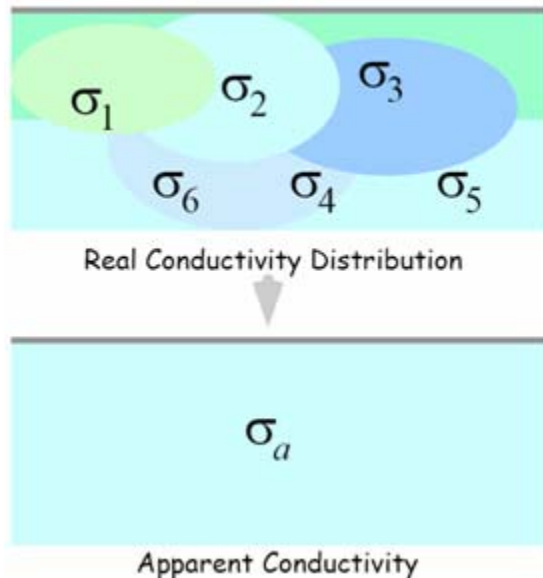
Equation (5.B.1)



Figure 5.B.1: A figure that shows the difference between the apparent conductivity and the real conductivity for the subsurface [2].

The apparent resistivity is the volume average of a heterogeneous half-space, except that the averaging is not arithmetic and dependent on each instrument and how it is used [1].

Moreover, the apparent conductivity can be calculated, which has the exact definition as the apparent resistivity except it represents the conductivity, which is the materials ability to conduct the current flow, (Figure 1). In other words, the apparent resistivity is the inverse of the apparent conductivity and vise versa.

Apparent resistivity plots give an idea about the resistivity/conductivity distribution for the subsurface, thus could be interpreted as geological features. They also could indicate the presence or absence of fluids, since fluids may have a different resistivity/conductivity compared to the background of soil or rocks.

Apparent resistivity will not be the same if we change geometries since the averaging will depend on the distances between the electrodes which are known as electrical arrays. Electrical arrays in resistivity prospecting, the arrangement of electrodes, also called configuration. There are many common arrays to collect the data and each one has its own advantages and disadvantages. In the next section, we will be covering three arrays [1].

## Current Flow in the Earth [4]:

In a homogeneous half-space, a single current electrode placed in the earth results in a hemispherical charge release. In reality this would be an open circuit, but if the second electrode is placed a large distance away current will flow and this model holds to a first order approximation.

Determining current density then becomes the simple problem of dividing the magnitude of the current by the surface area of the sphere where it has spread.

**The Geometric Factor [4]:**

In practice, a DC survey measures the resistance between the two potential electrodes. Knowing the current passing through the ground and the potential at MN provides the total resistance between M and N.

However, this is not a material property and not useful. Knowing the geometry between the four electrodes allows apparent resistivity values to be calculated. Resistivity is a material property and is useful in geophysical interpretations. Converting resistance (R) values to apparent resistivity (ρa) is possible with a relation known as the geometric factor. To derive this we begin with Ohm's law which relates voltage (V), current (I), and resistance (R) as is shown in equation (5.B.2).

*V=IR*                                                                                   Equation (5.B.2)


Alternately, Ohm's law can be written as shown in (5.B.3).

*J=σE*                                                                                 Equation (5.B.3)

In this equation **J** is current density, **E** is the electrical field, and $\sigma$ is conductivity.

**Basic Concepts of the DC Resistivity Arrays:**


1. Schlumberger:

This electrode arrangement used in surface resistivity surveying consists of four collinear electrodes, with the outer two serving as current sources and the inner two which are closely spaced about the midpoint of the outer pair serving as potential-measuring points [1].



Schlumberger array, n>2

Wenner array, n = l
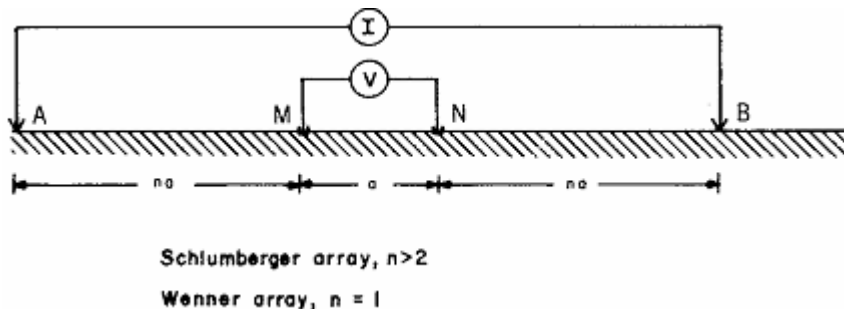
Figure 5.B.2 Schlumberger array set. It takes two current electrodes A and B and two potential electrodes M and N. As we increase the distance between A and B and keep M and N distance constant, then we are increase the current flow which increase the depth of penetration and therefore the depth of investigation [1]. This could be modified to Wenner array by setting the n factor to 1.

## 2. Wenner:

Four equally spaced inline electrodes; either the electrodes are all moved along a traverse or their separation is successively expanded [1].

## 3. Dipole-Dipole:

An array in which one dipole (a pair of electrodes, one positive and one negative) injects current into the ground and the other dipole serves as the potential-measuring pair. The separation between pairs (*na*) is *n* times greater than the separation of the dipole pair (*a.*) The separation is increased to increase the depth of investigation [1].



Dipole-dipole array
Axial dipole array
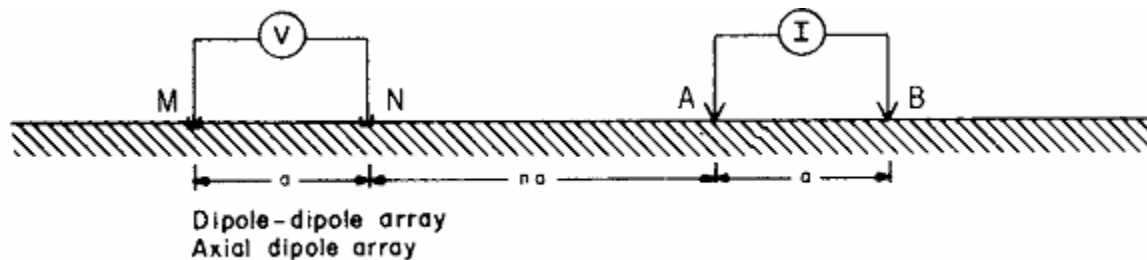
Figure 5.B.3: An example of dipole-dipole array. Here, N factor could be any number except zero[1].

## Survey Design:

All of the DC resistivity sounds were performed on the North Site. The surveyed were carried out on a series of seven lines placed strategically in the area. These lines were used for a multitude of other surveys including Hammer Seismic, GPR, and EM. Diversifying the survey techniques over the same lines allows for cross correlation from method to method to verify data.

The seven lines, orientation and line spacing are listed below and shown on the map in Figure 5.B.4.
**Line 3W:**
N to S, 5m spacing
**Line 3E:**
N to S, 5m spacing
**Line 1**
E to W, 5m spacing
**Line 2:**
N to S, 2 m spacing
**Line 3W**
Schlumberger line – S to N, 5m spacing
**Line 4:**
E to W line, 20 m spacing
**Horseshoe:**
A U-shaped array with 13 stations on each side.

Lines 3W and 3E cross the dry riverbed above the irrigation ditch.   Ideally these lines should show if there is any up-dip groundwater recharge stemming from the irrigation dip.  Line two is located below the irrigation ditch crossing the same dry ditch to characterize the down dip effect.  Lines 2 and 4 run parallel to dip and cross the ditch to characterize the water table in the same manner.
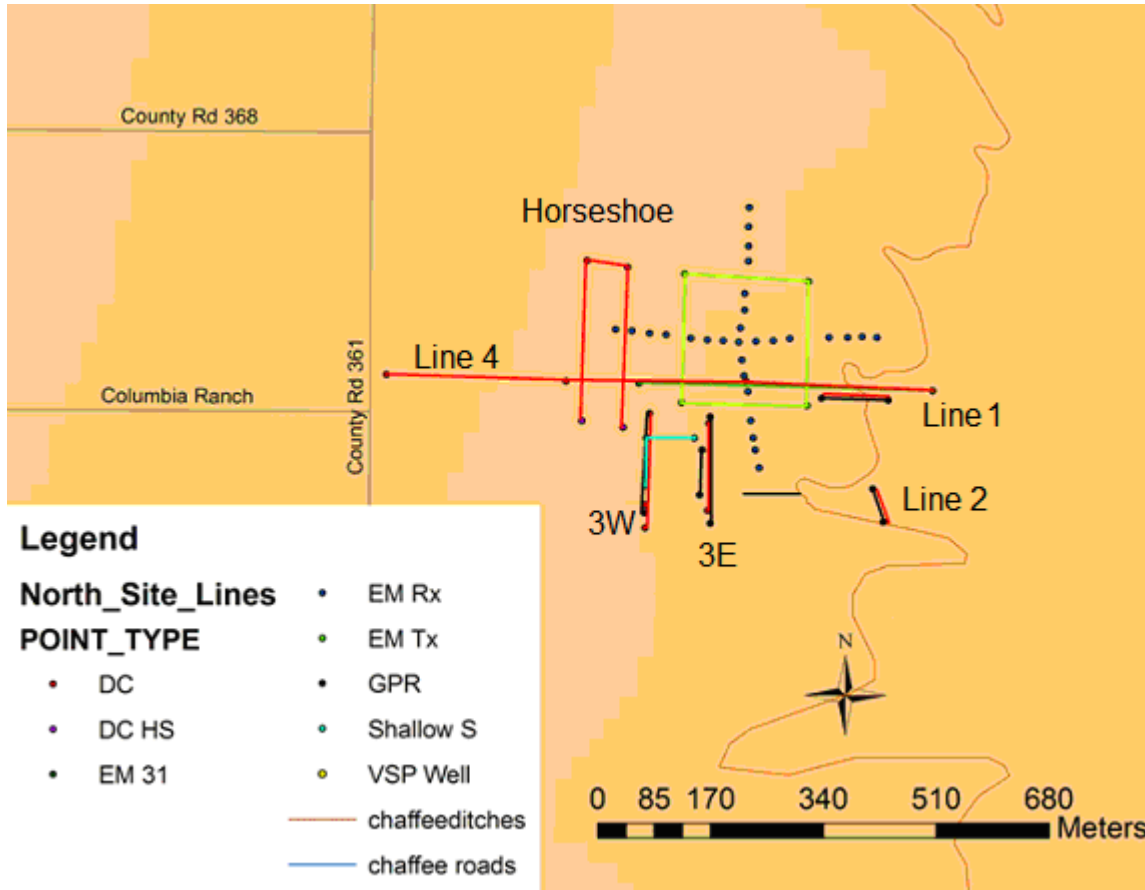


Figure 5.B.4:  A general view map for the location of all the geophysical surveys in the north site. You can see that the DC surveys were sometimes overlapping other methods in order to correlate all the methods together for better understanding of the subsurface.

## Data Analysis and Processing:

I. Data:

After collecting all the data and correlating the dataset to the map, the data was processed. the data set includes the A, B, M and N locations and the array type. Also, it gives a measurement of apparent resistivity and the ratio between the potential difference and the current. Moreover, there is another column for instrument error (Table 1).

**Table 5B.1**

An example of our basic data set as obtained from the Super Sting.

| Ax | Bx | Mx | Nx | V/I | Current(mA) | Rho | Error (%) |
|----|----|----|----|-----|-------------|-----|-----------|
| 5 | 0 | 10 | 15 | 3.1133 | 234 | 293.418 | 0 |
| 5 | 0 | 15 | 20 | 0.6708 | 234 | 252.903 | 0 |
| 5 | 0 | 20 | 25 | 0.2328 | 234 | 219.378 | 0 |
| 5 | 0 | 25 | 30 | 0.1134 | 234 | 213.668 | 0.1 |
| 5 | 0 | 30 | 35 | 0.064 | 234 | 211.195 | 0 |
| 5 | 0 | 35 | 40 | 0.0363 | 234 | 191.73 | 0.2 |
| 5 | 0 | 40 | 45 | 0.0278 | 234 | 220.164 | 0.1 |
| 5 | 0 | 45 | 50 | 0.0168 | 234 | 190.235 | 0.2 |
| 10 | 5 | 15 | 20 | 3.0041 | 223 | 283.131 | 0 |
| 10 | 5 | 20 | 25 | 0.5999 | 223 | 226.163 | 0.2 |
| 10 | 5 | 25 | 30 | 0.2248 | 223 | 211.859 | 0.1 |
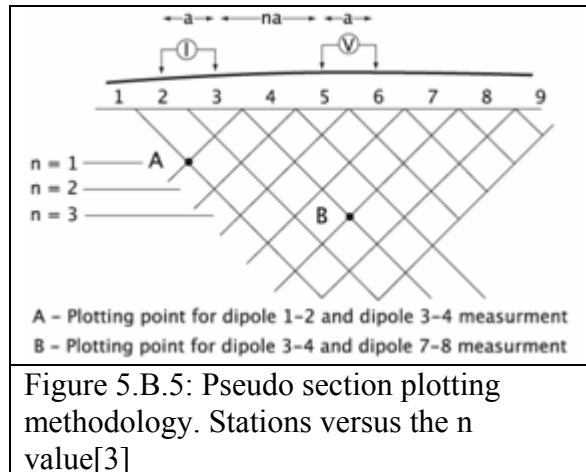


Figure 5.B.5: Pseudo section plotting methodology. Stations versus the n value[3]

The data was plotted using a pseudo section. A Pseudo section is a plot of electrical measurements or calculations, often of apparent resistivity or induced polarization as a function of position and electrode separation, which is a non-linear relation to the depth of investigation. A pseudo section indicates how the parameter varies with location and depth, but it can only be converted into a 2D model by inversion. For the dipole-dipole electrode configuration, the data are plotted beneath the midpoint between the dipoles at a depth of half the distance between the dipole centers. For the Schlumberger array, the data are plotted beneath the potential electrodes at a depth of half the separation of the current electrodes AB/2 [1].

However, the pseudo section does not show a real depth. It is just an arbitrary depth with no relation to the real depth. Therefore, an inversion model is necessary to convert the data to a format in which it can be interpreted. An inversion model is basically deriving from field data a model to describe the subsurface that is consistent with the data, determining the cause from observation of effects [1].

Hence, the inversion model will not be unique and could have different solutions with different parameters and calculation methods. Thus, it will be helpful to have an inversion model that fits our raw data and compare the inversion models to the pseudo sections (See Appendix D for Pseudo Sections).

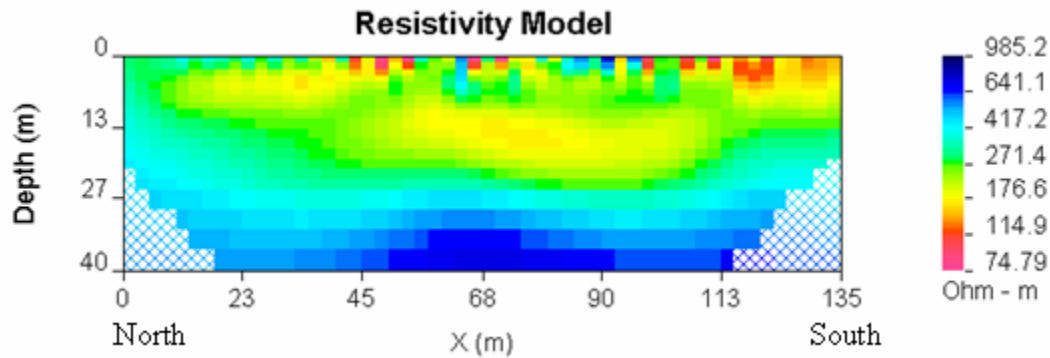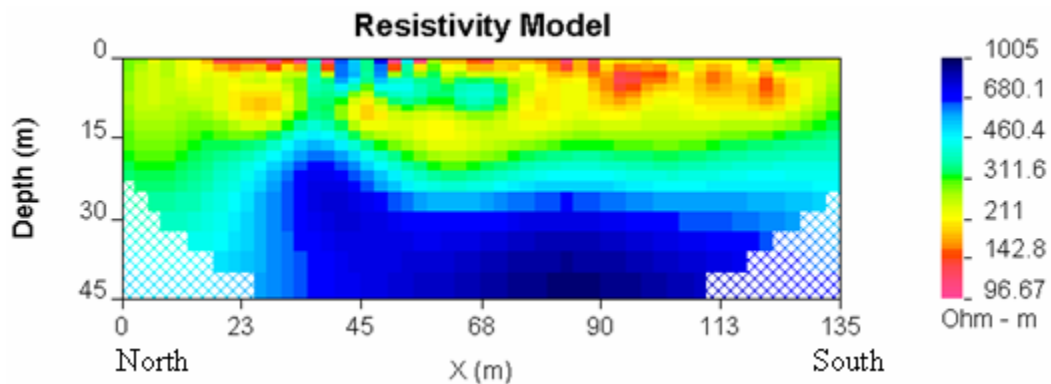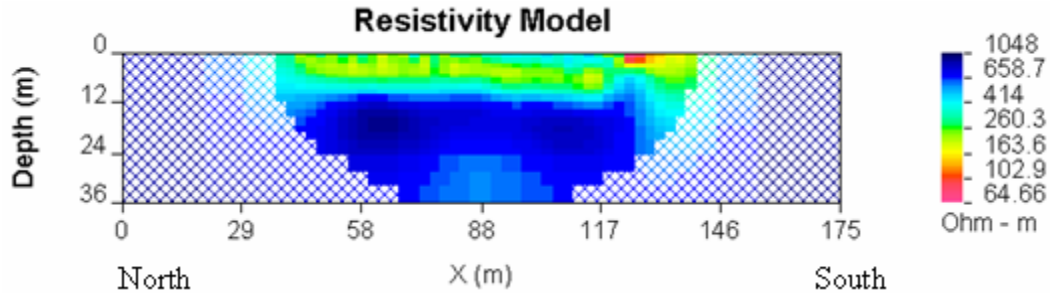## II. Inversions and Interpretations:



Figure 5.B.18:  An inversion model for Line 3W; N to S, 5m spacing. An inversion using two reference models with 1000 ohm-m and 10 ohm-m resistivity compared to each other with 30 iterations and a default chifact. We assumed flat topography and a cutoff value of 0.3.

**Interpretation of Figure 5.B.18:**
The first conductive layer appears close to the surface, (0-3 m) and seems mixed with the second layer. The first layer of low resistivity might be either noise, or rain water drain through the subsurface. In addition, Line 3W runs along two dry gullies, (between stations 3-5 and 7-10) which explains the heterogeneity of the resistivity in the first layer. To conclude, there are three major layers here with different resistivity values.



Figure 5.B.19:  An inversion model for Line 3E; N to S, 5m spacing. An inversion using two reference models with 1000 ohm-m and 10 ohm-m resistivity compared to each other with 30 iterations and a default chifact. We assumed flat topography and a cutoff value of 0.3.

**Interpretation of Figure 5.B.19:**
Line 3E runs along another dry gully between stations 4-8 (20m-40m of the beginning of the line). Since Line 3E runs parallel to Line 3W, we should expect similar geological features. Hence, we can see the three major layers in higher resolution and less noise compared to Line 3W.
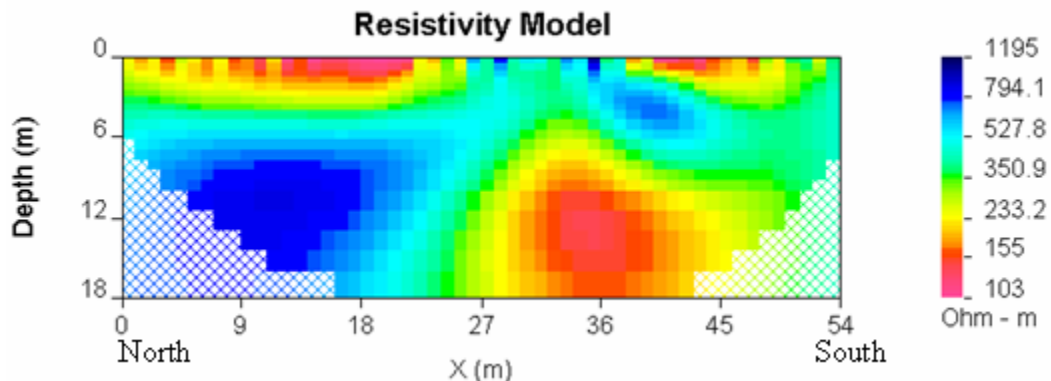
Figure 5.B.20:  An inversion model for Line 1(dipole-dipole); E to W, 5m spacing. An inversion using two reference models with 1000 ohm-m and 10hm.m resistivity compared to each other with 30 iterations, a default chifact. We assumed flat topography and a cutoff value of 0.3.

**Interpretation of Figure 5.B.20:**
Line 1 runs on a ditch but with different orientation compared to other lines. We did this line to help us understand the three dimension image of the subsurface. Here, we can identify the existence of the three major layers with no dipping direction as the previous lines showed too. Third layer might be an impermeable interface controlling the water table taking the fact that we can see the water drainage from the ditch (120m-133m) which has less resistivity value. Possibly that the drainage water could not go beneath this impermeable layer (layer #3, dark blue, 1365-2562 ohms).



Figure 5.B.21
An inversion model for Line 2 (dipole-dipole); N to S, 2m spacing. An inversion using two reference models with 1000 ohm-m and 10 ohm-m resistivity compared to each other with 30 iterations and a default chifact. We assumed flat topography and a cutoff value of 0.3.

**Interpretation of Figure 5.B.21:**
Line 2 runs over a gully which has many pine tries and a small ditch to the south end of the line. Line 2 still shows the same geological features but with more noise where we have three major layers except it shows a break into the layers at 35 m south of the beginning.  The large conductive area at 35 meters is possible a plume of water being fed by the drainage ditch.
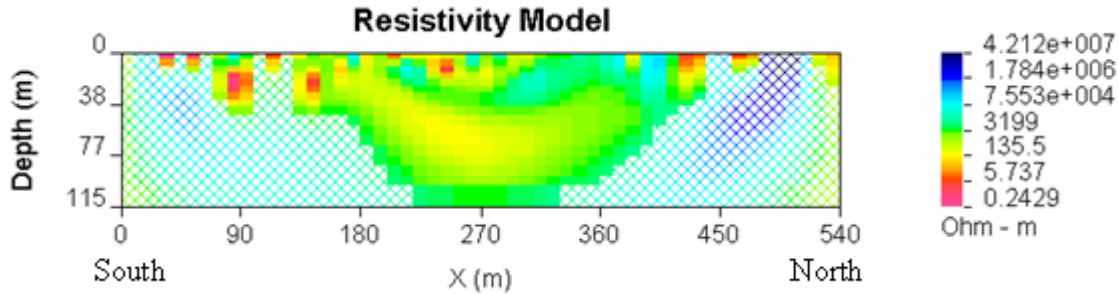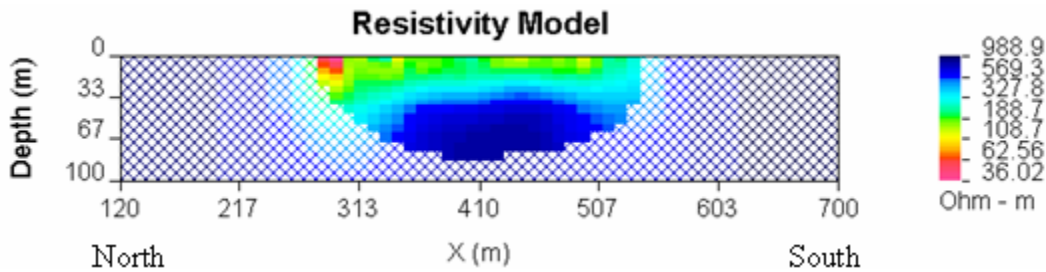
Figure 5.B.22:  An inversion model for the horseshoe array line AB (dipole-dipole). An inversion using two reference models with 1000 ohm-m and 2500 ohm-m resistivity compared to each other with 30 iterations and a default chifact. We assumed flat topography and a cutoff value of 0.3.

**Interpretation of Figure 5.B.22:**
Line AB from the horseshoe array has a greater depth of investigation than other lines and therefore went deeper and lost resolution in the near surface. This result shows two unique features. First, a low resistive body surrounded by higher resistive layers between 200-300 m at 60 m depth. Second, it shows an arc shape highly resistive body around 500m. Since, there is no other evidence to support such a feature this might be explained as noise or error. Noise and error will be discussed later in the section.



Figure 5.B.23:  An inversion model for the horseshoe array line CD (dipole-dipole). An inversion using two reference models with 1000 ohm-m and 10 ohm-m resistivities, compared to each other with 30 iterations and a default chifact. We assumed flat topography and a cutoff value of 0.3.

**Interpretation of Figure 5.B.23:**
Line CD runs parallel to Line AB. This line shows again the three major layers with the ditch anomaly at 290 where you can see a very conductive layer from the surface that extends to around 15m. These high conductive areas could be the water draining from the ditch into the subsurface.  It has also affected the entire resistivity layer to around 80 m depth, where a bowl-shape in the highly resistive third layer can be seen.
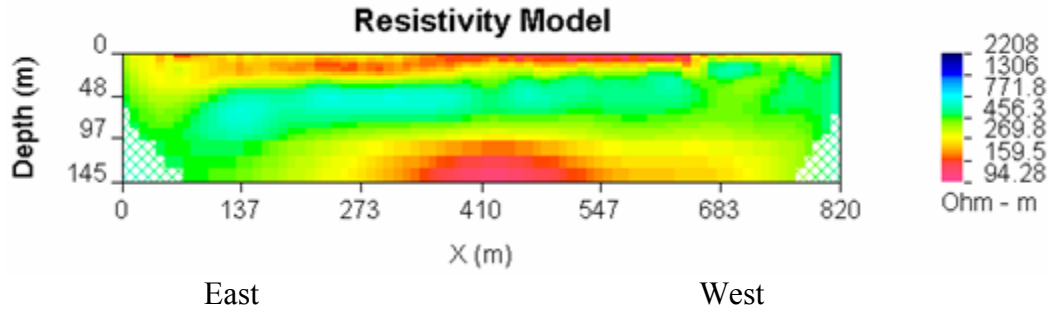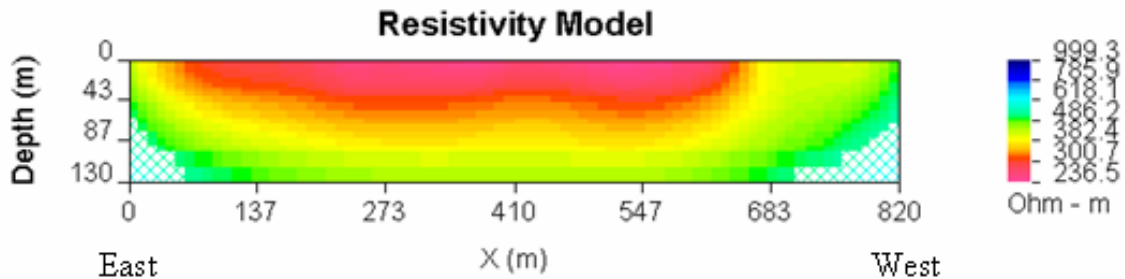
Figure 5.B.24:  An inversion model for Line 4 (dipole-dipole). An inversion using two reference models with 1000 ohm-m and 10 ohm-m resistivity compared to each other with 30 iterations and a default chifact. We assumed flat topography and a cutoff value of 0.3.

**Interpretation of Figure 5.B.24:**

Notice the two highly conductive layers around the resistive package at about 30-50 meters deep. This image shows a clear indication of the aquitard shown in the other surveys.  Also notice that there appears to be some penetration into the resistive layer towards the eastern edge of the image.  This area correlates with where the line crossed the irrigation ditch and shows possible recharge of the system.



Figure 5.B.25:  An inversion model for Line 4 (Wenner). An inversion using two reference models with 1000 ohm-m and 10 ohm-m resistivity compared to each other with 30 iterations and a default chifact. We assumed flat topography and a cutoff value of 0.3.

**Interpretation of Figure 5.B.25:**

This inversion of the Wenner Array data shows a contradictive result to that of figure 5.B.24. One important feature to notice is the small anomaly around 410 meters.  This may correlate to some faulting or small scale facies changes within the area.  This same anomaly can be seen in Figure 5.B.24 in the resistive layer.
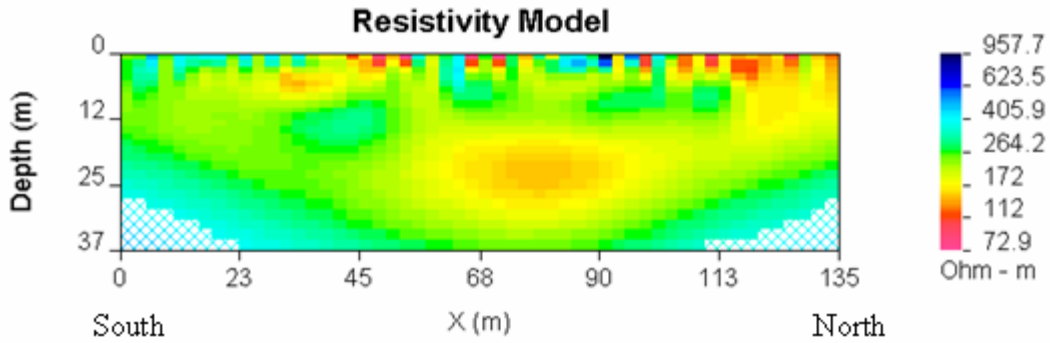
Figure 5.B.26:  An inversion model for the Line 3W; South to North with 5m spacing  (Schlumberger). An inversion using two reference models with 1000 ohm-m and 10ohm-m resistivity compared to each other with 30 iterations and a default chifact. We assumed flat topography and a cutoff value of 0.3.

**Interpretation of Figure 5.B.26:**
This section shows the same feature that Line 2 did. A highly conductive body appears around 114m to 228m depth and from 260m to 570m on the horizontal scale.
Moreover, it does not seem like that there is any fluid drainage to the highly conductive body neither discharging since the body is surrounding by higher resistivity layers (yellow).
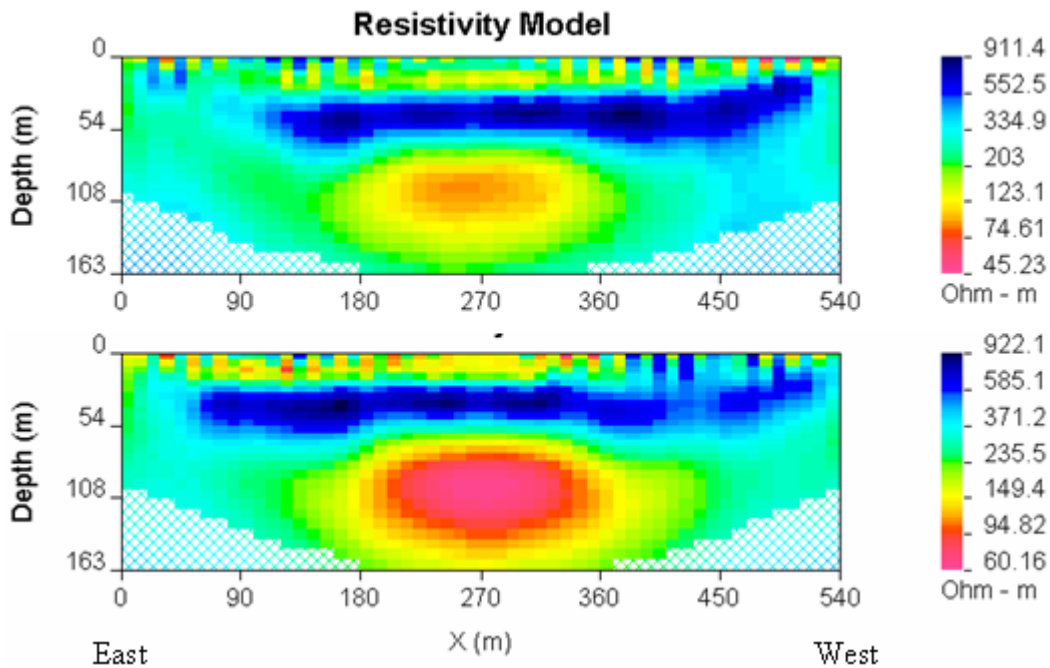


Figure 5.B.27:  An inversion model for the Line 4 (Schlumberger). This inversion is done where the two lines overlapped each other exactly at the middle. So, the last part of the top is the first part of the bottom one. This inversion uses two reference models with 10 ohm-m and 1000 ohm-m compared to each other with 30 iterations and a default chifact. We assumed flat topography and a cutoff value of 0.3.

**Interpretation of Figure 5.B.27:**

Top model: Line 4, which runs on the ditch around 450m from the beginning, shows the same feather as Line 2. A highly conductive body appears around 114m to 228m depth. It also shows a resistive layer (light blue) below a conductive layer (yellow) between 50-70 m down from the surface. The yellow layer might be the water table which could not go beneath an impermeable resistive layer. This figure also shows another interesting feature, a fourth resistive layer (dark blue) that appears between 120m and 420m around 70-80 m depth in the middle of the second layer. This layer has a resistivity value between 1000-1200 ohms and it is surrounded by less resistive layers (500-700) ohms.

Moreover, it does not seem like that there is any fluid drainage to the highly conductive body neither discharging. Moreover, it does not seem like that there is any fluid drainage to the highly conductive body discharging since the body is surrounding by higher resistivity layers (yellow). The bottom model in (Figure 5.B.28) Line 4 which runs on the ditch around 150 m from the beginning shows the same feather that Line 2 did. A highly conductive body appears around 100m to 150m depth and from 150m to 390m on the horizontal scale.)
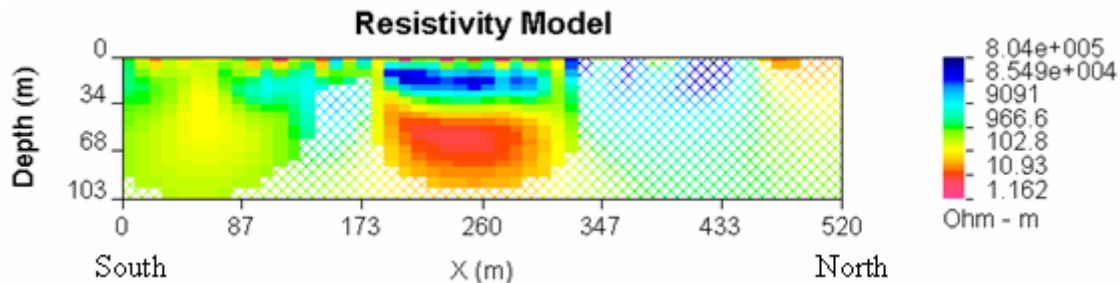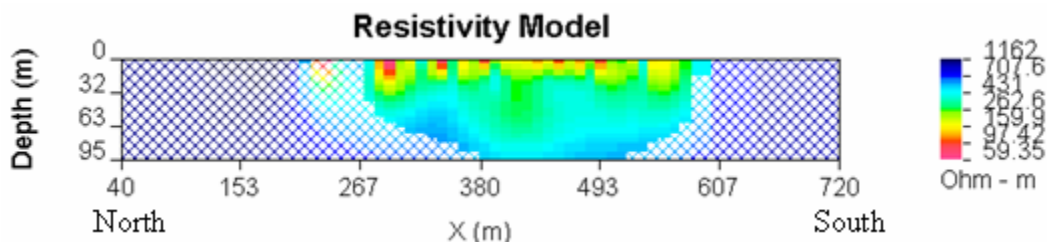


Figure 5.B.28: An inversion model for the horseshoe array Line AB (Schlumberger) using two reference models with 1000 ohm-m and 10 ohm-m compared to each other with 30 iterations and a default chifact. . We assumed flat topography and a cutoff value of 0.3.



Figure 5.B.29: An inversion model for the horseshoe array Line CD (Schlumberger) using two reference models with 1000 ohm-m and 10 ohm-m compared to each other with 30 iterations and a default chifact. We assumed flat topography and a cutoff value of 0.3.

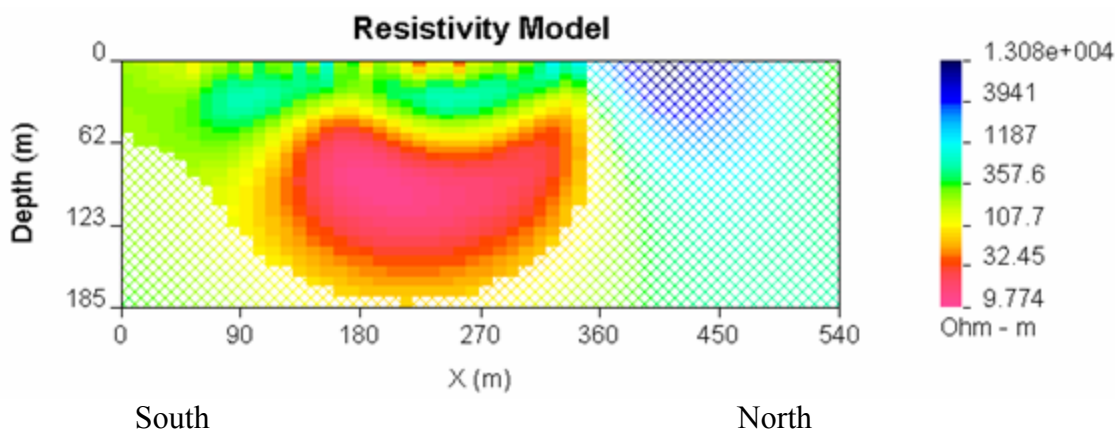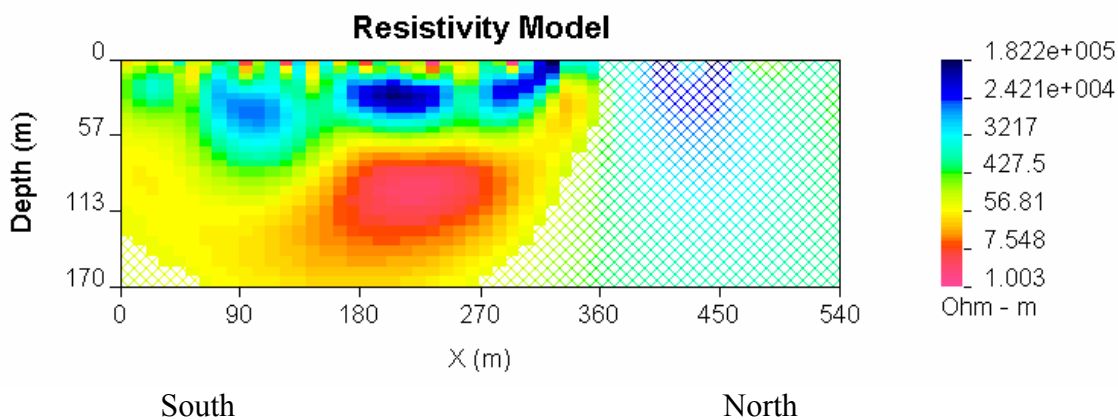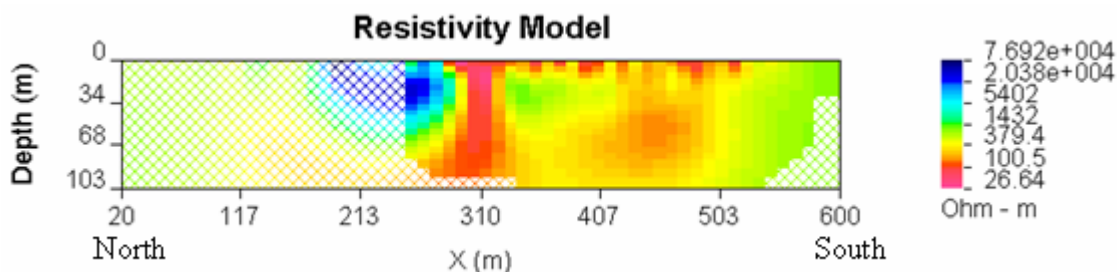South                                                    North

Figure 5.B.30:  An inversion model for the horseshoe array Line AB (Inverse Schlumberger) using two reference models with 1000 ohm-m and 10 ohm-m compared to each other with 30 iterations and a default chifact. We assumed flat topography and a cutoff value of 0.3.

South                                                    North

Figure 5.B.31:  An inversion model for the horseshoe array Line AB (Wenner) using two reference models with 1000 ohm-m and 2500 ohm-m compared to each other with 30 iterations and a default chifact. We assumed flat topography and a cutoff value of 0.3.

North                                                    South

Figure 5.B.32:  An inversion model for the horseshoe array Line CD (Wenner) using two reference models with 1000 ohm-m and 2500 ohm-m compared to each other with 30 iterations and a default chifact. We assumed flat topography and a cutoff value of 0.3.

## Error Analysis:

In DC surveys, there are three major sources of errors, field errors, human errors and processing errors. Field errors include lack of coupling between the electrodes and the ground, power lines and surveying errors. We assumed flat topography and most cases were running over ditches and non-flat topography.

Human errors are about the way the field's notes were taken. Field notes were quite messy and most of handheld GPS readings were missing. Moreover, orientations were not accurate in most cases but we solve that by comparing the anomaly to known surface anomalies such as the ditch. Processing errors go into the inversion assumption. It also carries all errors from the field and accumulates the error during the inversion. Our inversion models were doubled checked with the pseudo sections with 30 iterations to make sure that the inversion is correct. However, we will be getting different inversion models as we keep using different reference models and cutoff value.

## Conclusion:

The data collected using DC methods came out noisy in parts. However, similar anomalies were detected using multiple methods and on multiple lines which increases the confidence interval on the results. A highly resistive impermeable layer dipping to the west side between 45-70 m deep, and about 60m thick is apparent in many of the sections. Correlating DC resistivity with EM-31, it was found that the irrigational ditches do not penetrate deeper than 30 meters due to the impermeable layer.   Also, a highly conductive anomaly deep around 108m shows promise for deeper groundwater in the area, the recharge capabilities of which are hard to distinguish at this time.  Overall the near surface DC soundings at the North Site have proved invaluable to the understanding of the groundwater characteristics and will contribute greatly to the overall interpretation in the area.

## *Electromagnetics*

## Introduction

The geophysical method of using electromagnetics to image the subsurface was employed at the North Site in several distinct locations.  These included multiple survey lines and a large, 2D grid.  There were two different EM methods drawn on at the 2007 field camp experience:  Time-Domain and Frequency-Domain.  The Time Domain EM (TDEM) method's investigation used the 2D grid, taking measurements at many points disseminating from the center of the grid outward in all four cardinal directions with respect to the grid's parameters.  The Frequency Domain EM (FDEM) method was applied to neighboring survey lines.  These survey lines had already been examined by another technique previously mentioned, the DC-Resistivity method. This was done with the purpose of comparing data interpretations from both methods for quality control as well as attaining a more complete and thorough subsurface picture.

## Time Domain EM

## Background

The foundational principle behind the TDEM method is Faraday's Law of Induction. Time-variant current flows through a transmitter coil placed on the ground with alternating periods when the current is "on" or "off". Shutting "off" the current does not occur instantaneously, but over a slight time interval (on the order of milliseconds), called the ramp time, which induces a time-variant magnetic field [1]. This magnetic field, in turn by Faraday's Law of Induction, induces a current, called the induced (secondary) current which, by the same principle, induces a second, time-variant magnetic field. It is exactly the time-varying nature of this induced current and its secondary magnetic field that provides the basis for TDEM. Any change seen in the induced current will be seen correspondingly in the secondary magnetic field. This induced current propagates through the subsurface as a smoke ring would disseminate through air. Please see Figure 1. How quickly this induced current (smoke ring) diffuses down and outward in the subsurface depends on the conductive or resistive nature of the subsurface layers. The induced current will spend more time in a conductive layer, sandstone containing conductive pore fluids, and less time in a resistive layer, shale with minimal porosity and permeability. By measuring the corresponding changes of its magnetic field with respect to time, one may deduce an approximate idea of how the subsurface is layered with respect to each layer's conductivity/resistivity.

TDEM is an effective method for a geophysical subsurface investigation when the desired depth of study requires only the dimensions of the transmitter coil. The larger the transmitter coil, the larger the depth of investigation. However, as size increases, resolution by corresponding fashion tends to decrease. Additional, one may increase the depth of investigation by increasing the pre-set ramp time as greater ramp times will see greater successive depths being penetrated by the induced current.
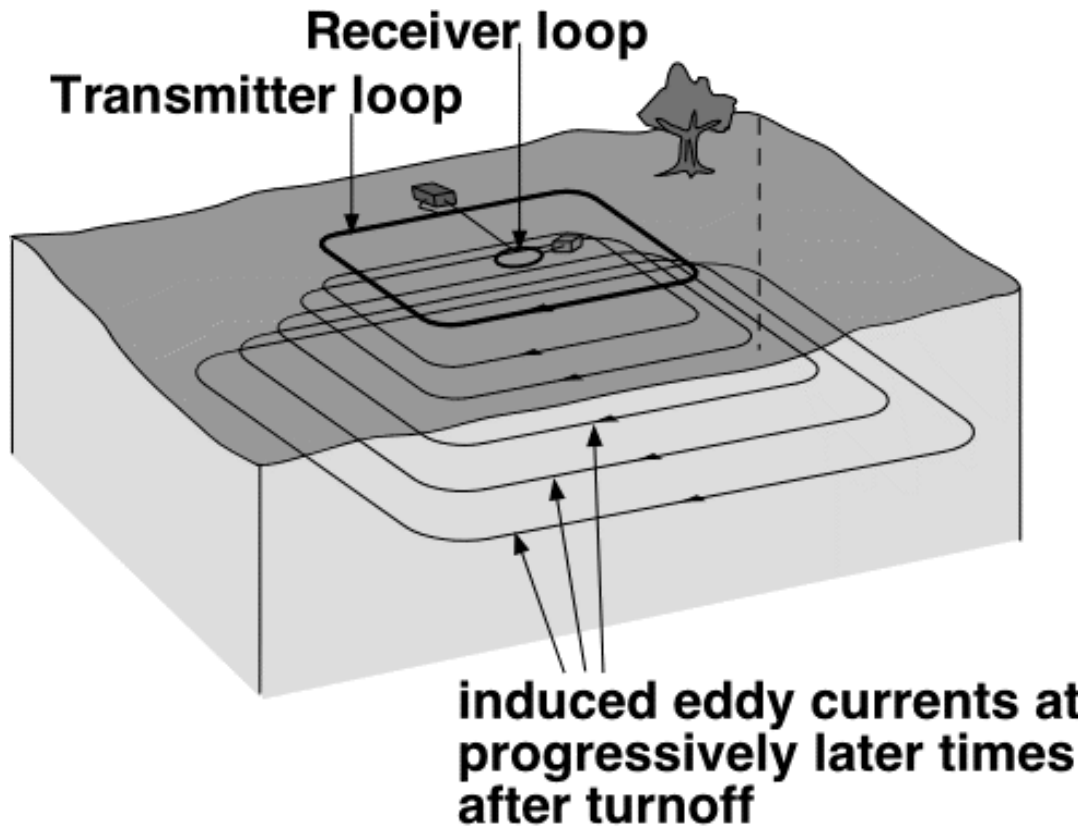
Figure 5.C.1:  Schematic of "smoke-ring" concept [1]


## Survey Design and Implementation

TDEM was handled with the EM 57 instrument, incorporating a transmitter coil attached to its associated transmitter box and a receiver coil attached to a Protem digital receiver.  The transmitter and digital receiver work in synchronization using a quartz crystal in each device for accuracy.  For power, the transmitter utilized a generator while the receiver exploited several batteries.  The transmitter coil was laid out with dimensions of 200m by 200m; the receiver coil's effective area was 100 m$^2$.  The transmitter coil was square in shape with sides oriented north-south and east-west.

As previously mentioned data stations, with a station spacing of 25m, were located starting at the coil's center and diffusing outward in all principle directions so that two distinct lines intersected each other at the loop's center and also intersected the midpoints of the loop's sides.  Each survey line had three data stations inside the loop on either side of the loop's center as well as four stations outside the loop on either side.  In all, 29 data stations, center loop included, were incorporated in the EM57 survey.  Please see Figure 2 for comparison.  At each data station, a measurement in the change of the secondary magnetic field was made for each Cartesian component.  Also, additional measurements were made for each component at a variety of data stations as a check for the accuracy of the instrumentation and crystal synchronization.

Figure 5.C.2:  Survey Layout for EM57

## Data Processing

The recorded time domain EM data consisted of 29 receiver loop locations.  Each receiver location contained three components, X, Y, and Z measurements (the receiver loop was held at three different orientations).   Each component consisted of 20 voltage measurements taken at known times after the primary field was shut off.   Each of these 20 voltage versus time measurements was repeated 5 times.  These 5 records were averaged to give 20 voltage versus time measurements per component per receiver loop location.

Each voltage measurement was then converted to $\dfrac{dB}{dt}$, the time derivative of the magnetic field, using the equation:

$$\frac{dB}{dt} = 19.200V(\frac{I}{2^n Rx_a})$$

V: Geonics download number

$Rx_a$: Effective receiver coil area (100 m$^2$)

I: Transmitter current in Amp

n: Gain number

This equation gives $\frac{dB}{dt}$ in $\mu$ V/m$^2$.

After the data was converted to $\frac{dB}{dt}$ format, it became apparent that there was some problems. First, the data was horizontally inconsistent. Data recorded at adjacent receiver loop locations was different by several orders of magnitude in many cases. The values also changed from negative to positive at many unexpected locations. (See Figure 5.C.3.) This prevented us from reliably determining the horizontal variations in the $\frac{dB}{dt}$ decay. Also, the data was inconsistent between measurements taken at the same station. Figure 5.C.4 shows the decay curves for two Z component soundings taken at the center of the Transmitter loop. These measurements were taken on different days. These curves are different in both shape and magnitude
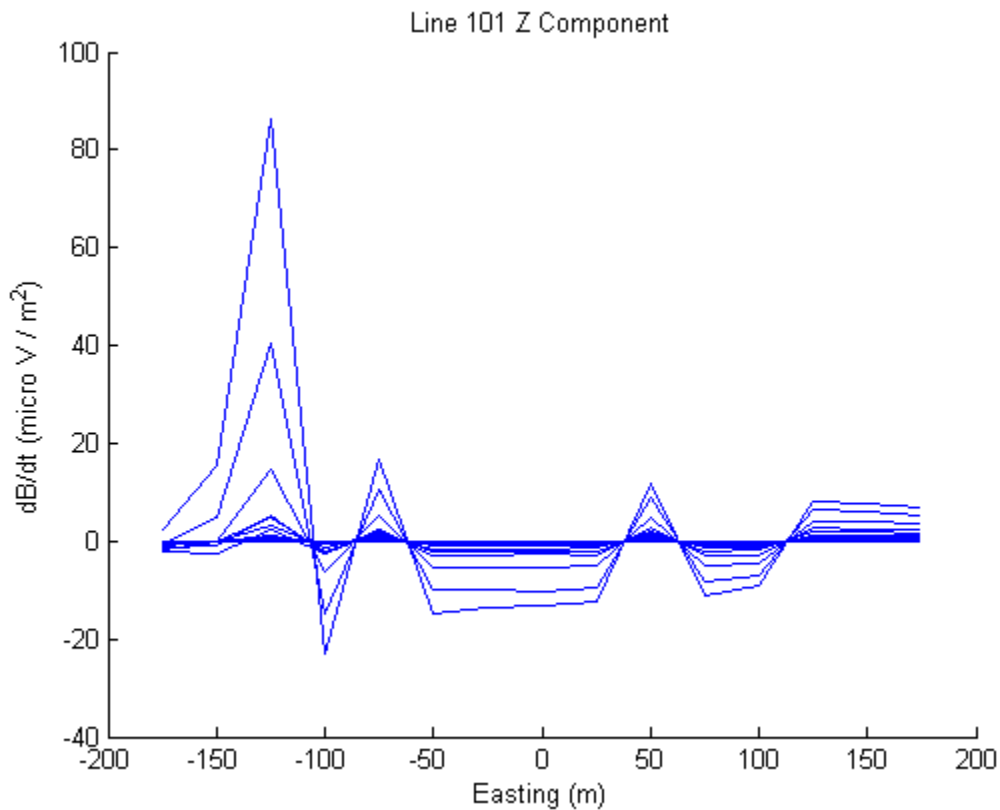


Figure 5.C.3 This figure shows the Z component of $\frac{dB}{dt}$ versus horizontal location. Each line represents measurements taken at different time gates.
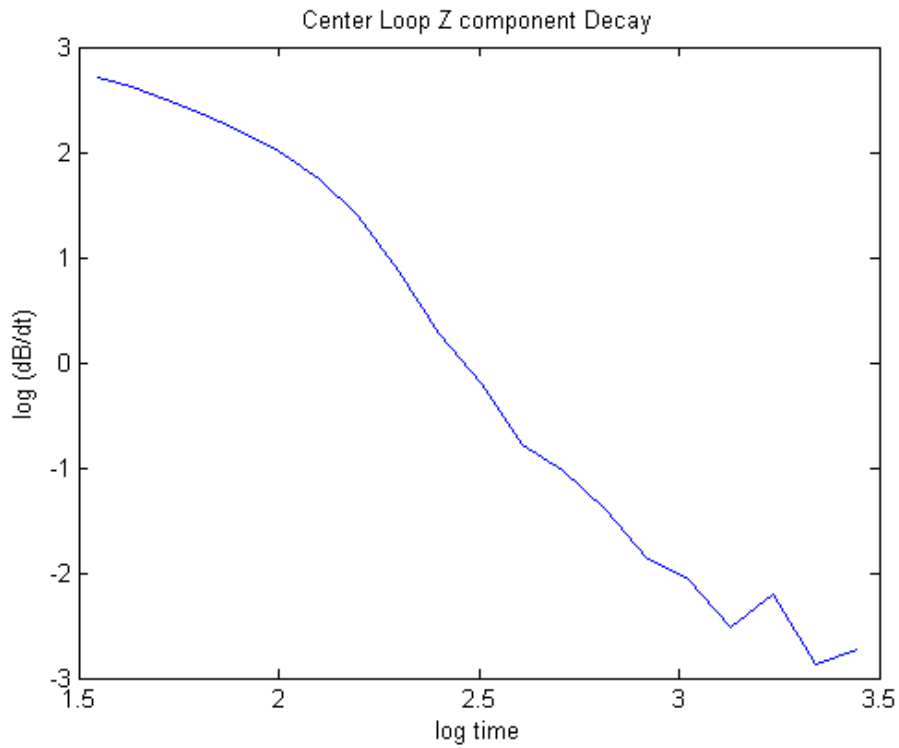
a.)
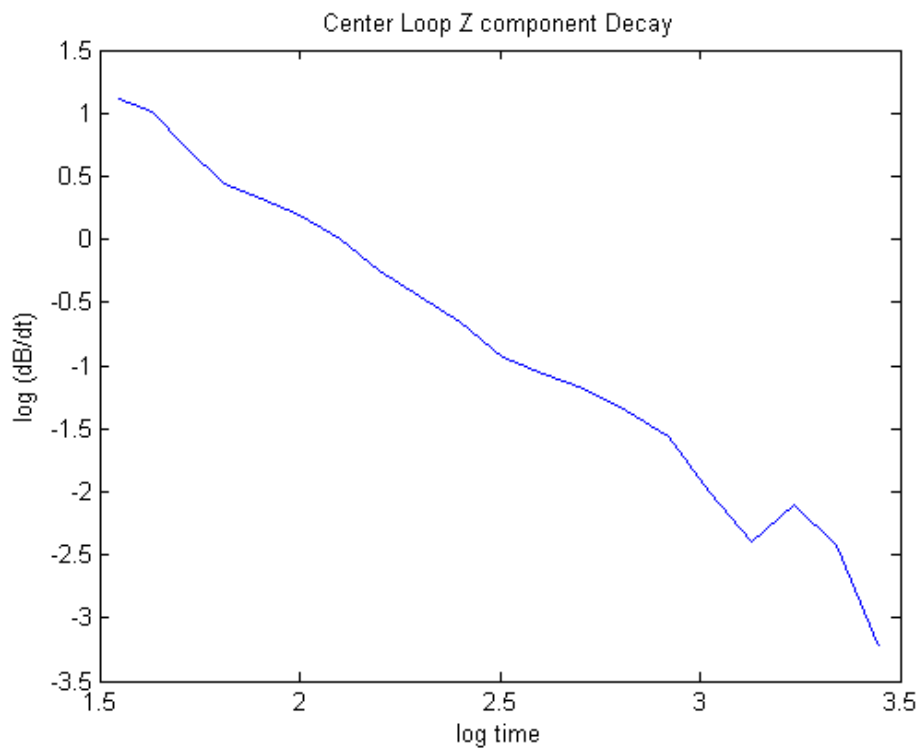


b.)

Figure 5.C.4 Figure 4 shows the decay curves for two Z component soundings taken at the center of the Transmitter loop plotted on log-log scale.  These measurements were taken on different days.

Figure 5.C.4B shows a linear decay on the log-log scale. This is characteristic of horizontal subsurface layers. Figure 5.C.4A shows a curve that could be the superposition of an exponential and linear decay on the log-log scale. This is characteristic of horizontal layers and confined conductors. It was determined that the data shown in figure 5.C.4A was of better quality by Dr. Yaoguo Li, Center for Gravity, Electrical, and Magnetic Studies at CSM.

A 1D inversion was attempted on the central loop sounding data shown in figure 4A using IX1D (inversion software from Interpex). However, we were unable to produce a subsurface conductivity model that would accurately fit the data. IX1D was then used to forward model the $dB/dt$ decay curve (a three-layer conductivity model) using depth and conductivity values determined through the DC resistivity inversions. The results did not match the observed data. This is shown in figure 5.C.5.
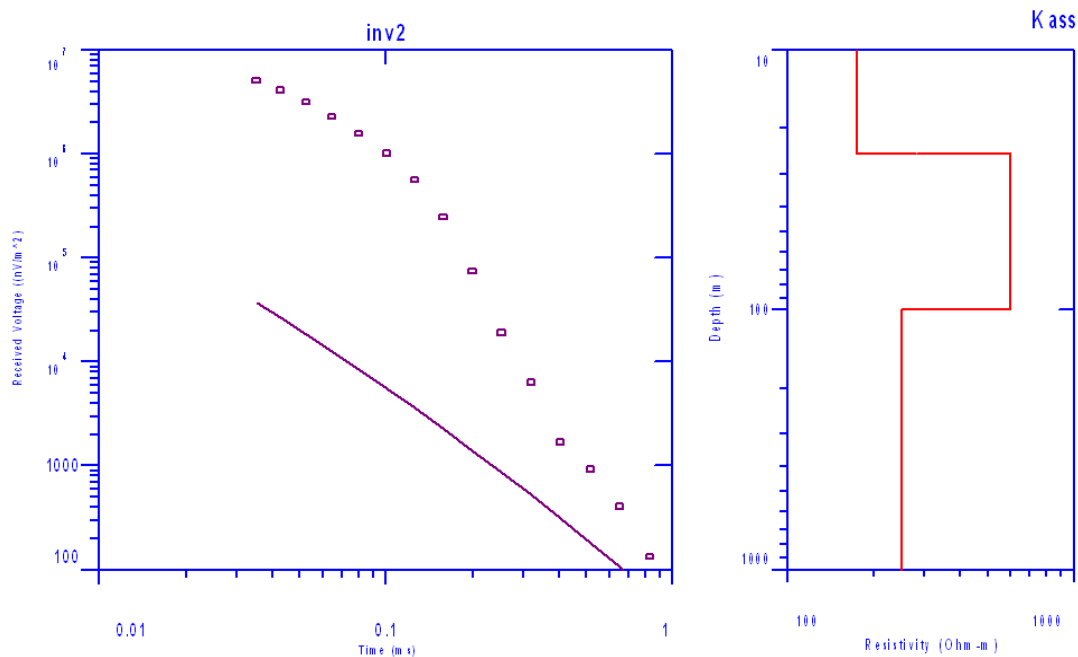


Figure 5.C.5 Figure 5.C.5 shows the forward model of the $\frac{dB}{dt}$ decay curve) a three-layer conductivity model) using depth and conductivity values determined through the DC resistivity inversions. The plot on the right shows the subsurface conductivity model. It plots resistivity (inverse of conductivity) versus depth. The plot on the left shows $\frac{dB}{dt}$ versus time after the primary field is shut off. The solid purple line is the decay expected for the conductivity model shown on the right. The purple squares show the observed data points.

Interpretations

Since the data was so inconsistent, it was hard to form interpretations from it. The data was not repeatable so any interpretation would be unreliable. For these reasons we have decided not to base any of the North site interpretations on the EM57 data.

Error

The EM57 data was inconsistent and unrepeatable to the point that no reasonable interpretations could be made. We are not certain what caused these problems. One possible source of error could be the transmitter coil leaking current into the ground. If the transmitter coil is not well insulated, some of the current can flow into the subsurface and interfere with the voltage measurements. This was observed at least once in the field. It is also possible that the instrument was not taking readings properly. Also measurements were taken by different people who may have used different techniques. This could have influenced the measurements, but not to the level of inconsistency that was observed in the data.

**Frequency Domain EM**

Introduction

In order to confirm the results from the DC resistivity surveys along the North Site lines, conductivity values were measured using frequency domain electro-magnetics. By having redundant data sets produced from different techniques, the idea is that the independent data sets should confirm each other and form the basis for a corroborated interpretation of the subsurface resistivity structure.

Background: EM31

Using an EM31, data was collected along four of the DC resistivity survey lines. The EM31 is a frequency-domain electro-magnetic induction instrument for measuring ground conductivities. It functions by producing a primary magnetic field of constant frequency at the transmitter dipole (TX) located at one end of the instrument. The instrument then measures the secondary magnetic field produced by eddy currents induced in the conductive ground by using a receiver coil (RX) at the opposite end of the instrument. The primary EM wave from the transmitter and the secondary EM waves produced by the eddy currents are separated by a phase lag. Using this lag, the secondary waves can be isolated and decomposed into real and imaginary parts according to Euler's Theorem. The quadrature, which is the imaginary term of the secondary wave, is proportional to the conductivity of the subsurface. Therefore, the EM31 can be calibrated to yield

the bulk conductivity of a surveyed area. The depth of investigation for the EM31 is about six meters, so its application is mainly in near surface geophysics.

## Results/ Interpretation/Error Analysis

The results from the surveyed lines are of mixed quality. Because of device malfunctions and inadequate data for some survey marker positions, the only recoverable data is from the North Site Line 4. Figure 5.C.6 shows the plot of the apparent conductivity across the survey line. The step function appearance of the survey line profile is due to an instrument quantization error. However, the long wavelength features are deemed reliable. The far East end of the line shows a relatively low conductivity of approximately 11 mS/m. This is likely due to its close proximity to the poorly conductive water in the irrigation ditch. The irrigation ditch has a conductivity of a mere 9.6 mS/m. The conductivity in the irrigation ditch is low due to a lack of dissolved solids. Having low dissolved solids means the water is insufficiently saturated with ions to behave as a good electrolyte. The water in the irrigation ditch was discovered to have a total dissolved solids (TDS) count of 0.062 g/L. By comparison, ocean water typically has a TDS count of approximately 30-35 g/L.
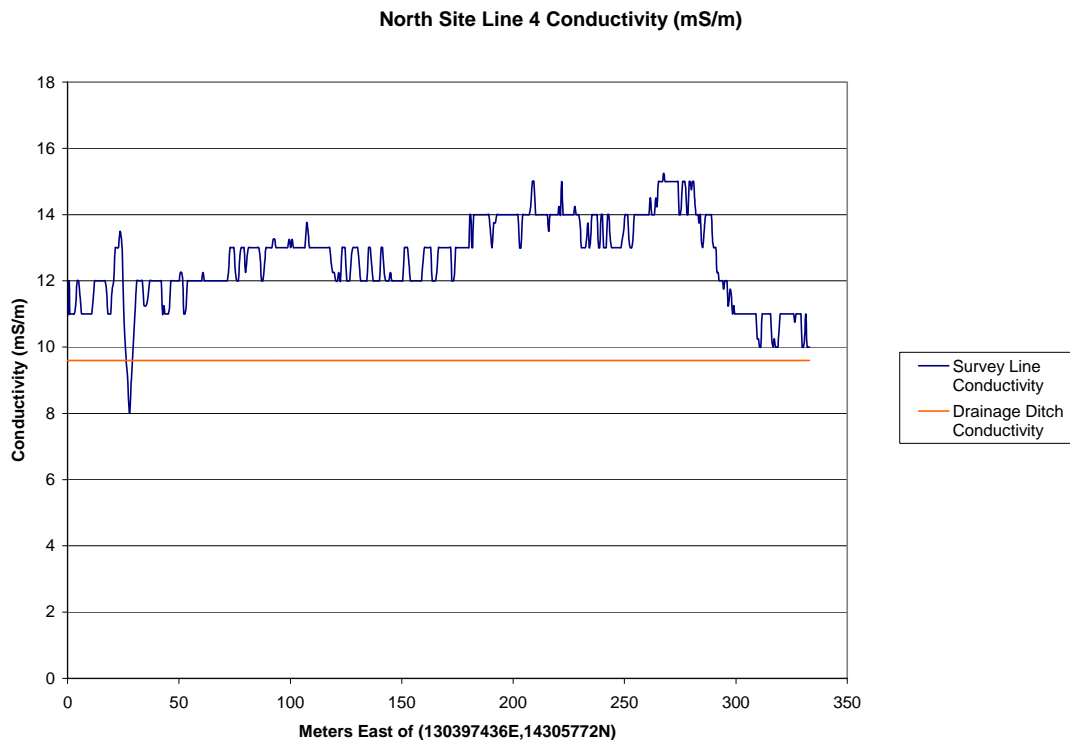


Figure 5.C.6: Plot of conductivity of North Site Line 4 compared to the conductivity of the irrigation ditch. The step function appearance of the survey line profile is due to malfunctioning of the EM31, however the trend of the conductivity values is reproducible and supported by the DC resistivity data. Note that the irrigation ditch would appear approximately 5 m East of the far East end of the figure.

The correlation between dissolved solids and conductivity might explain the shape of the plot in figure 5.C.6. While very close to the irrigation ditch, the measured conductivity is low probably because of high concentration of poorly conductive ditch water.  As the water diffuses slightly farther from the ditch, it gains ions along the way and causes the spike in conductivity seen at approximately 275 m along the line. As distance from the irrigation ditch increases further, the concentration of water from the irrigation ditch becomes lower, and corresponds to the slope of the conductivity trend.

## Conclusions

The results from the EM31 are in excellent agreement with the results from the DC resistivity surveys. Figure 5.C.7 shows that the inversion model from the dipole-dipole DC resistivity survey behaves exactly as would be expected from the conductivity values measured by the EM31. This reinforces the interpretation that water from the ditch is leaking, at least into the near subsurface. Figure 5.C.8 shows the full inversion model from the dipole-dipole DC resistivity survey along North Site Line 4. This model clearly reveals a conductive region near the surface that correlates well with the leaking irrigation ditch water. However, the presence of a large aquitard located at approximately 50-100 m depth appears to prevent the irrigation ditch water from penetrating to the deeper ground water, at least along North Site Line 4 where the data was recorded. This would suggest that though the irrigation ditch is leaking, it may not be charging the deeper subsurface aquifer.

Figure 5.C.7: North Site Line 4 plot of conductivity values from EM31 compared to the resistivity model from the inversion of Dipole-Dipole DC resistivity data.  The conductivity of the irrigation ditch water was discovered to be 9.6 mS/m, which is equivalent to 104.2 Ohm-m.

Figure 5.C.8: North Site Line 4 resistivity model from inversion of Dipole-Dipole DC resistivity data. Note that the irrigation ditch water is restricted to the top 30 m of the subsurface and does not appear to penetrate the large aquitard that separates the surface from deep ground water.

## *Ground Penetrating Radar*

## Background

Ground penetrating radar is a geophysical tool used to image the shallow subsurface. A transmitter emits an electromagnetic pulse—light wave—into the ground via an antenna. A second antenna is used to receive the signal. The wave travels at different velocities through different materials. When the wave encounters changes in dielectric permittivity, the wave is divided into a part that is reflected and a part that is refracted and a part that is transmitted. By stacking the signals returned to the receiver, an image of the subsurface can be produced. The depth that radar can image is influenced by the materials in the ground as well as the frequency of the signal. The higher the frequency, the shorter the wavelength, and the quicker the signal is attenuated.

## Survey Design

Two types of ground penetrating radar surveys were performed at the North Site. The first is a common offset survey. Lines 1, 2, 3E, and 3W were surveyed using common offset GPR. In a common offset survey, the transmitter and receiver are a constant distance apart. The transmitter sends a pulse every 0.5 seconds. Meanwhile, the antennas are moved together at a constant speed so the trace spacing can be determined during processing. This type of survey is beneficial for quick acquisition to get an idea of the subsurface. Unfortunately, since there is only one offset, subsurface radar velocities cannot be determined, and therefore neither can material properties.

In addition to the common offset surveys, two multi-offset surveys were conducted to help constrain the velocities of the reflectors seen in the data. One line ran parallel to and located between 3E and 3W, while the other ran perpendicular to and east of line 3E.

All surveys used Sensors & Software's PulseEkko 100A system with specially designed 50 MHz resistively loaded antennas. The survey parameters are listed in table 5.D.1

Table 5.D.1:  GPR Parameters

| Survey | Common Offset | Multi-offset |
|---|---|---|
| System | Sensors & Software PulseEkko 100A | |
| Transmitter Voltage (V) | 400 | 400 |
| Frequency (MHz) | 50 | 50 |
| Source-receiver offset (m) | 2 | 2 – 10.5 |
| Sampling interval (ns) | 1.6 | 1.6 |
| Stacking | 16 | 16 |
| Inline receiver spacing (m) | ~ .3 | .5 |
| Transmitter spacing (m) | ~ .3 | 1 |
| # Receivers per transmitter position | 1 | 18 |

## Processing

Both types of surveys are pre-processed the same way in Matlab. First the signal is dewowed to remove the low frequency part of the signal. Next, the t-zeros are aligned for all the traces. Then a power gain is applied and the background noise is removed. Finally, the data is transferred to ProMAX for further analysis. In ProMAX the surveys are corrected for elevation statics. A velocity analysis may then be performed on the multi-offset surveys to determine material properties. In the case of the GPR lines that were acquired, however, the geometries are not accurate in the header data so neither the elevation statics nor the velocity analysis could be completed.
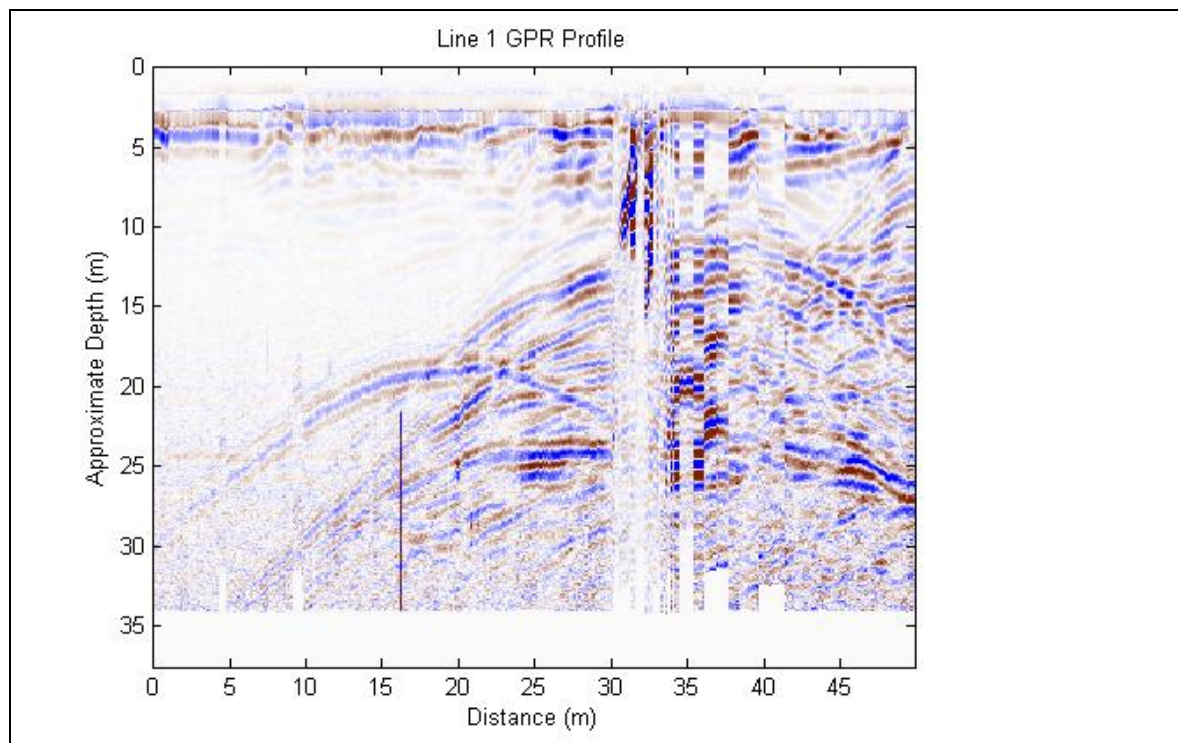


Figure 5.D.2: In Line 1, the noise seen in the data 30 m along the line is caused by the antennas being lifted off the ground while passing over the irrigation ditch. The reflection at 25 m depth correlates well with the other GPR surveys in the area as well as other surveys over the same line. This is interpreted as the upper boundary of the aquitard separating the near surface water from the deeper aquifer.
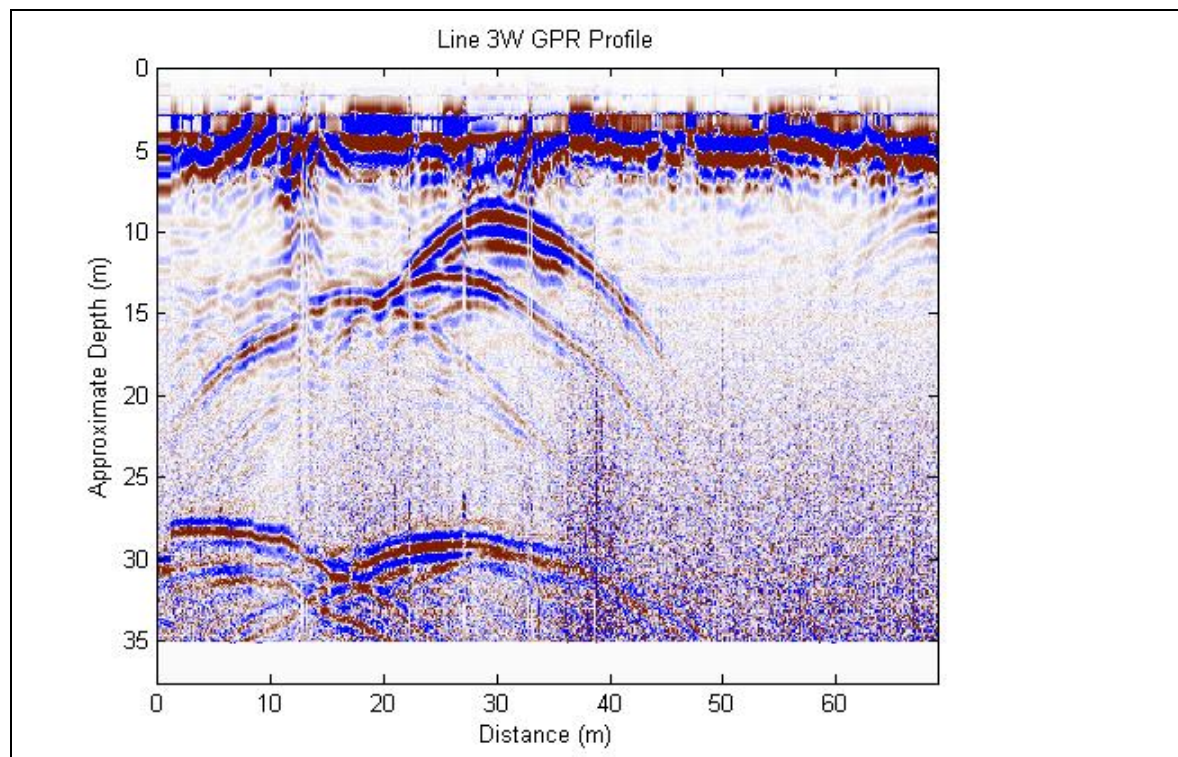
Figure 5.D.3: In Line 3W, the prominent diffractions between the depths of 10 and 15 m are likely from the walls of the ditch.  The diffractions at 30 m depth are not in the correct location to have been caused by any surface features. Because they correlate well with location of the upper aquitard boundary as seen in the DC Resistivity data, it is interpreted that the diffractions represent this same feature.
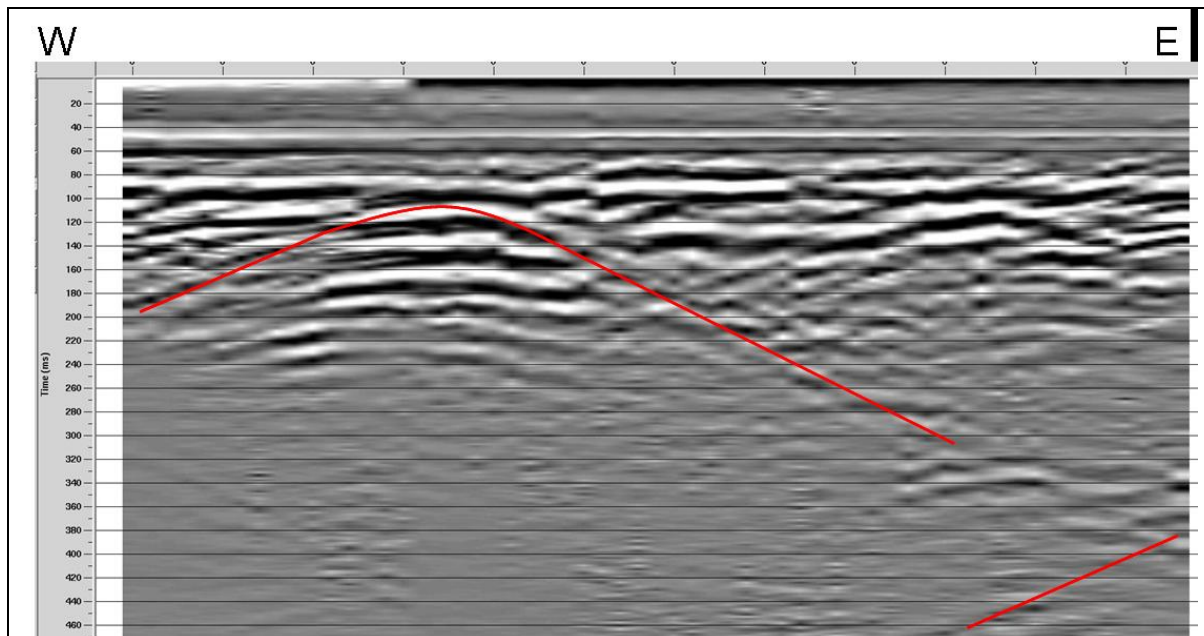
Figure 5.D.4: GPR line running from approximately 5 m east of Line 3E towards the irrigation ditch.  There are two interesting features in this profile.  The first is the large diffraction with the vertex at 100 ms.  This cannot be attributed to any surface effects.  Also, there is a west dipping reflector on the east side of the profile that likely relates to the aquitard boundary in the DC resistivity data.

## Interpretation

Interesting reflectors, though little is known without velocities.  Most of the interesting diffractions are results of the ditch walls, a velocity analysis would likely show the velocity of the diffraction roughly equal to the velocity of light through air.  The other prominent reflections are all around 30 m deep.  Since a velocity analysis was not available this is interpreted to be the upper boundary of the aquatard based on the interpretation of other methods.

## Error Analysis

The most significant source of error would be the position control of the surveys.  Since an odometer wheel was not available, the transmitter had to be triggered at constant time intervals while the cart was pulled at an approximately constant speed.  The trace spacing was then determined by dividing the total distance by the number of traces.

Another source of error influenced the processing and interpretation of the data.  The geometries did not integrate smoothly into ProMAX, and so elevation statics corrections could not be made.  More information could be gained by determining the velocities of the materials in the subsurface, however the velocity analysis module in ProMAX was not working.

*Shallow Seismic*

## Refraction Seismic Theory

The seismic refraction method is based on the measurement of the travel time of seismic waves refracted at critical angles through the interface between subsurface layers of different velocity. Acoustic energy is sent into the subsurface by a source on the surface. For shallow applications this source is generally provided by a hammer and plate, weight drop or small explosive charge (blank shotgun cartridge). Energy radiates out from the source point, either traveling directly through the upper layer (direct arrivals), or traveling down to and then laterally along higher velocity layers before returning to the surface (refracted arrivals). This energy is detected on the surface as small perturbations in the subsurface by using a linear array (or spread) of geophones spaced at regular intervals. At a distance from the source, called the cross-over distance, the refracted signal is observed at the same instant as the direct arrival, as it moves quicker through the lower faster velocity material.  Observation of the travel-times of the direct and refracted arrivals provides information on the depth profile of the refractor. To improve the signal-to-noise-ratio, several shots may be stacked until coherent data is acquired.

Shots are deployed at and beyond both ends of the geophone spread in order to acquire refracted energy as first arrivals at each geophone position.
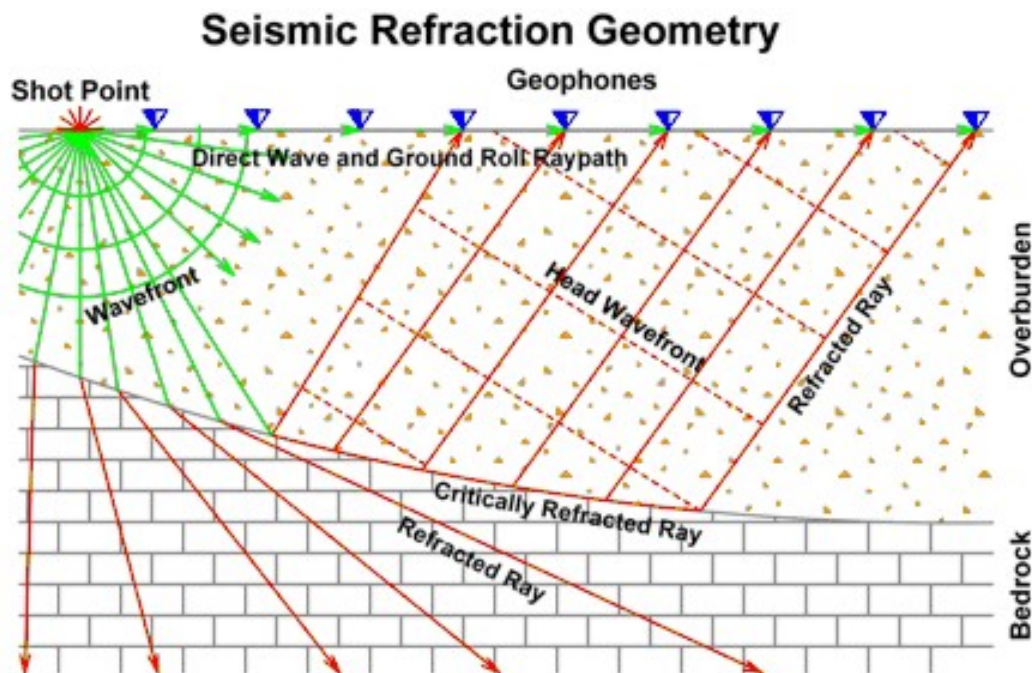


**Figure 5.E.2 - Typical seismic refraction geometry. The source in this case is a 10/20 pound steel hammer. (Diagram after Timothy D. Bechtel, Ph.D., www.enviroscan.com/html/seismic_refraction_versus_refl.html)**

Data observed through the geophones is recorded on a seismograph and later downloaded to a computer for analysis. Distance versus travel-time graphs are constructed and velocities calculated using the first arrivals.  These velocities can be used to calculate for the overburden

and basement layers. Depth profiles for each refractor layer are produced by an analytical procedure based on consideration of shot and receiver geometry and the measured travel-times and calculated velocities. The final output comprises a depth profile of the refractor layers and a velocity model of the subsurface.

## Reflection Seismic Theory

Reflection seismic is based on acoustic waves that travel through the subsurface and reflect off interfaces between two differing layers of materials. These interfaces can be caused by a difference in density or a difference in material properties of each layer, which in turn leads to an interface that will partially reflect acoustic waves. These reflections are measured along an array of geophones at the surface. The travel times from the source to the geophones are recorded for all reflections and are later used for processing. This processing is used in conjunction with the processed information from the refractions to solve for a clean migration of data and pick accurate layer depths and velocities.

## Survey Design

The shallow seismic surveys were conducted at the Northern Chaffee County location along County Road 385. Multiple lines were shot in both the north-south direction and in the east-west direction to allow for optimum analysis of the subsurface layers. Shown below in Figure 2 is an aerial view of the location of all the surveys that were completed during the weeks of May 14th and May 21st 2007.



Figure 5.E.3 - Aerial view of some of the surveys completed during the weeks of May 14th and May 21st 2007. These surveys were in the same area in order to produce complete information about the subsurface structure and material properties.

The receiver geophones were laid out at a separation of 3 meters between each geophone with a total of 24 geophones in the line. These 72 meter lines were always laid in either a north-south

direction or an east-west direction as shown above in Figure 1.  The sources that were used for these surveys varied in location and type.

Shot locations that were meant to measure reflections within the subsurface were always done along the same points as each geophone.  A shot would begin at one end of the geophone line and be stacked four times for each geophone location as the shot was moved down the line.  When surveys were done with the hope of gathering refraction data, shot points began at one end of the geophone line and moved at three meter intervals parallel away from the geophone line.  A shot would be taken and stacked four times at each three meter location heading away from the end of the line until 45 meters was reached.  Distances beyond 45 meters were often too noisy because it is difficult to send a strong enough acoustic wave into the ground that will travel the needed distance through refraction and result in a clear seismic trace record.

A majority of the surveys used a 10 or 20 pound hammer with a steel strike plate to send an acoustic wave into the subsurface.  This hammer and plate method is very cost effective and simple to complete.  A Denver based company called Sound Blasters donated some time and materials to the Colorado School of Mines by providing an impulsive acoustic source that they are currently developing.  This source is a powerful directed explosion that hits the ground with a high force and causes a consistent planned impulse source with great repeatability.

## Data Processing

The primary applications of seismic refraction are for determining depth to bedrock, bedrock structure and the water table. Due to the dependence of seismic velocity on the elasticity and density of the material through which the energy is passing, seismic refraction surveys provide a measure of material strengths and consequently can be used as an aid in assessing rock properties. The technique has been successfully applied to mapping the depth to base of backfilled quarries, depth of landfills, thickness of overburden and the topography of groundwater.

During data acquisition individual shot records are displayed as variable area wiggle traces displaying distance versus travel-time (shown in Figure 3).
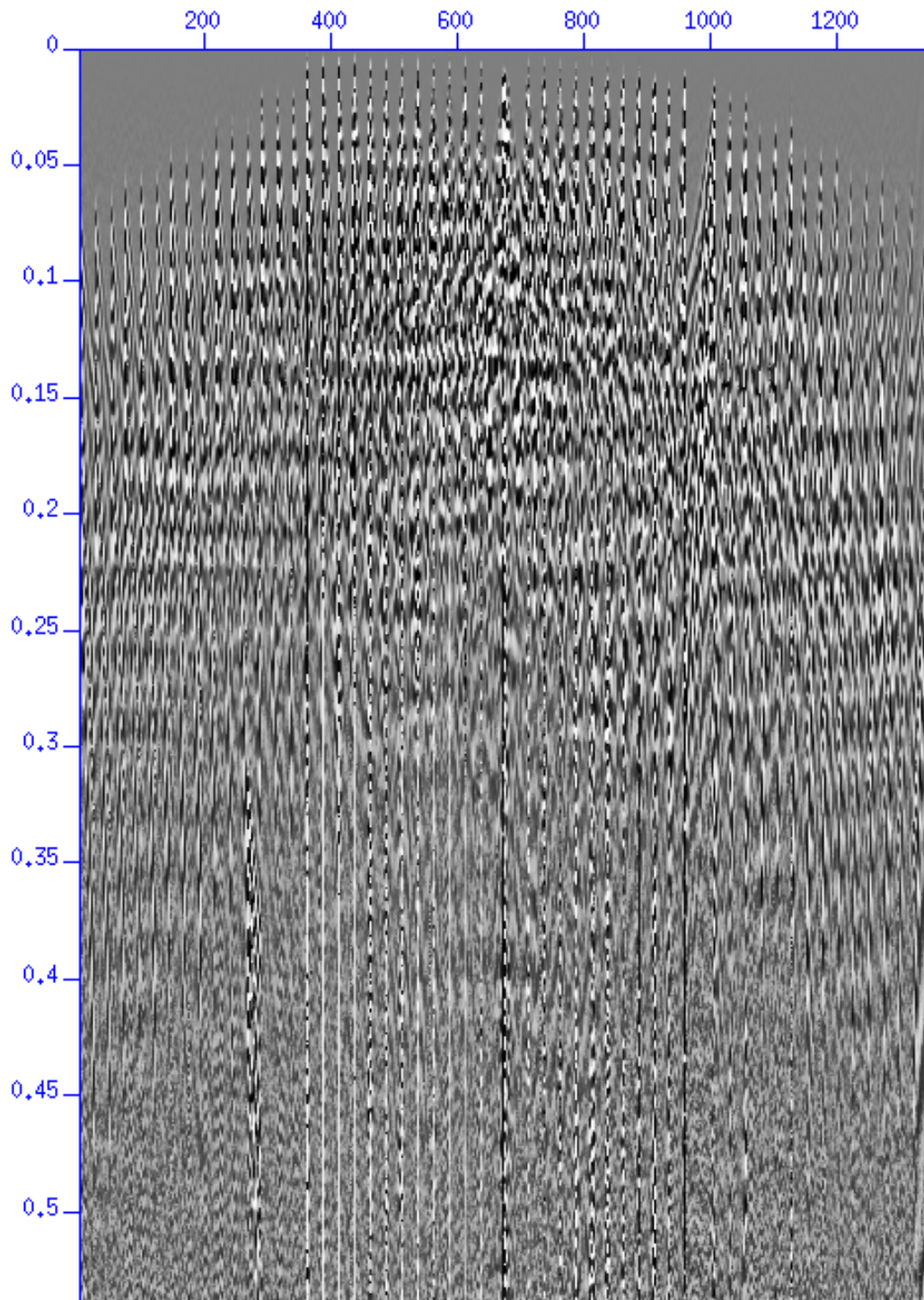
Figure 5.E.4 - This image shows the complete set of traces 1 through 54 that cover from 45 meters east of the line to 45 meters west of the line.  This is a sorted image created by the flow shown at the end of this section. Y-axis is time (s), X-axis is trace number.
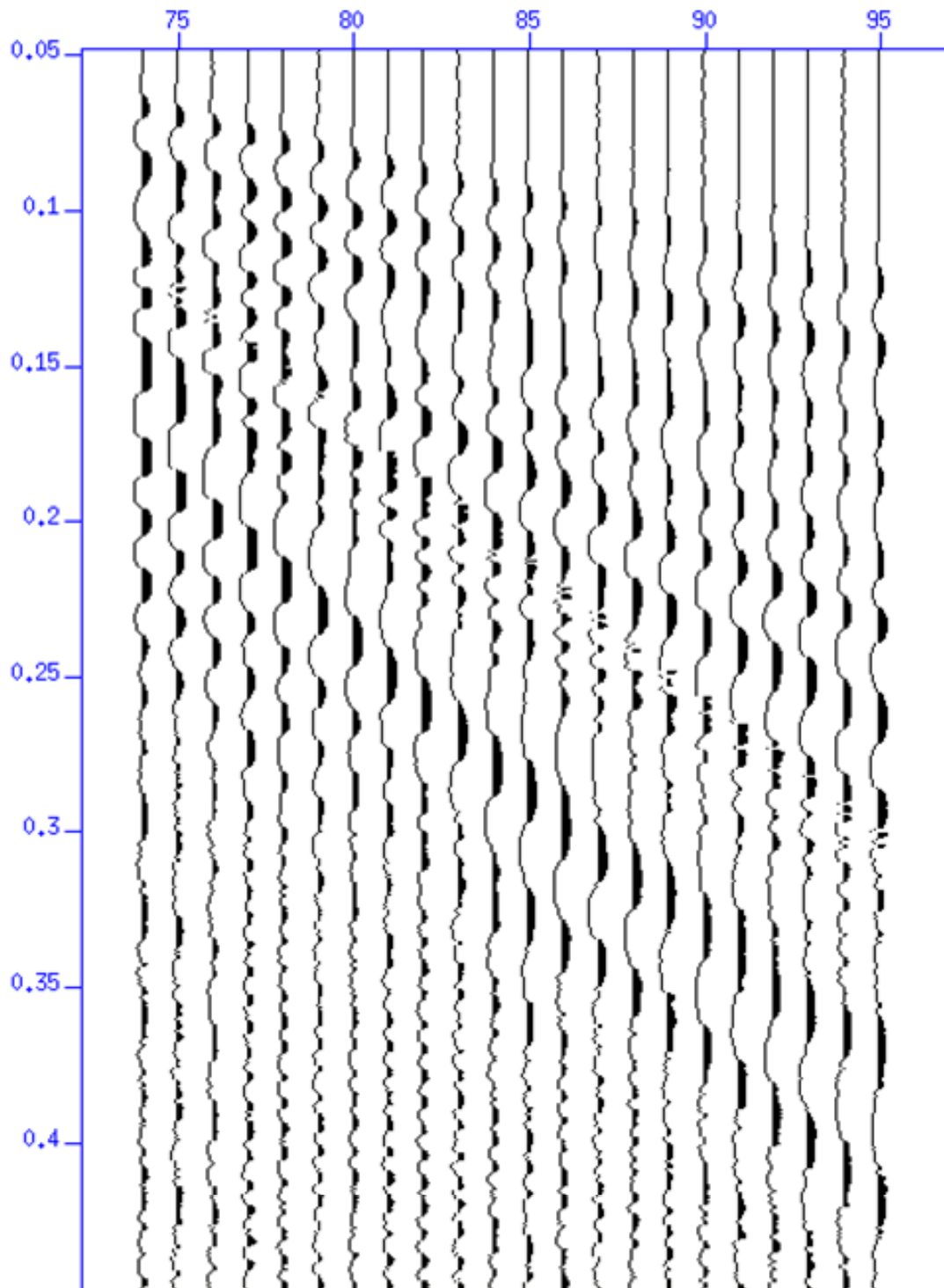
Figure 5.E.5 - This figure is a wiggle image of a single trace.  The source began to the left (west) of the trace and caused the ground motion that was measured and recorded by the geophones.  Y-axis is time (s), X-axis is trace number.

These enable an initial calculation of overburden and refractor apparent velocities and provide an important check on the quality of the data. Following acquisition, wiggle traces are used to display the data during picking of the first-arrivals for each geophone position and shot.

Refraction calculations are done using the change in the slope of the first arrivals. Initially the direct wave is the fastest moving wave, but after some time and distance, a wave that was refracted at the critical angle along an interface is able to overcome the direct arrival wave. This distance is known as the crossover distance. The varying slopes of the first arrival allow for a calculation of an intercept time. This time is used in conjunction with the crossover distance to calculate for the depth of the interface between two different velocities layers.

Seismic Un*x is a processing program developed by the Colorado School of Mines, which was used to produce Figures 3 & 4 by following the following flow:

- seg2segy 1.dat 54  (54 files - put into temp.sgy)

- segyread tape=temp.sgy endian=0 verbose=1 conv=0 | segyclean > temp.su  (converts temp.sgy into temp.su)

- sugain jon=1 < temp.su | suxwigb xcur=3   (gains and corrects temp.su using jon parameter)

- susort sx offset < temp.su | sugain jon=1 > gain.sort.temp.su  (sort temp.su by offset - then gain using jon=1  - creates gain.sort.temp.su)

- suximage < gain.sort.temp.su perc=99  (image the sorted gained file  Figure 2)

- suxwigb < gain.sort.temp.su perc=99  (image using wiggle traces Figure 3)

Normal moveout was applied to the seismic traces as a check for possible reflections. A common depth point (cdp) gather was created from gain.sort.temp.su using Seismic Un*x. This cdp gather was then used to calculate for the normal moveout based on the refraction velocities and travel times. Unfortunately, the trace gather was too cluttered by the noise created from the direct arrivals and refracted waves. This prevented any interpretation of reflections occurring within the subsurface.

## Data Interpretation

The processed data is normally presented as a depth profile for the identified refractors and a velocity profile for the overburden and refractors. Any existing ground truth information such as borehole logs, EM and DC resistivity data are overlain on the depth profile in order to help calibrate the seismic results and then provide an indication of the level of correlation along the survey line.

Shown in the next eight figures are calculated refraction depths and velocities based on the information that was gained from the hammer seismic performed in the east-west direction and the north-south direction as shown in the aerial view of Figure 2.
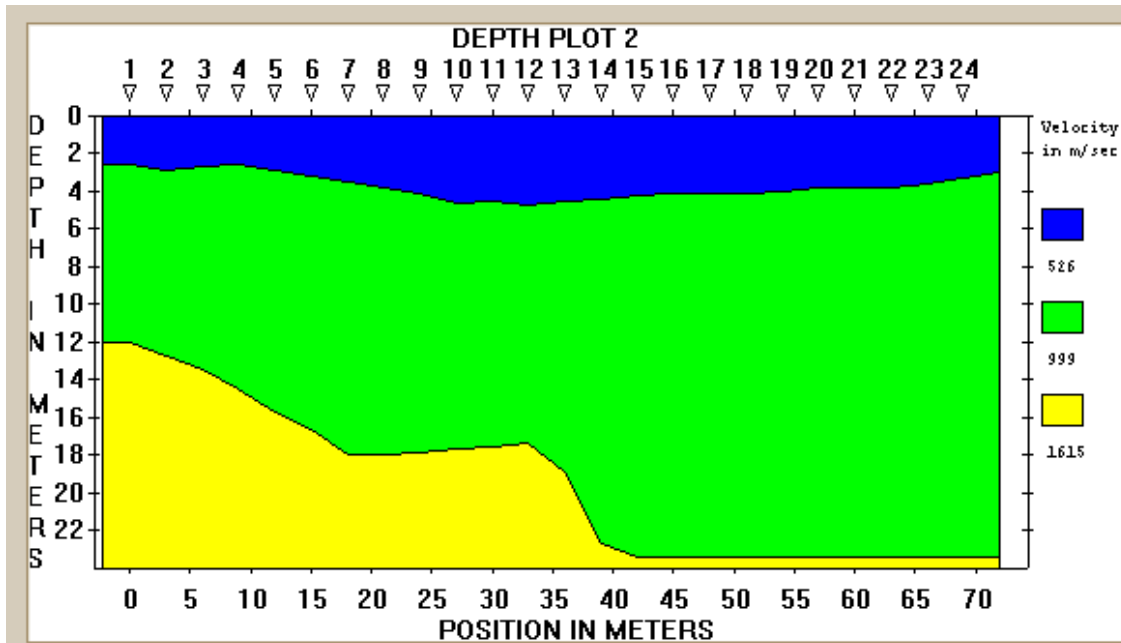
East-West Line



Figure 5.E.6 – This refraction cross section was developed using the traces taken from the shot point being along the western end of the refraction survey.
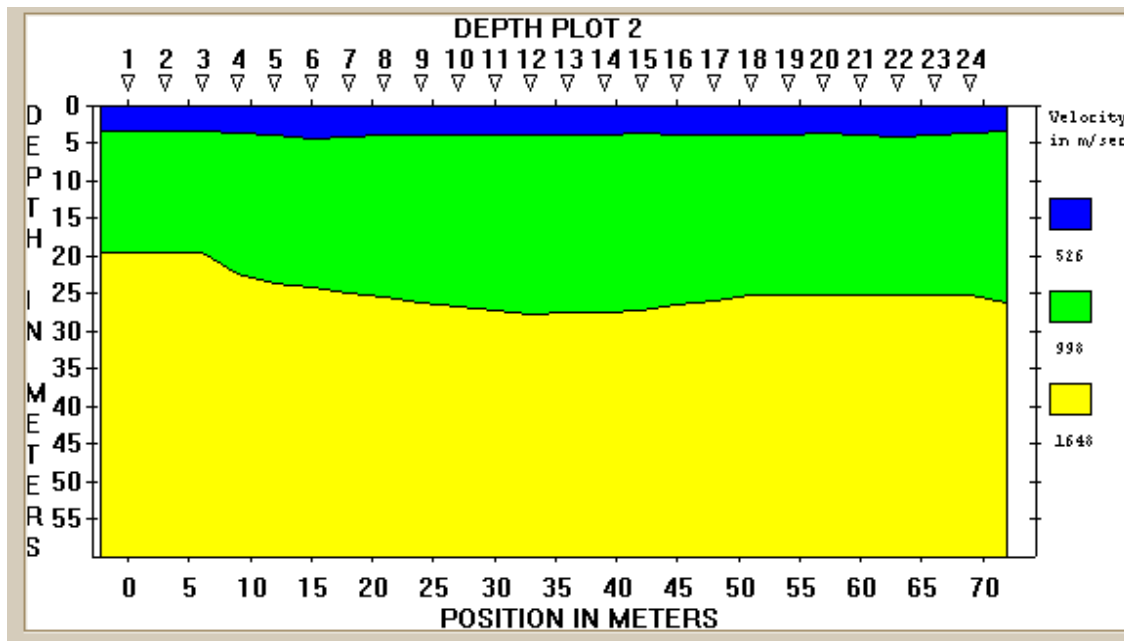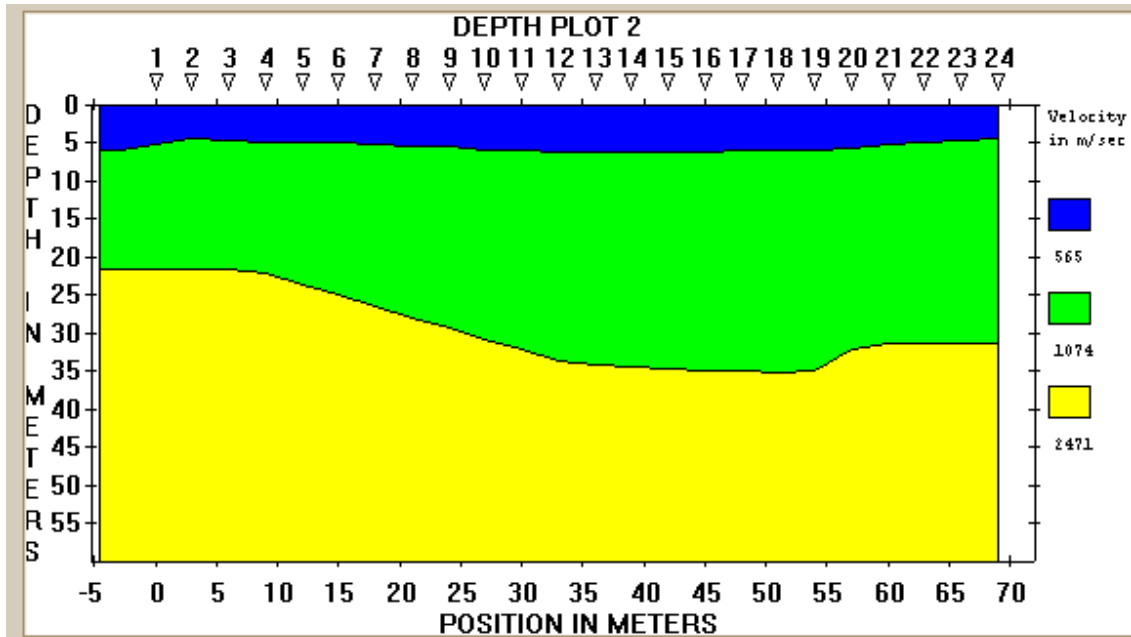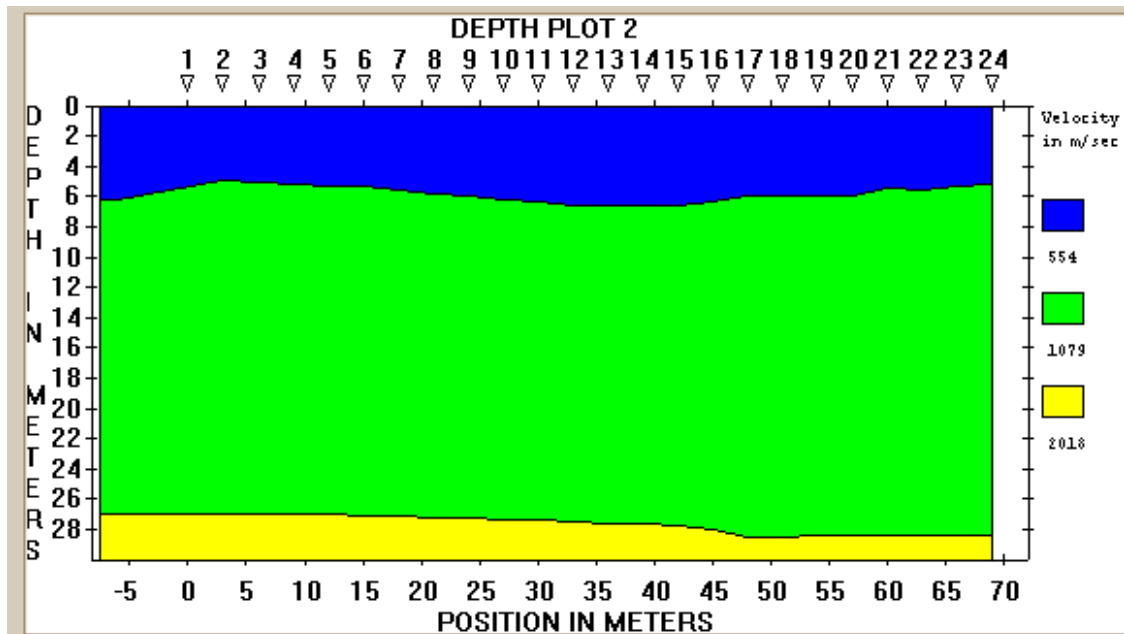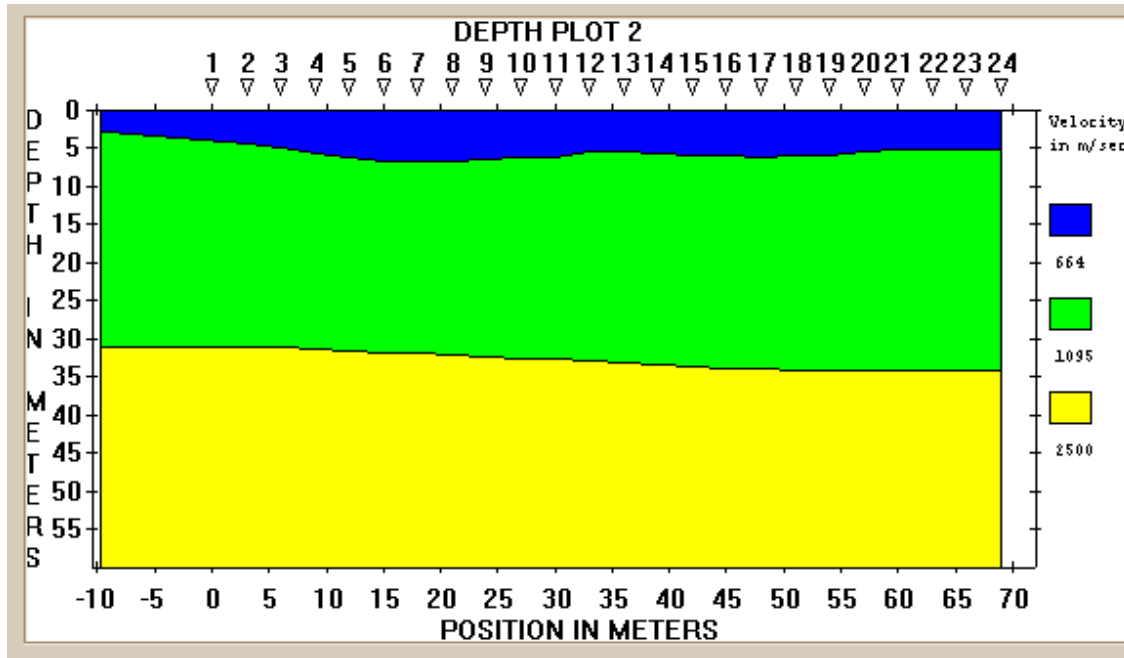


Figure 5.E.7 - This refraction cross section was developed using the traces taken from the shot point being along the western end of the refraction survey.
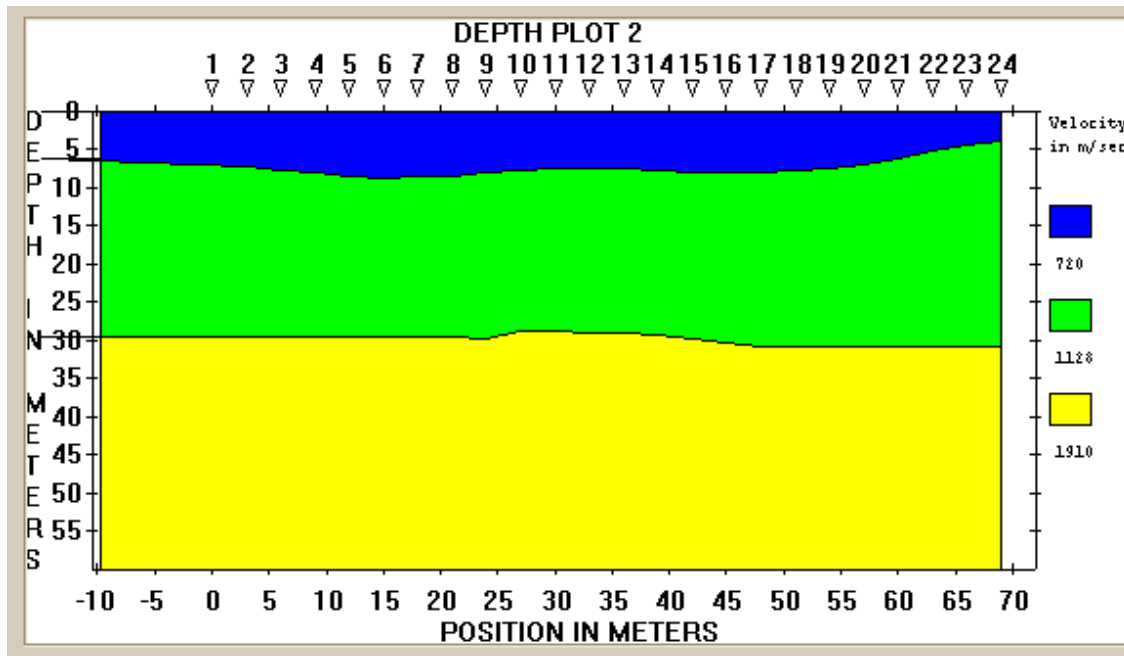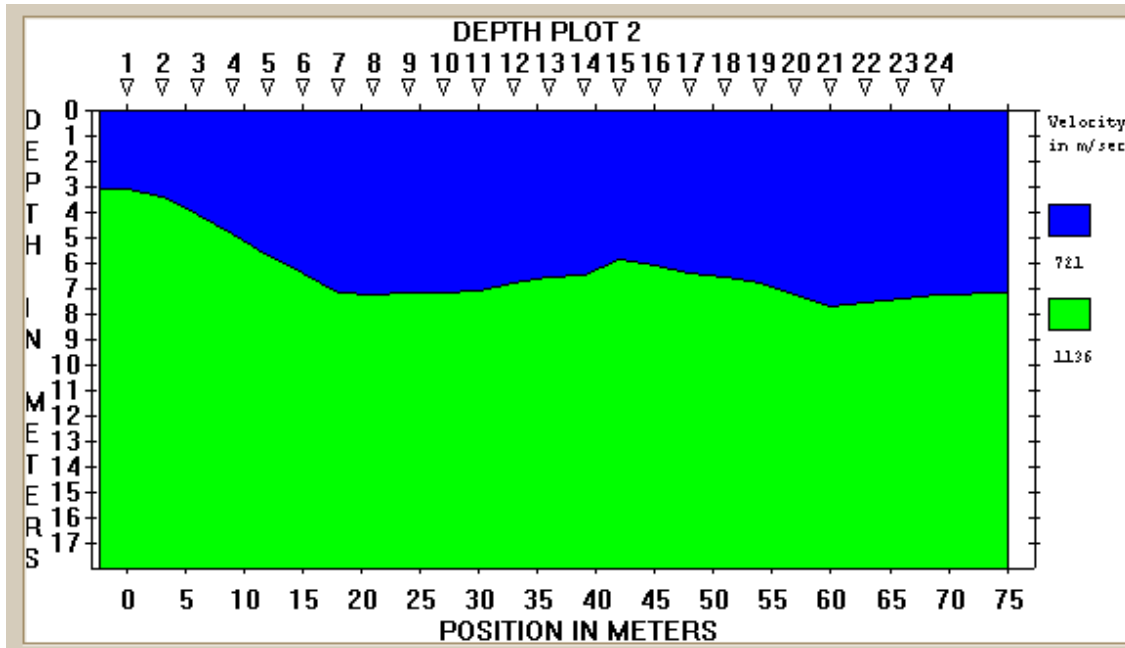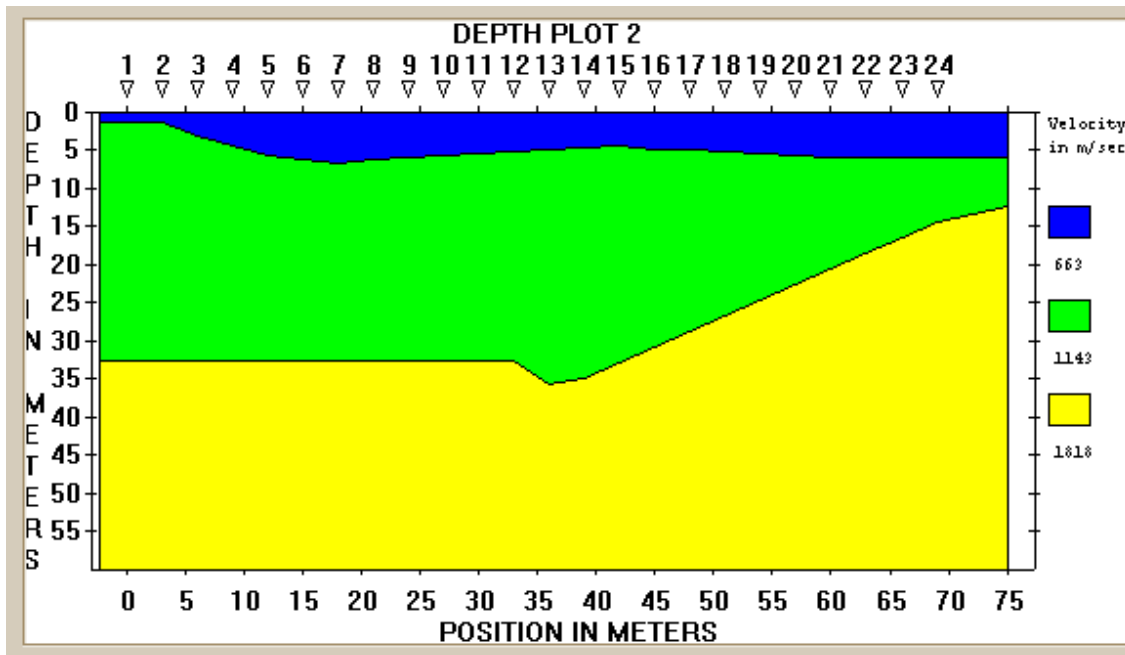
**East-West Line**



Figure 5.E.8 - This refraction cross section was developed using the traces taken from the shot point being along the eastern end of the refraction survey.



Figure 5.E.9 - This refraction cross section was developed using the traces taken from the shot point being along the eastern end of the refraction survey.

North – South Line (Walk_Away_Hammer_Seismic)



Figure 5.E.10 - This refraction cross section was developed using the traces taken from the shot point being along the southern end of the refraction survey.



Figure 5.E.11 - This refraction cross section was developed using the traces taken from the shot point being along the southern end of the refraction survey.

**North – South Line (Walk_Away_Hammer_Seismic)**



Figure 5.E.12 - This refraction cross section was developed using the traces taken from the shot point being along the northern end of the refraction survey.



Figure 5.E.13 - This refraction cross section was developed using the traces taken from the shot point being along the northern end of the refraction survey.

Based on interpretation through Figures 5-12, it is possible to create an estimate of the velocities and depths of the first two layers of the subsurface. The first layer has a depth that ranges from 3 meters to 6 meters down and a velocity of $550 \pm 50$ meters/second. The second layer has a depth ranging from 20 meters to 25 meters down and a velocity of $1000 \pm 100$ meters/second. Based on the data shown above, calculating a third layer depth or velocity is very uncertain. The approximate velocity of the third layer is $2000 \pm 400$ meters/second.

Based on Figures 9-12, there is a slight southward dipping of the second layer beneath the subsurface. This can be interpreted because the velocity estimated by the refraction calculations is slightly faster along the southern side of the line than along the northern side of the line. This means that as the source from the south was sent out, it traveled directly to the refractor and slightly 'uphill' towards the receivers, which would lower the total travel time. The opposite is true for sources along the northern side of the receiver line. This observation results in a small angle dip in the eastward direction for second layer of the subsurface.

When combining these observations of depth and velocities with the data acquired through direct current resistivity, it is very clear that there is a direct correlation between the layers. The top layer is highly resistive and shows approximately the same depth as estimated through refraction analysis. This layer is likely recent glacial till or alluvium fill from the mountain fronts to the west. The second layer could possibly be the dry union layer or a glacial till that has been compacted more than the first layer and is more conductive. The direct current resistivity survey shows an approximate depth of 20 meters for the second layer, which correlates nicely with the data gathered through shallow seismic. The third layer is apparent in many of the direct current resistivity models as being highly resistive which may correlate with the high velocity as being basement rock.

## Error Analysis

The way that shallow seismic data is collected allows for ease of use and an overall reduction in the possible sources of error. Once everything has been connected together and is ready to collect data, the system is nearly self sufficient, and does not require much interaction, therefore preventing human error. All data is saved in a complete format that can be edited later using preprocessing techniques. The largest source of error that does occur happens during analysis and processing of the collected data.

Often noise is collected along with the source acoustic wave, thereby obscuring the data and making it much more difficult to interpret. Along with the noise there are often problems with processing the data using a geometry that correctly displays the setup of geophones and sources that was used. This geometry is often one of the largest problems in processing for larger deep seismic data sets.

## Conclusion

Based on the results from refraction processing and the results from the direct current resistivity, there are a few conclusions that can be made. There are three distinct layers within the subsurface, layer one at 3-6 meters depth with a velocity of $550 \pm 50$ meters/second, layer two at a depth ranging from 20 meters to 25 meters and a velocity of $1000 \pm 100$ meters/second and layer three with a velocity of $2000 \pm 400$ meters/second. Combining this depth information with the resistivity information, it is feasible to assume that the water aquifer of this area is strictly limited to the shallow second layer where the resistivity is not too high, and the velocity is lower, which could imply looser compaction than the high velocity of the third layer.

## *Vertical Seismic Profiling*

## Introduction

A vertical seismic profile (VSP) is when a receiver is lowered into a borehole to record the down-going and upgoing waves produced from a seismic source at the surface [1]. In May, 2007, a vertical seismic profile was performed at the well drilled in 1971 off of county road 321 at Universal Transverse Mercator location 13S 04400410E 4295618N. The United States Geological Survey has named this well "Test Well SC01407830DAA". The well is 1000 feet deep, and the water level begins about 26 feet below the surface of the earth. The elevation of the well is 8086 feet. The well is encased in a steel casing that is approximately six inches in diameter. [2] A geophone (the receiver) was lowered into the borehole starting at a depth of ten meters and then lowered at five meter intervals to a depth of sixty meters. At each depth location, a surface source was triggered starting five meters west of the well and progressing at five meter intervals away from the well to an offset of fifty meters. The surface sources were triggered by people pounding a sledge hammer on a steel plate five to ten times to stack acoustic waves into the ground. Dylan Mikesell from Olson Engineering assisted in survey design and data acquisition.
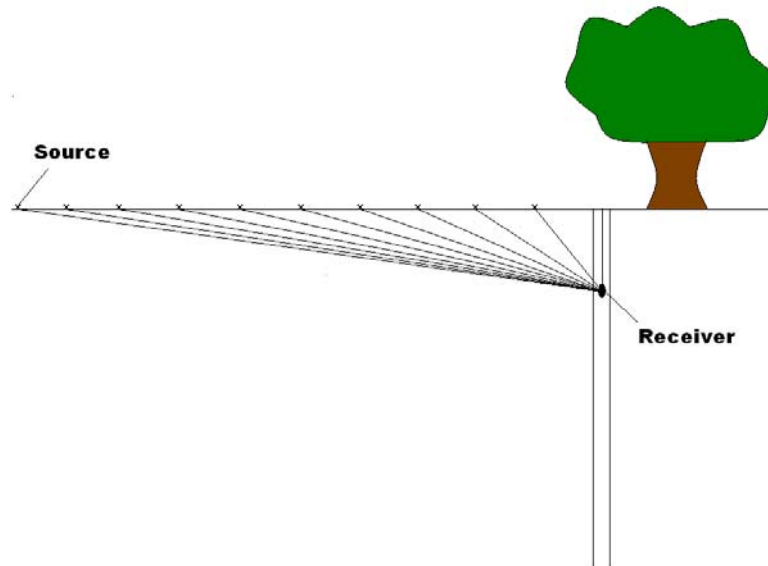
Figure 5.F.1:  Cartoon of how the receiver receives direct waves.

Figure 5.F.1 shows how the geophone in the borehole receives the direct waves from the source at the surface.  Figure 5.F.1 nicely shows the advantage of a vertical seismic profile over surface seismic: one-way travel time.  Surface seismic uses two-way travel time because the receiver has to wait for the wave to be reflected off of a reflector.  This is not the case for a VSP.  Direct waves make analyzing VSP data easier than surface seismic data.  Once the VSP data is downloaded, amplitudes are picked using a seismic un*x software.  These picks are then analyzed in a graphing program to compare the picks with an estimated velocity.  Figure 5.F.3 is an example of how velocities are picked from raw data, called shot gathers.  Vertical seismic profiling is used by many people.  It can be used to determine the lithology of the shallow subsurface.  Knowing the geology of the subsurface helps determine where the water table is or how water moves in the subsurface.  Different geological layers, faults and other geologic structures can also be seen using a vertical seismic profile.
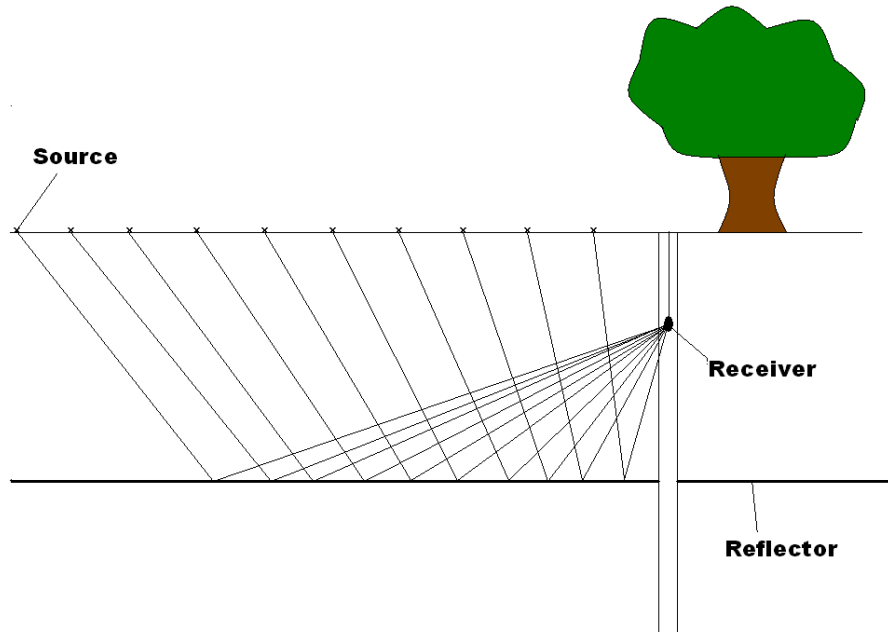
Figure 5.F.2:  Cartoon of how the receiver receives reflected waves.

Figure 5.F.2 shows how the geophone receives reflected waves.  This is similar to Figure 1 except that the waves arrive later because their travel path is much longer.  Reflected waves were not easy to see in the data that was collected; this made interpretations difficult to make.
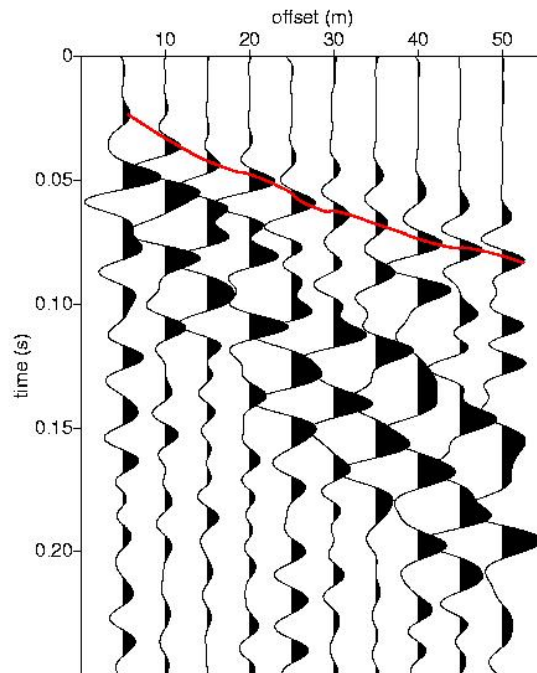


Figure 5.F.3:  The velocity picks on the raw shot gather at 10 meter depth.

The equation used for VSP is a simple one:  $h^2 = v_0^2 t^2 - d^2$, where h is offset, d is the depth of the receiver, t is one-way travel time from the source to the receiver, and $v_0$ is the material velocity. Velocity is the unknown.  The units of h and d are meters; the units of t are seconds; and the units of $v_0$ are meters per second.
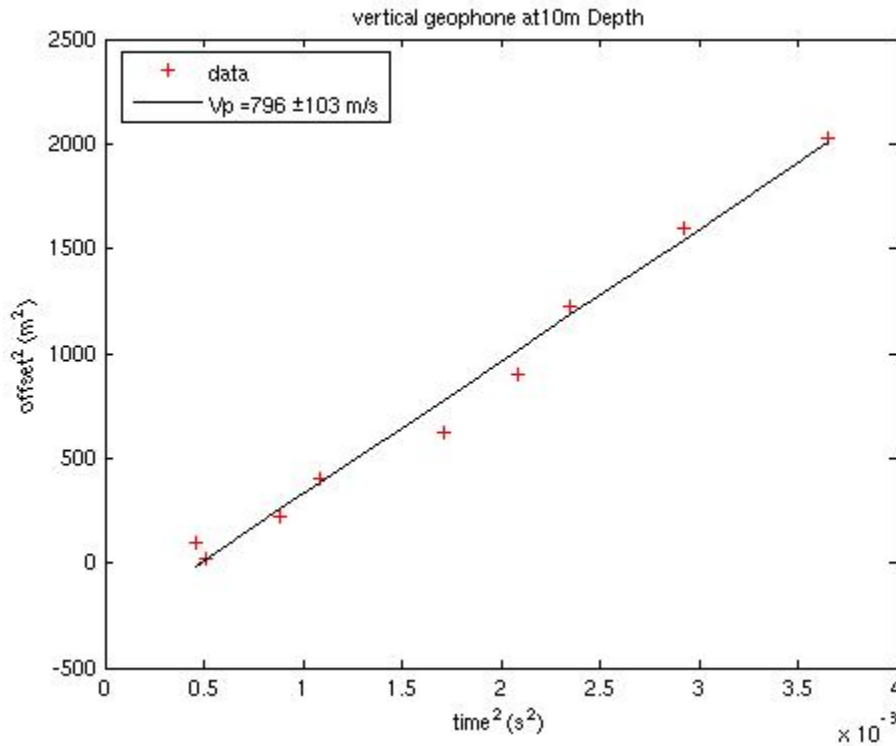


Figure 5.F.4:  Velocity fit using the 10 meter depth data.

Figure 5.F.4 shows the raw data ('+') for the vertical component of the waves collected at each offset with the geophone at a depth of 10 meters.  The data was fit hyperbolically to find the standard deviation of the data.  For the vertical component fits at each depth, the near offsets usually follow the fit closely because the vertical component is more prominent.  At far offsets, the horizontal components are more easily measured.

## Interpretation

Due to the metal casing on the borehole, it is difficult to interpret different layers in the first sixty meters in the subsurface.  The average velocity in the first sixty meters is approximately 704 meters per second with a standard deviation of 66 meters per second.  This conclusion correlates well with the interpretations made from the shallow seismic data.  The shallow seismic data showed that there are at least three layers in the subsurface at this location.  The first layer, which extends down about five meters, has a velocity of approximately 550 meters per second.  The second layer, which is about twenty meters thick, has a velocity of approximately 1000 meters

per second.  The average velocity of these top two layers is about 775 meters per second.  This average velocity is very close to being within one standard deviation of the average velocity calculated using VSP.

An educated guess that can be made is that there is anisotropy in the subsurface.  In Figure 5.F.3, one can argue that there are two slopes:  a slower one from 0 to 20 meters offset and then a faster slope from 20 to 50 meters (see Figure 5.F.5).  These two slopes could be caused by a vertical change in geology.  The slope of the first 20 meters is approximately 600 meters per second; the slope of the second 30 meters is approximately 1200 meters per second.  This guess also fits nicely with the shallow seismic data.  This interpretation also fits fairly well with the known geology in the area.  The thin layer of glacial till on the surface is unconsolidated and will have a slower velocity that the tightly packed Dry Union beneath.
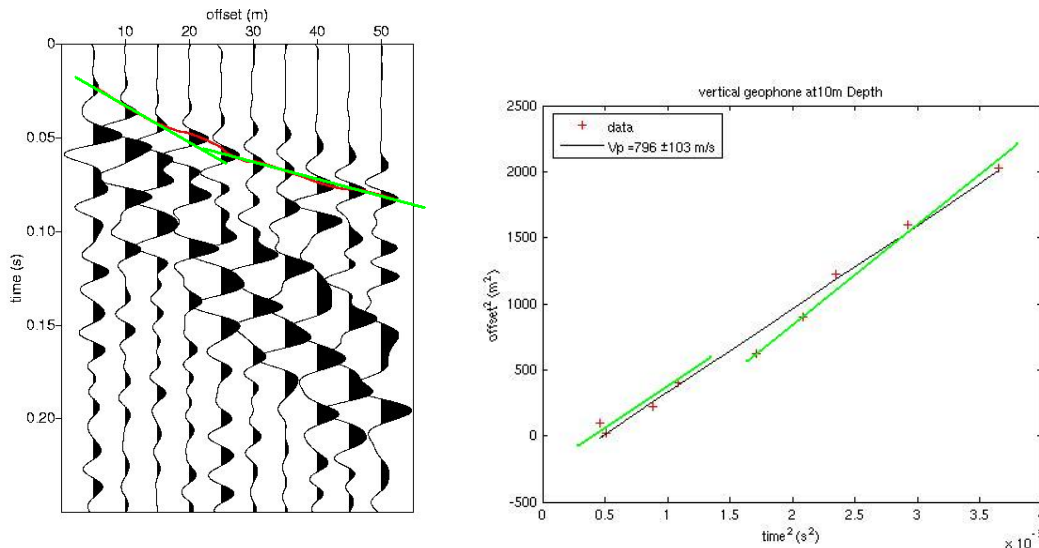


Figure 5.F.5:  This shows the two different slopes (in green) from Figures 5.F.3 and 5.F.4.

## Error Analysis

Most of the error in the VSP data is human error.  Ideally, the hammer should have hit the plate with the same force and at the same place every time.  A few different people took turns swinging the hammer and each person has a different technique, so the source trigger was not the same each time.  Also, all of the data collected at the fifty meter offset at each depth location were not used.  Throwing out this data decreased the standard deviation at every depth.  Another problem in the field was lowering the geophone in the well.  As it was lowered, it twisted.  Since it twisted, we do not really know the orientation of the receiver, which makes it difficult to measure the shear and transverse waves.  The data that we have to the shear and transverse waves may not be entirely accurate if the geophone twisted and measured the opposite wave.  A large source of error is the metal casing around the borehole.  This made picking velocities difficult because many of the waves were transferred through the metal casing.

## Conclusion

After analyzing the vertical seismic profile collected on a well off of Chaffee County Road 321 by the junior geophysics class at the Colorado School of Mines, the average velocity in the first sixty meters of the subsurface is 704 meters per second, plus or minus 66 meters per second.

One recommendation for improving a vertical seismic profile is to work on a well that is uncased.  If an uncased borehole cannot be found, try to find one that is cased in plastic rather than steel.  The metal absorbs too many of the waves and makes it difficult to see the actual data.  If another well cannot be found, one recommendation is to use the same well and use offsets that move North and South of the well.

## *Conclusion of North Site Geophysical Surveys*

Based on evidence produced using multiple independent techniques, including hammer seismic, GPR, DC resistivity, and frequency domain EM, it is possible to build a corroborated interpretation of the north site that may help characterize water movement in the Upper Arkansas River Valley. It was shown consistently that throughout the north site, a large resistive body appears about 30 meters below the surface.  This feature appears in all data sets that were able to image to the necessary depth. The hammer seismic shows a large change in acoustic impedance at approximately 25 meters depth, dipping slightly toward the south at about 4-5°. In support of this finding, the ground penetrating radar shows a large change in dielectric permittivity at about 30 meters depth. As further evidence of this stratigraphic boundary, the inversion models produced from the DC resistivity data show a large resistive feature dipping at about 5° to the west and at the same depth as seen in the hammer seismic and GPR data. Additionally, the DC resistivity shows that the feature is approximately 50 meters thick and behaves as an aquitard, separating surface ground water from deeper subsurface ground water. The frequency domain EM data confirms the DC resistivity data, showing that the surface water diffuses mostly to the west rather than down.

The location and characteristics of this aquifer correlate well with the expected location and the structure of the Dry Union Formation. Therefore, a possible conclusion from the combined analysis of the data sets is that in the North Site, the Dry Union formation acts as an aquitard, having the characteristics of being approximately 50 meters thick and dipping at approximately 6-7° to the southwest. This layer is overlain by alluvial deposits that allow for water transmission and is underlain by a large aquifer. Though there is evidence of faulting, connectivity between the near surface ground water and the deeper aquifer cannot be established from the recorded data sets.

# Chapter 6: Final Interpretations

## *Integration of Deep Geophysical Data from Past Field Camps*

Over the last three summer field camps in Chaffee County, Colorado, a vast amount of deep seismic and gravity data has been acquired throughout the Upper Arkansas River Valley extending from Buena Vista to Salida. The deep seismic and gravity survey lines all have an approximate west to east orientation. Differences and similarities in these data sets provide valuable information concerning the overall interpretation of the valley.

## Deep Seismic Lines (Northernmost line to Southernmost line)

### 2006 North Seismic Line

The northern-most deep seismic line is the 2006 north seismic line 2. Layers of alluvium, Dry Union, Paleozoic sediment, and Precambrian basement can be seen in the data. Highly characteristic of a rift system, there are two sub-vertical extensional faults that extend from the Dry Union to the basement rock.

Figure 6.A.1    The figure above is the seismic profile from the 2006 North Seismic Line. The vertical axis is time in milliseconds and the horizontal axis is distance. The length of this profile is about 3.5 km.

Figure 6.A.2    The figure above is a cross section of the 2006 North Seismic Line.  Both the vertical and horizontal axes are distances.  The cross section is about 3.5 km in length.


## 2006 South Seismic Line

Moving to the south, the next seismic line is the 2006 south seismic line.  This line extends further to the east than the 2006 north seismic line.  The same succession of alluvium, Dry Union, Paleozoic sediment, and Precambrian basement can be seen in the data.  However, along this line the beds dip to the west with an average dip of about 20 degrees [1].  The basement rock becomes shallower toward the east.  This data is consistent with the model of a rift valley.
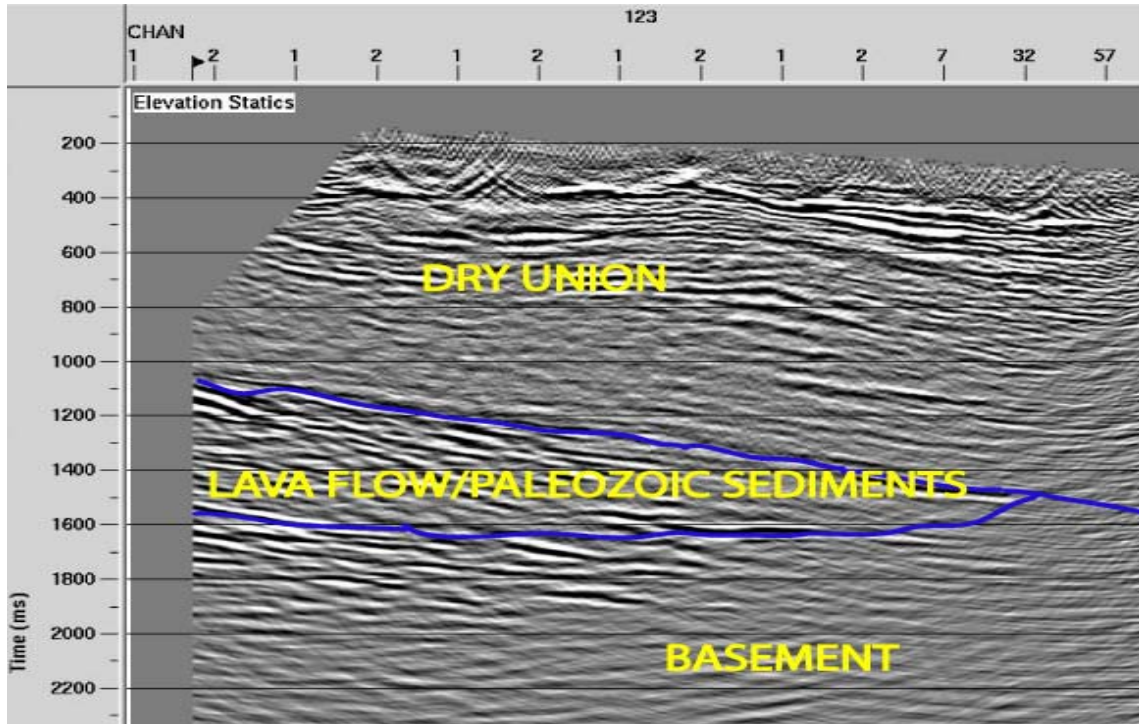
Figure 6.A.3    The figure above is the seismic profile from the 2006 South Seismic Line. The vertical axis is time in milliseconds and the horizontal axis is distance.  The length of this profile is about 8 km.
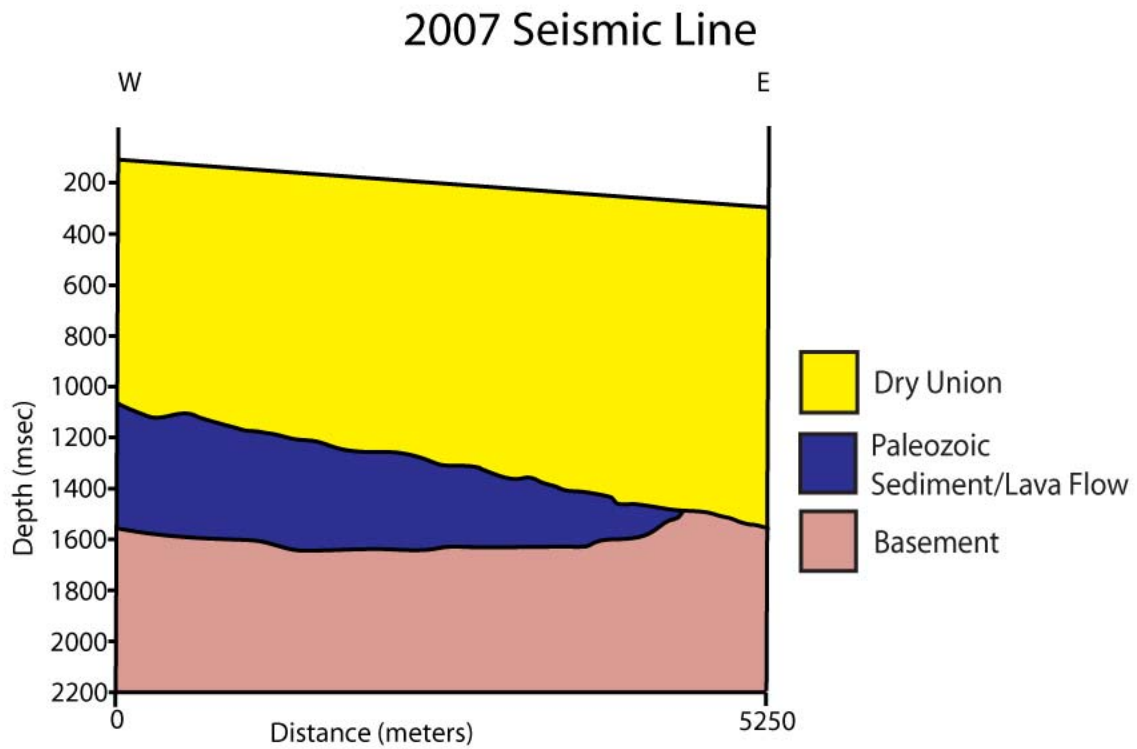
Figure 6.A.4    The figure above is a cross section of the 2006 South Seismic Line.  Both the vertical and horizontal axes are distances.  The cross section is about 8 km in length.

## 2005 Seismic Line

Two deep seismic surveys were performed in 2005 but only the data for one of the surveys still exists.  The 2005 seismic line was about 6 km long and was located on the far west side of the valley.  The data in this profile contains the alluvium, Dry Union, and the Precambrian basement but the Paleozoic sediments cannot be identified.  This might be due to low acoustic impedances between the alluvium and the Dry Union. A fault can be seen in this profile between the Dry Union and the basement rock with an average dip of about 40 degrees to the East [1].  The dip of this fault is consistent with the dip of the faceted spurs seen on the surface.

Figure 6.A.5    The figure above is the seismic profile from the 2005 Seismic Line.  The vertical axis is time in milliseconds and the horizontal axis is distance.  The length of this profile is about 6 km.

Figure 6.A.6    The figure above is a cross section of the 2005 Seismic Line.  Both the vertical and horizontal axes are distances.  The cross section is about 6 km in length.

## 2007 North and South Seismic Lines

The two southernmost deep seismic lines are those acquired during the 2007 field camp.  The 2007 North Seismic Line runs west along CR 251-1 from HW 285 for about 8 km and the South Seismic Line runs west along CR 250 for about 6 km.  Because both of these lines were very close together, the data acquired by both of the lines is very similar.  Both seismic profiles exhibit the Dry Union and Paleozoic sediment layers on top of the Precambrian basement.  There are possibly lava flows covering the Paleozoic sediments, but discerning between the two is difficult because they have similar velocities.  In both profiles, the Paleozoic sediments are pinched out to the East.  This is probably due to erosion.

Figure 6.A.7    The figure above is the seismic profile from the 2007 North Seismic Line. The vertical axis is time in milliseconds and the horizontal axis is distance.  The length of this profile is about 8 km.

Figure 6.A.8    The figure above is the seismic profile from the 2007 South Seismic Line. The vertical axis is time in milliseconds and the horizontal axis is distance.  The length of this profile is about 6 km.

Figure 6.A.9    The figure above is a cross section of the 2005 Seismic Line.  The
vertical axis is in time and the horizontal axis in distance.  The cross section is about 7
km in length.

*Gravity Lines (Northernmost line to Southernmost line)*

## 2005 North Gravity Line

The gravity data from the north line acquired in 2005 field camp shows the gravity effect on the
east side of the valley.  The gravity reading increases steadily toward the east.  This is to be
expected because the dense basement rock becomes shallower toward the east.
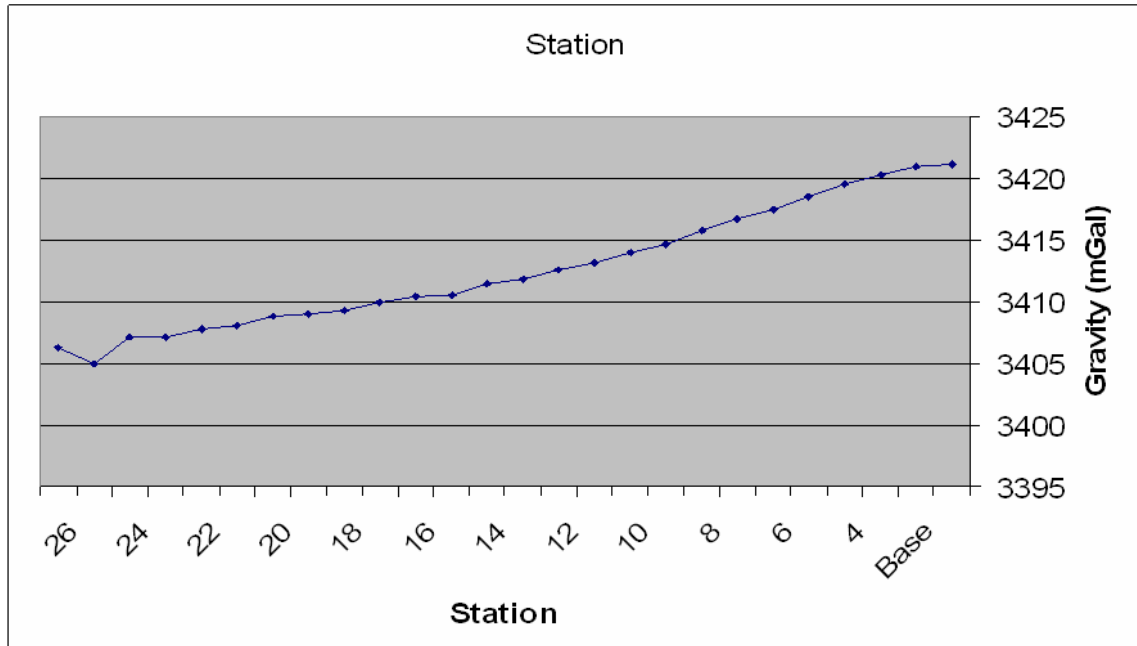
Figure 6.B.1    The figure above is a plot of the gravity data acquired on the 2005 North Line.  The horizontal axis is Station Number and the vertical axis is gravity in milligals. The length of this line is about 3 km.

## 2005 South Gravity Line

The data from the South Gravity Line was acquired further west than the 2005 North Gravity Line.  Therefore, the gravity effect of the basement rock on the west side of the valley can be seen in the plot.  The basement rock on the east side of the valley has a stronger effect than the basement rock on the west side, however, because the basement rock is closer to the surface in the East.  There are a few anomalies in the middle of the valley which could indicate faulting or horsts, but they are possibly due to human error when using the instrument.
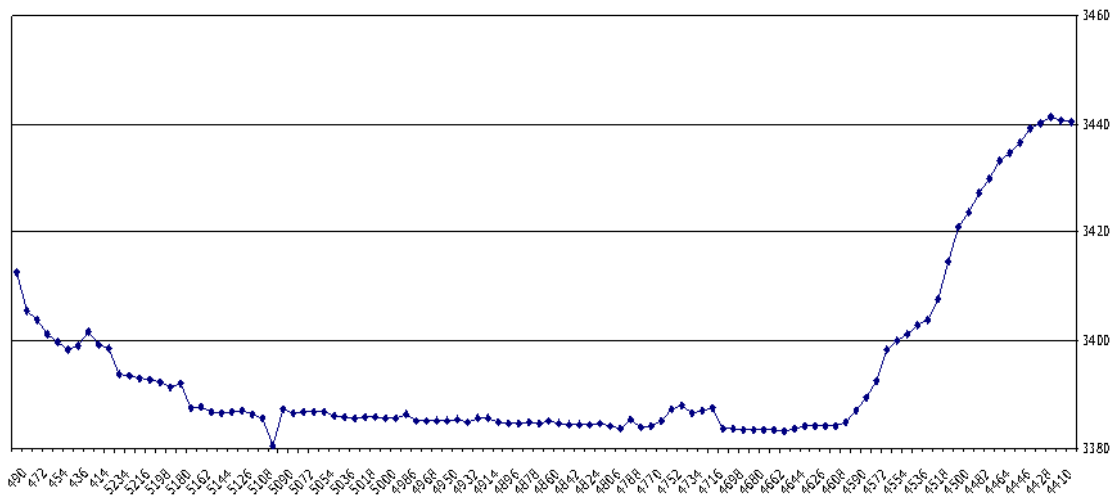


Figure 6.B.2    The figure above is a plot of the gravity data acquired on the 2005 South

Line.  The horizontal axis is UTM coordinate and the vertical axis is gravity in milligals.
The length of this line is about 6 km.

*2006 Gravity Line*
The 2006 Gravity line extends across the entire valley for a distance of about 12 km.  The data is
very similar to the 2005 data in that both lines show steep increases in gravity toward the east.
Because there is no terrain correction for this data, the data looks as if there is a gravity low in
the west.  However, if a terrain correction is applied, the presence of high density material could
probably be seen on the west side.
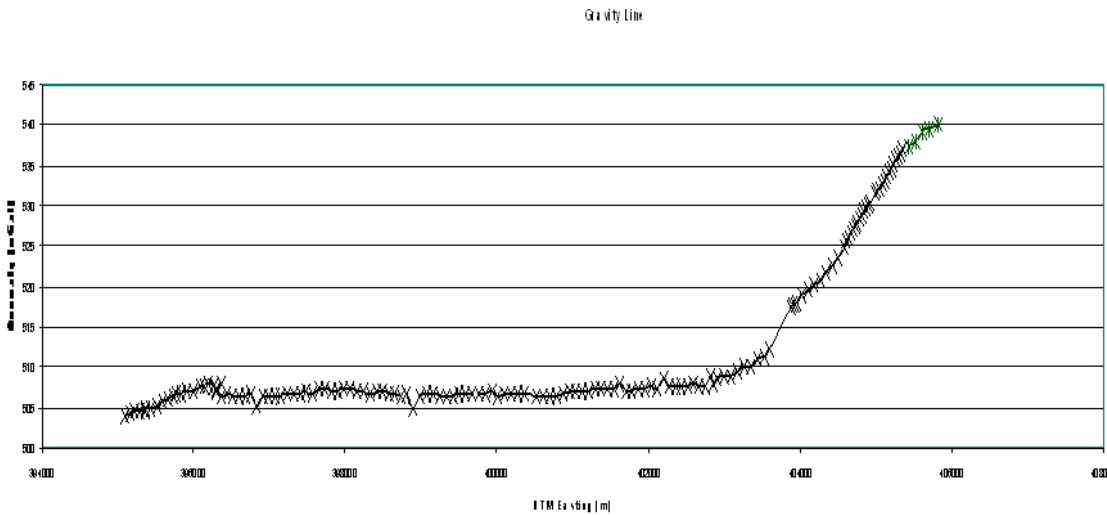


Figure 6.B.3     The figure above is a plot of the gravity data acquired on the 2006 Line.
The horizontal axis is UTM coordinate and the vertical axis is gravity in milligals.  The
length of this line is about 12 km.


## 2007 Gravity Line

The 2007 gravity line is about 11 km beginning in the middle of the valley and extending all the
way along CR 251-1 to the west.  The line was then extended even further up to the peak of
Mount Shavano.  The data acquired on this line is more chaotic than the data from other lines
further north but still follows the same general trend that the other lines do.  There is a gravity
high in the east and a slight increase in gravity in the west.  This is because the basement rock is
closest to the surface in these areas.  Also, the 2007 Gravity Line is the only gravity line that has
been corrected for terrain and is, therefore, very reliable.  The data is more chaotic on the 2007
Gravity Line than the other gravity lines which could be due to the fact that it is closer to the
Poncha Pass transfer zone.

Figure 6.B.4    The figure above is a plot of the gravity data acquired on the 2006 Line. The horizontal axis is Station Number and the vertical axis is gravity in milligals.  The length of this line is about 11 km.


## Basement Contours

Using depth to basement data and elevation data from the five deep seismic lines, the GIS software was able to create a contour map of the Precambrian basement rock.  The map shows the basement rock dipping to the East on the west side of the basin.  This dip is perhaps the extension of a major fault on the west side of the basin.  The map also shows the basement rock dipping slightly to the south toward the Poncha Pass transfer zone.  This indicates that the southwestern portion of the Upper Arkansas River Valley has the greatest depth to basement rock and, and therefore, the greatest amount of basin fill.  This area could possibly be the most ideal location for a water reservoir.
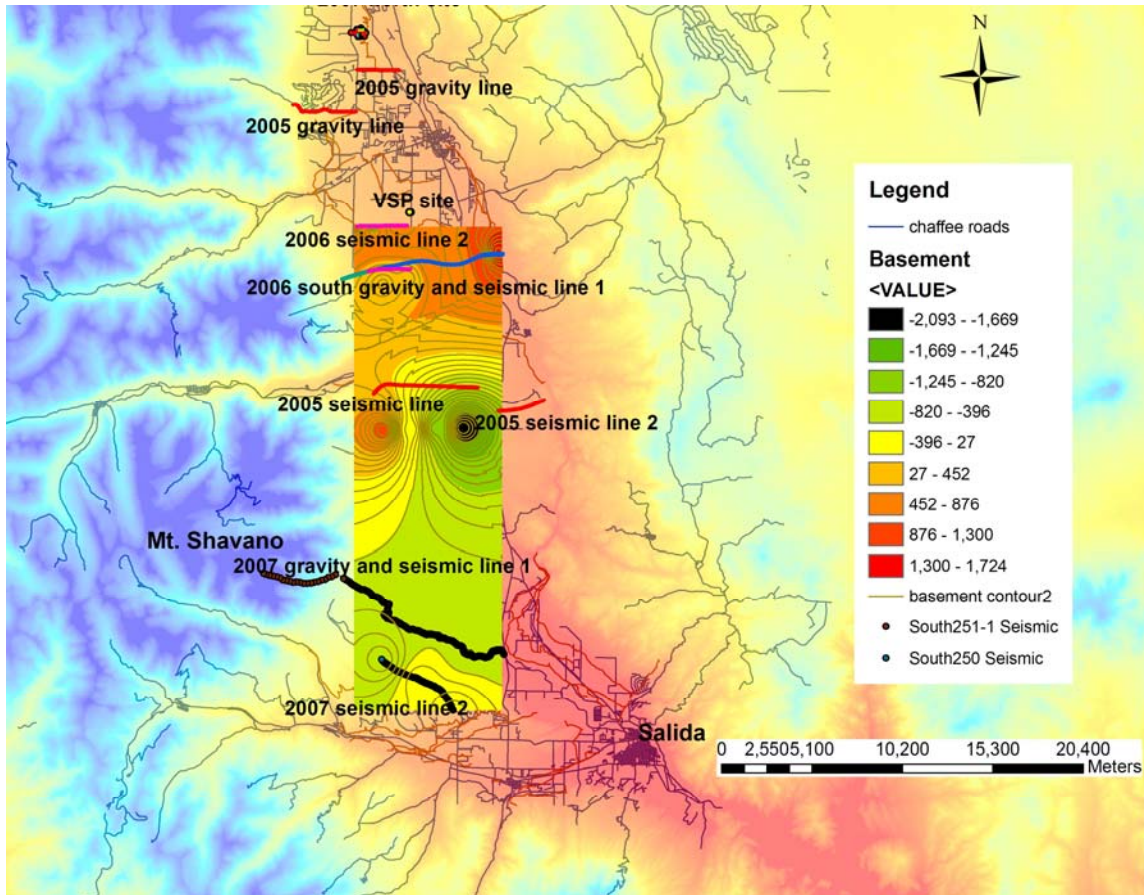
Figure 6.C.1: The rectangular portion that extends over all of the seismic lines is a contour map of the Precambrian basement rock. In general, the basement dips to the West and the South. This plot contains 24 data points over the entire basin and thus the interpolation method is low resolution. However the overall trend can still be seen as the basin gets deeper towards the south.
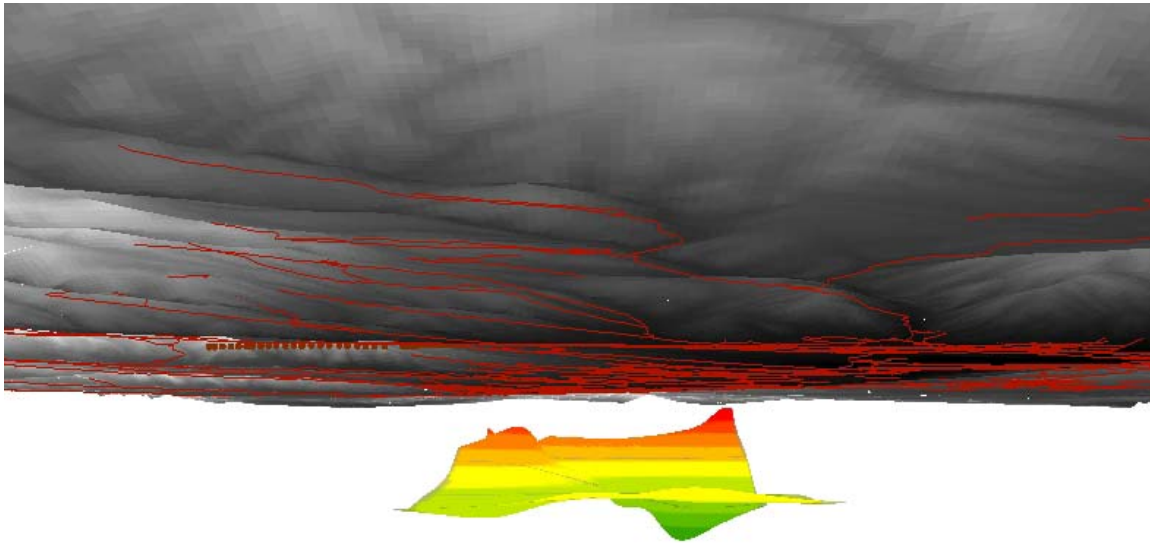
Figure 6.C.2:  The 3D colored surface plot is a contour map of the Precambrian basement rock.  The grey area above the contour plot is a 3D topography model of the entire Chaffee County.  This is a view from the South looking to the North.  In general, the basement dips to the West and the South.

## Conclusions

From the deep seismic and gravity data, many conclusions can be drawn.  Major faults exist on the west side of the valley which can often be seen on the surface as faceted spurs.  The Precambrian basement rock becomes shallower toward the East.  The deepest basin fill is in the west and some minor faults exist in the middle of the basin through the basin fill.  With the exception of the data acquired in 2007, the gravity data is consistent throughout the valley.  This might be due to the fact that the 2007 gravity data is the only data with a terrain correction.  The 2007 gravity line is closer to the complex region of the Poncha Pass transfer zone and, therefore, could be more chaotic due to more complex faulting.  Overall, the same trend exists in all gravity lines due to the fact that the basement is shallower to the east throughout the valley.

# Chapter 7: Field Camp 2008 Plan

## *Objectives*

For the past three years, the Upper Arkansas River Valley has been the focus of study by several junior classes in the Geophysical Engineering department of the Colorado School of Mines. The 2005 junior class studied one particular area of the Valley using the same geophysical methods discussed thus far. Similarly, the class of 2006 gave a different area its due attention, having moved south of the 2005 area. The junior class of 2007 attempted to study yet another area, having moved farther south down the valley. The succession of field camps in the Chaffee County was designed to gain a complete and accurate picture of the whole Upper Arkansas River Valley, starting at the northern end of the Valley and moving, in a general direction, down to the south end. However, more challenges still remain. In order to make a thorough analysis of the Upper Arkansas River Valley in its entirety, the 2008 junior class must conduct an exploration of the Poncha Pass transfer zone at the farthest southern extent of the Valley.

The Poncha Pass transfer zone is the area of Chaffee County spanning from the southern-most extent of the Upper Arkansas River Valley and the northern-most extent of the San Luis Valley, effectively forming the transition between the two valleys. Very little is actually known about the subsurface of the valley itself and even less is known about the transfer zone. One popular theory, proposed by Dr. Robert (Bob) Raynolds, is that the normal listric faults bounding the Collegiate Range at the west end of the Upper Arkansas River Valley and the Sangre De Cristo Mountain Range at the east end of the San Luis Valley die out at the transfer zone. Specifically, the slip of these listric faults decreases as the faults move to meet each other in the transfer zone. Figure 1 depicts this theory in detail. In addition, other theories abound with arguments for and against.
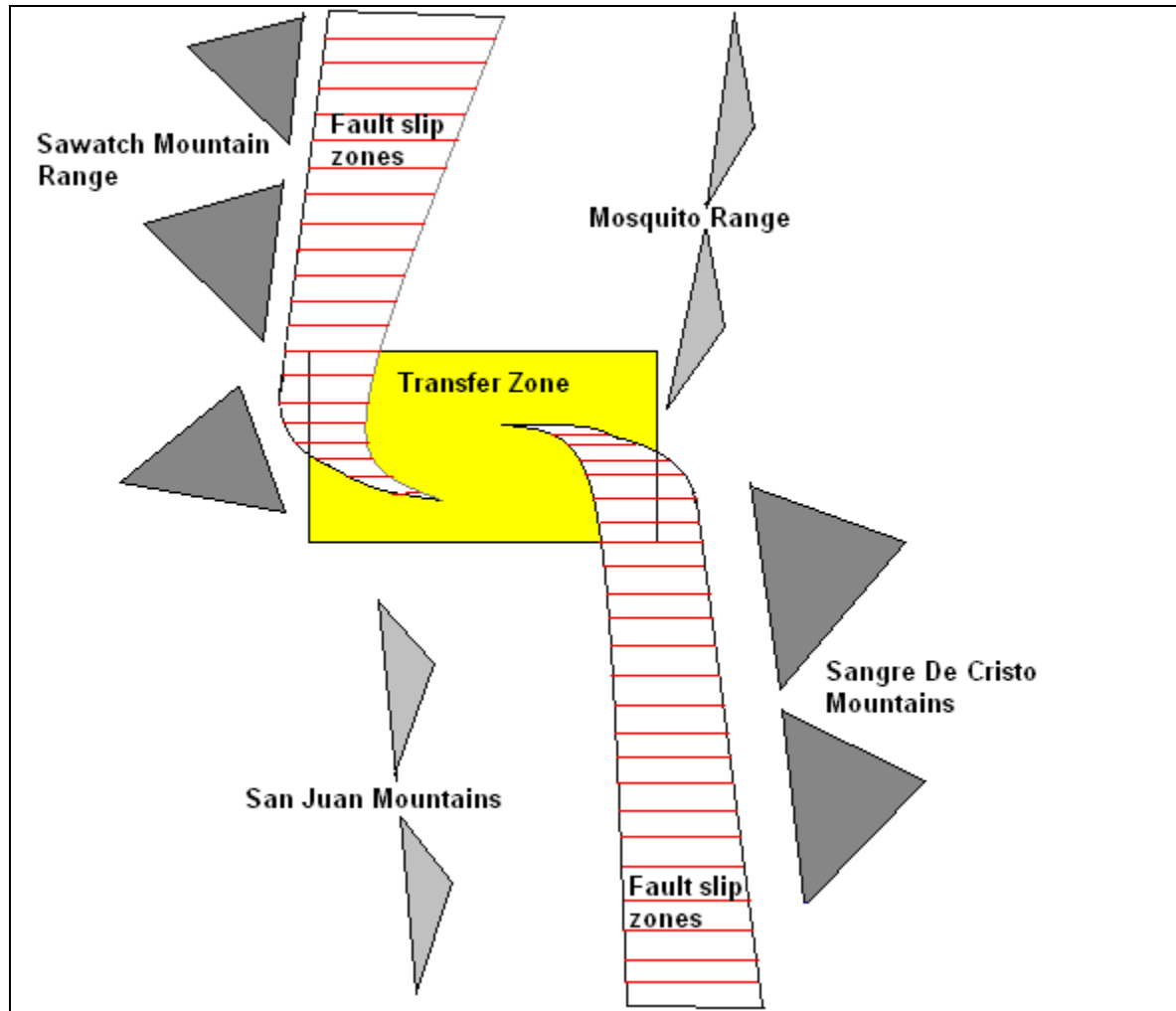
Figure 7.A.1:  Depiction of transfer zone between the Southern Upper Arkansas Valley and the Northern San Louis Valley.

We propose two possible deep seismic and gravity lines running from north to south that cross the northern part of the transfer zone.  We also propose a gravity line that runs south along US highway 285, south of Poncha Springs.  These three lines may give insight on how the fault switches from the west to east side of the valley.  The proposed lines are shown in figure 7.2.
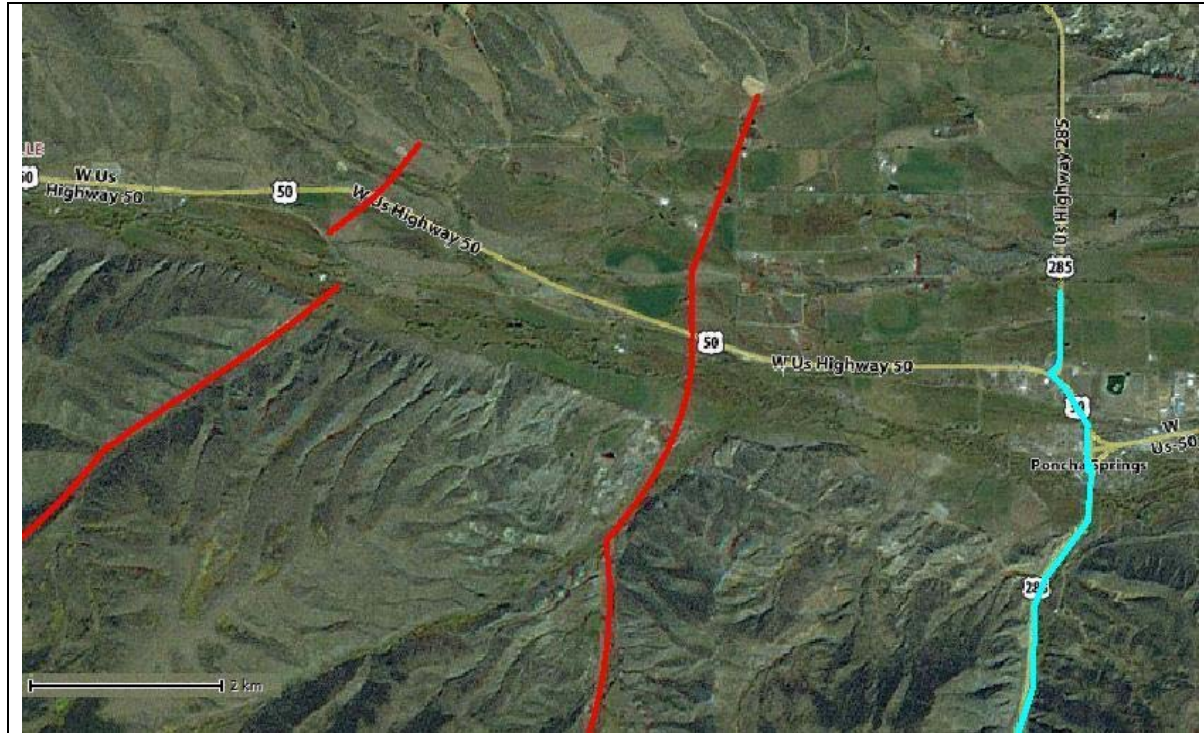
Figure 7.2: This figure shows the proposed gravity and deep seismic lines. The red lines are for gravity and seismic. The blue line is for gravity only.

## *Acquisition Plan*

The purpose of the 2008 Summer Field Camp session is to make a comprehensive study of the Poncha Pass transfer zone, focusing on structural geology of the Valley at that location as well as advancing the understanding of the groundwater situation. In order to accomplish this goal, the students of the junior class of 2008 will spend several days examining the geology of Poncha Pass from one outcrop to the next. In addition, they will make use of the variety of geophysical methods, such as deep seismic, gravity, direct current resistivity, and electromagnetics, to characterize the subsurface structure and complement their field observations. Like the 2007, the class of 2008 will use the deep seismic and gravity methods for characterization of the structural geology and the direct current resistivity, shallow seismic, and electromagnetics methods for near-surface research. We propose that the 2008 field camp returns to the same North site at Frosty Roe's property to investigate the effects of irrigation ditches on the water table. Figure 7.3 shows several proposed surveys at the North site.
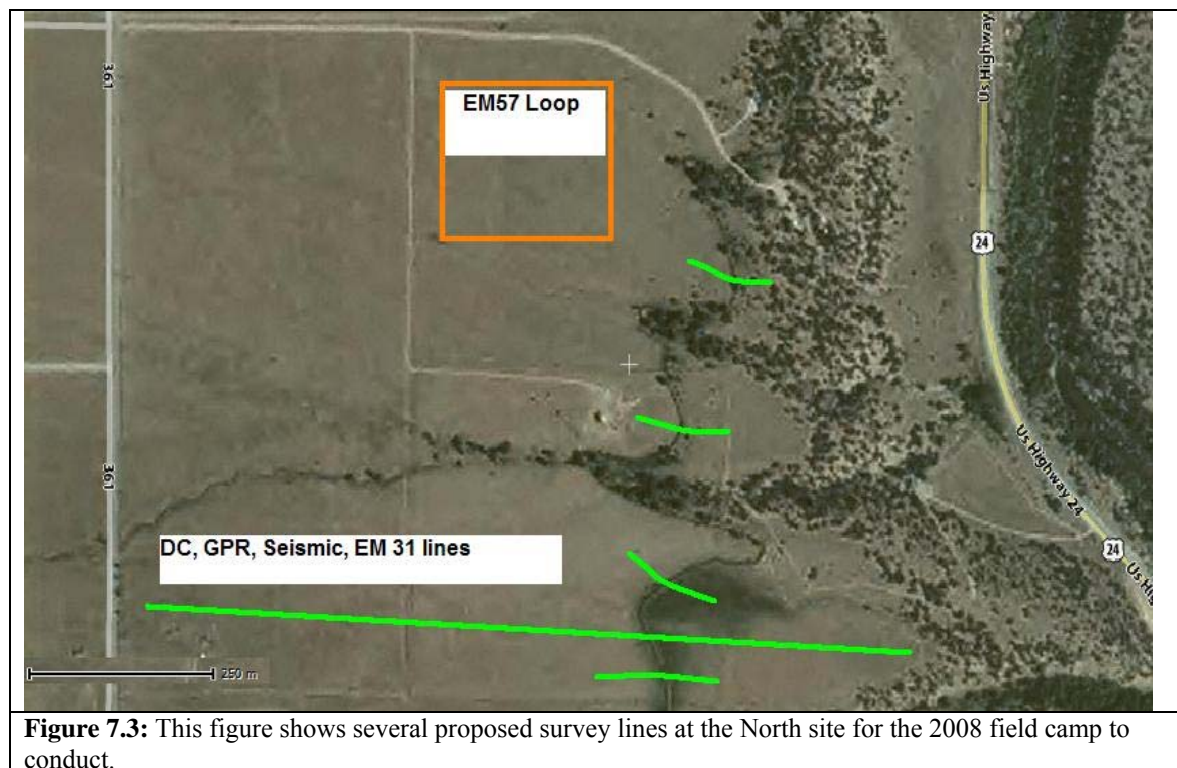
**Figure 7.3:** This figure shows several proposed survey lines at the North site for the 2008 field camp to conduct.

By performing another intensive analysis, the 2008 junior class of the Geophysical Engineering department at the Colorado School of Mines will have made their corresponding contribution to the Upper Arkansas River Valley investigation.

# Appendix A: Geologic Maps
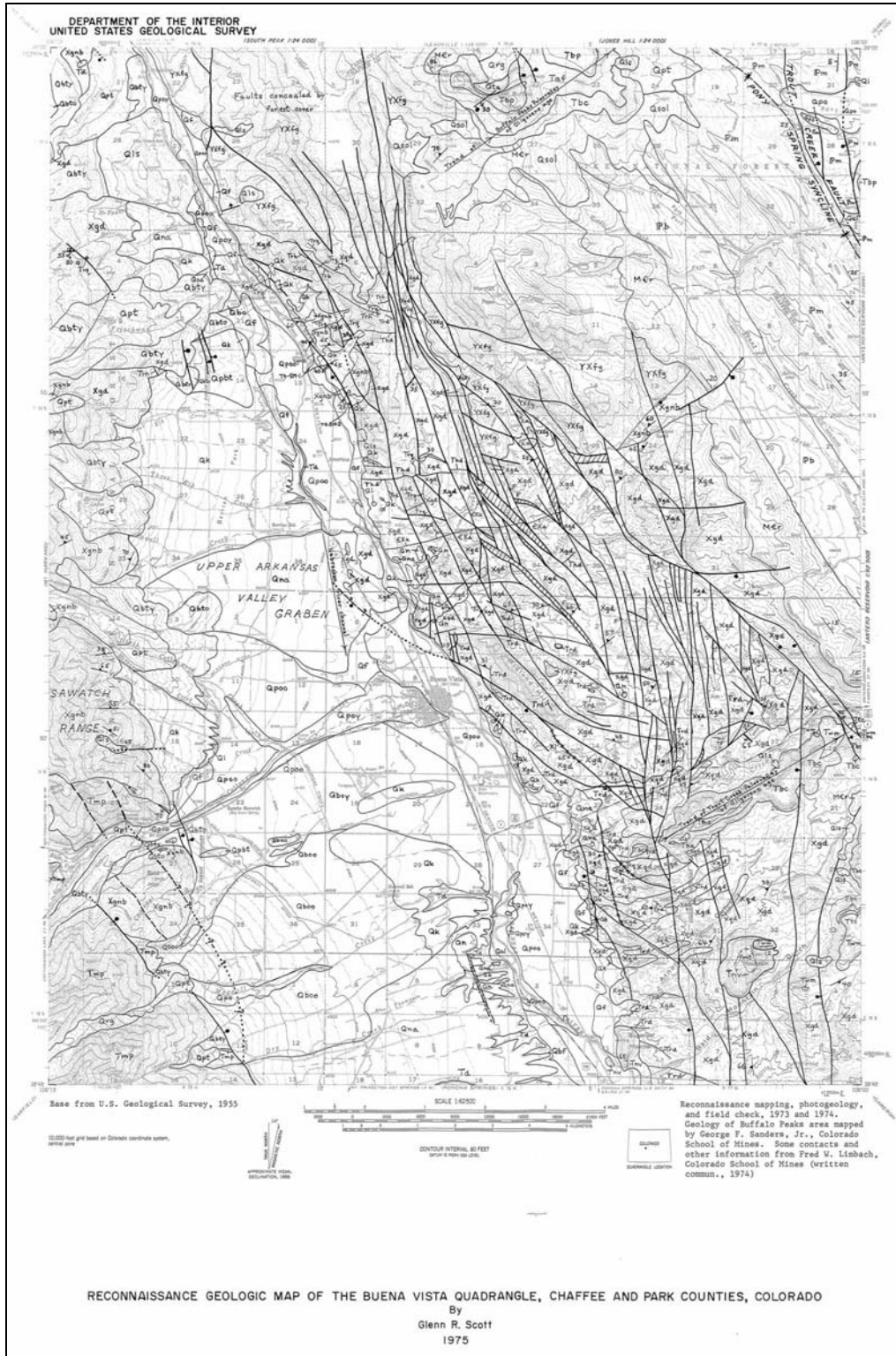


Figure 1A: Northern half of the UGSS Reconnaissance Geologic Map of the Buena Vista Quadrangle, Chaffee and Park Counties, Colorado [4]
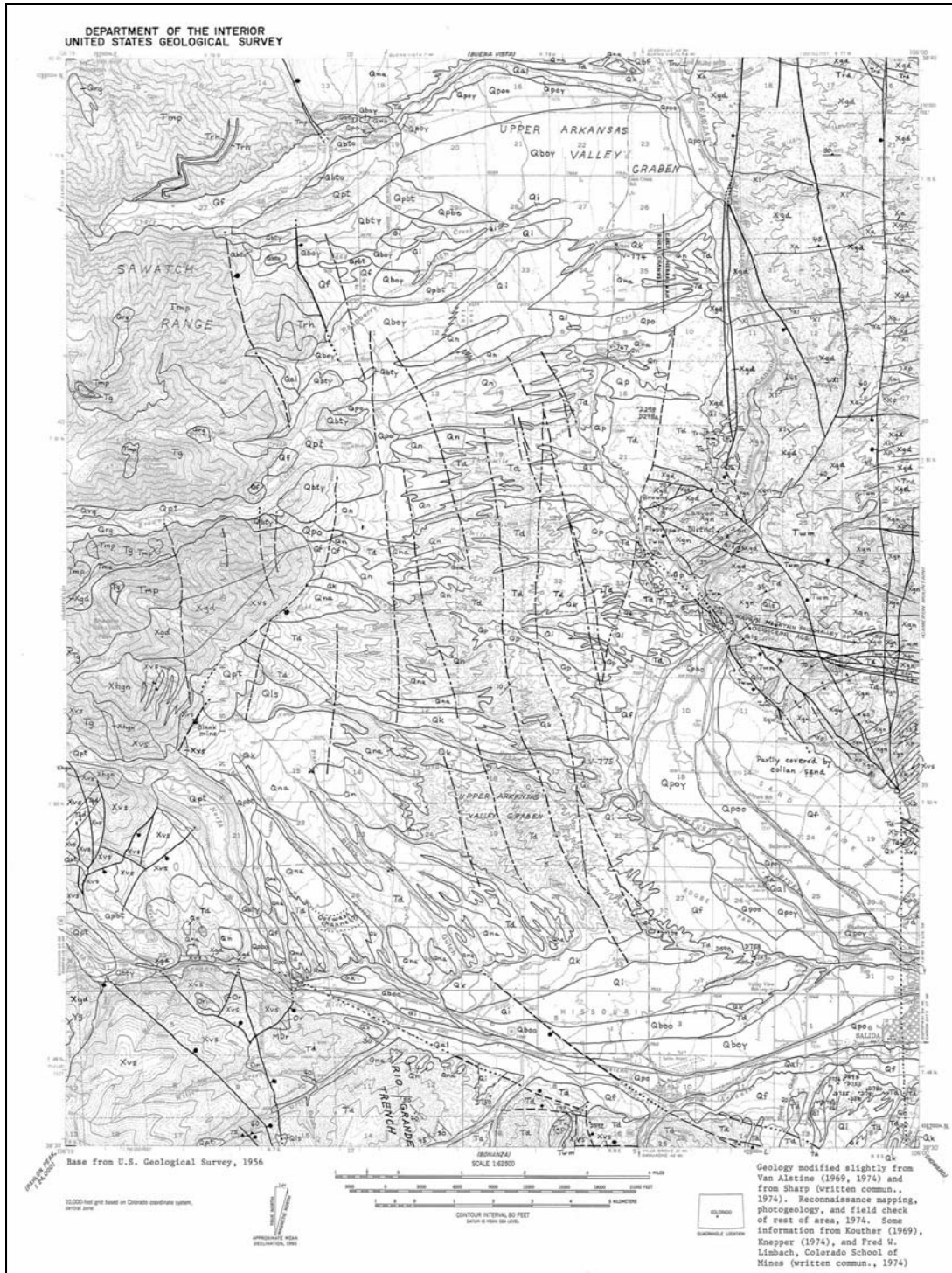
Figure 2A: Southern half of the UGSS Reconnaissance Geologic Map of the Buena Vista Quadrangle, Chaffee and Park Counties, Colorado [4]

Figure 3A: Map key, and Geologic Unit Description for the UGSS Reconnaissance Geologic Map of the Buena Vista Quadrangle, Chaffee and Park Counties, Colorado. [4]

## Appendix B: Deep Seismic Flows

This Appendix contains the read me file to operate the flows included in the Field Camp 2007 Data Disk.

All Seismic data, processing flows, etc. is on the DVD made for us by GX Technologies. The last pass on ln 30 (CR 250 has not been done yet)

To use:

1:  Create area in Promax...call it Archive for example
2:  Create appropriately named line in Archive
3:  Create appropriately named flow in above line
4: Add [List/Restore from Tape] to the flow

Type of operation:                              Restore
Type of files to restore/list:                  Area
Disable checking for available disk space?   No
Skip seismic trace files?                       No
        Use primare storage fore trace files? Yes
          Trace File restoration method:                Most Space
List file names as processed?               Yes
Ignore checksum errors?                          No
Type of storage to use:                          Disk Image
Enter DISK file path name:                       [enter path name here...dvd called fc2007_image]

5:  Execute Flow

## Appendix C: Gravity Correction Plots

Plots below follow the information provided in the Data Reduction section of the Gravity Report.
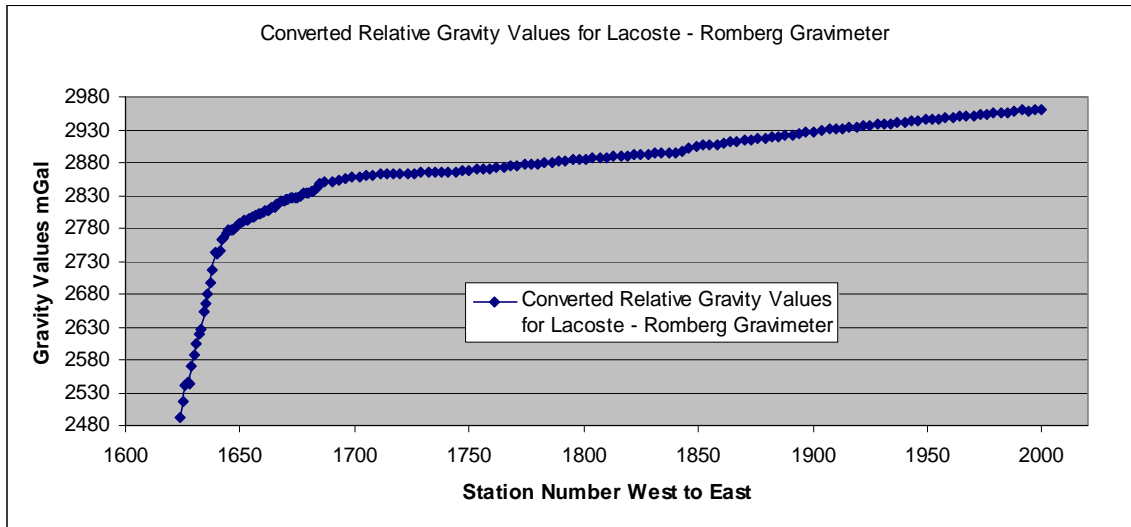


Figure 1C:  Original gravity measurement converted to scaled relative gravity using the conversion chart supplied with the Lacoste Romberg Gravimeter.
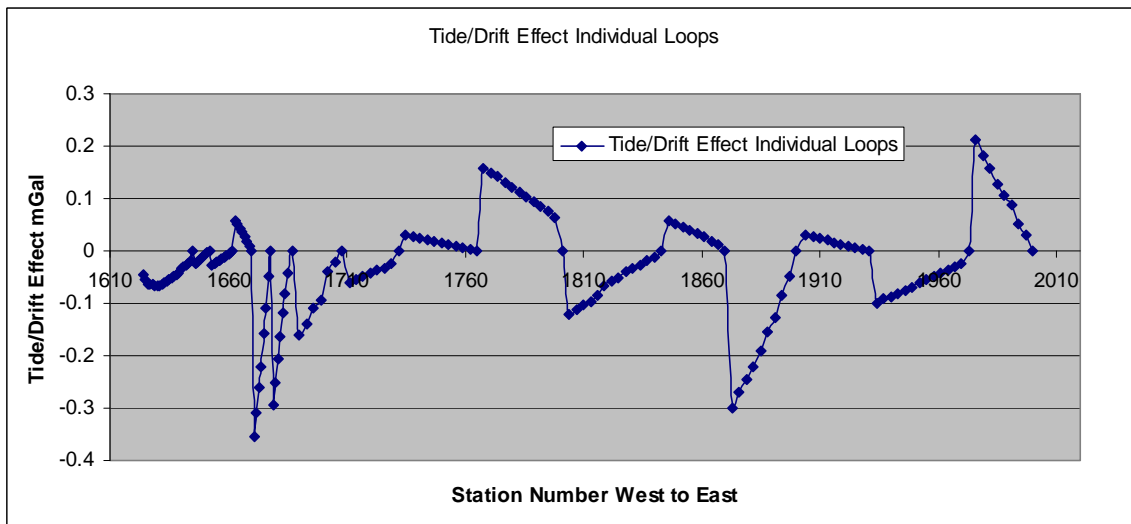


Figure 2C:  Tide/drift correction calculated over the entire line.  Notice the vertical scale being about 0.1-0.2 mGal, which is near the threshold of repeatability of the gravimeter.
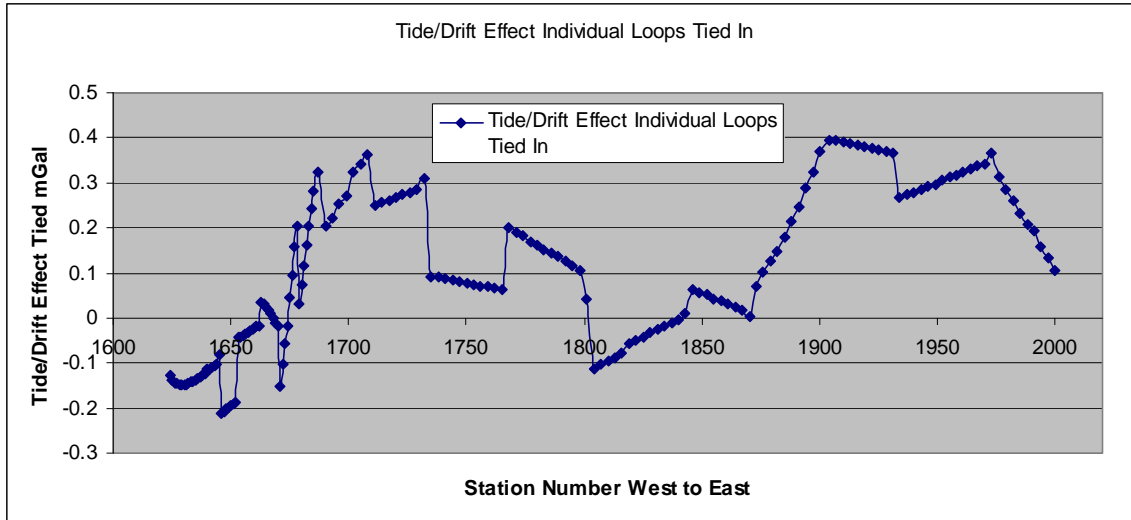
Figure 3C: Tide drift after the Base station loop to tie all of the base stations together.
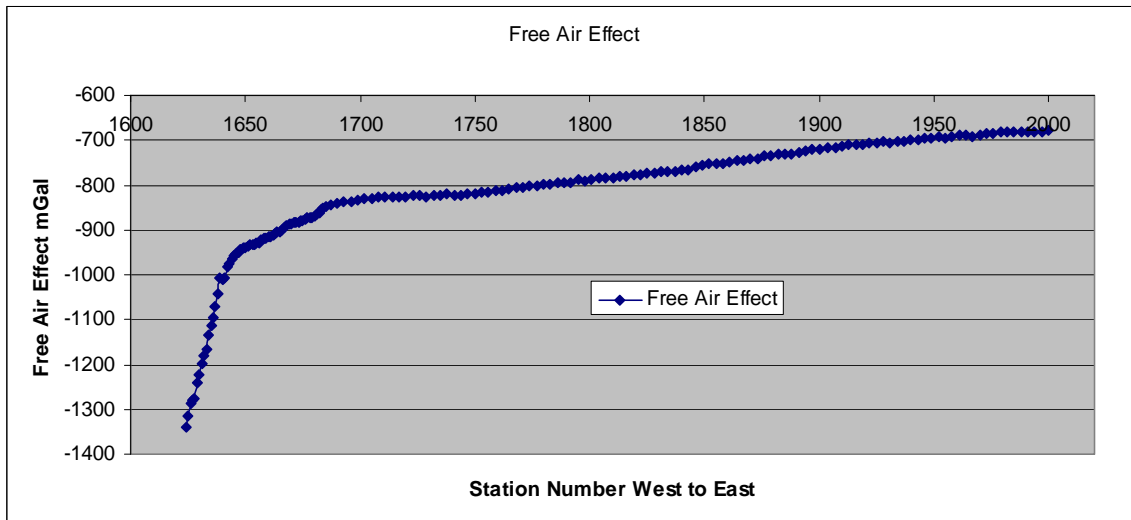


Figure 4C: Free air correction. Notice how significant these corrections are. This is the biggest source of error for the entire line.
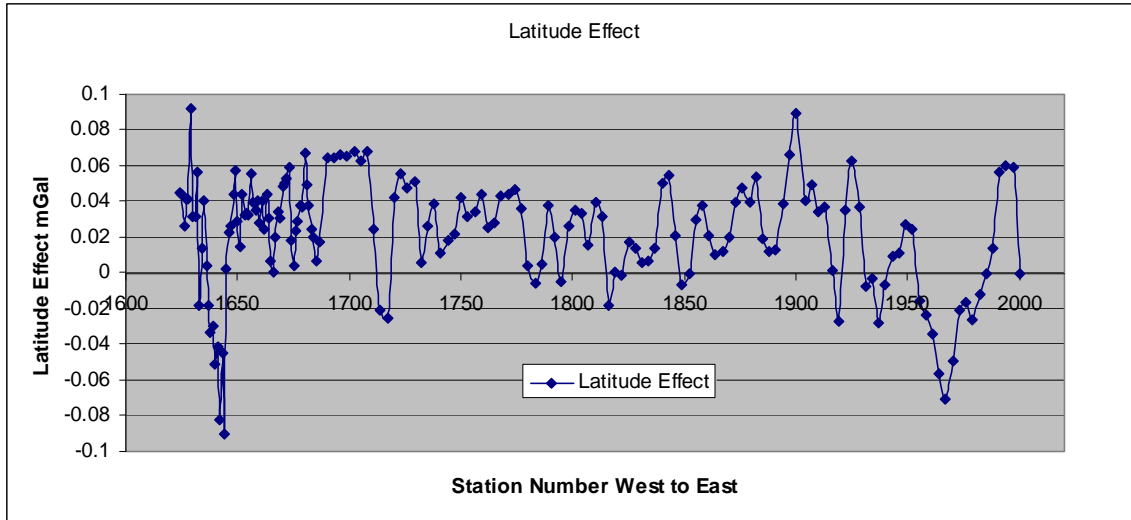
Figure 5C: Latitude Effect. Notice that this chart is almost insignificant since there was a relatively constant latitude on the East-West running line.
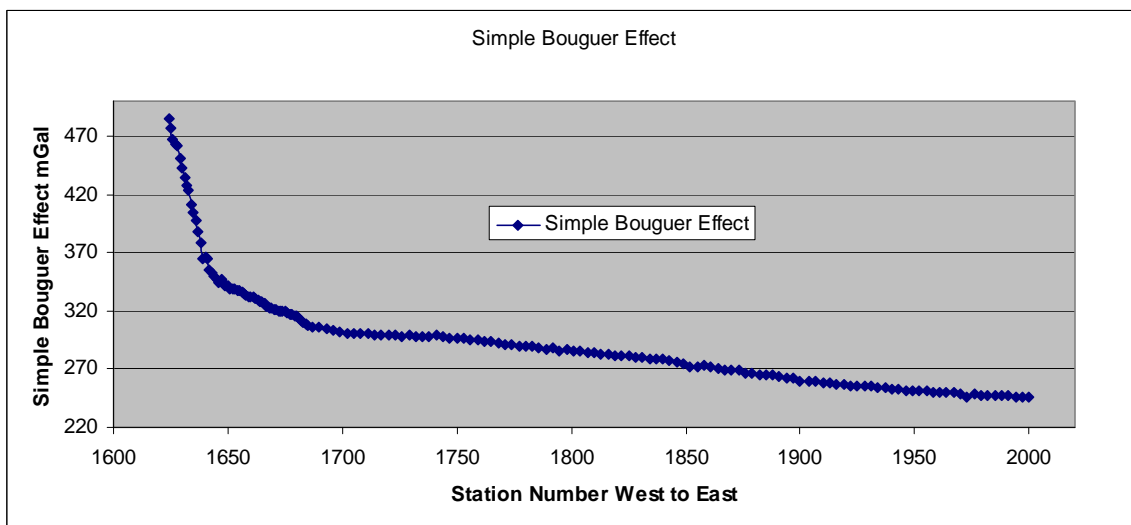


Figure 6C: The Bouguer effect is a mirror opposite of the free air correction. This correction essentially fills the area subtracted out by free air with an infinite slab of constant density.
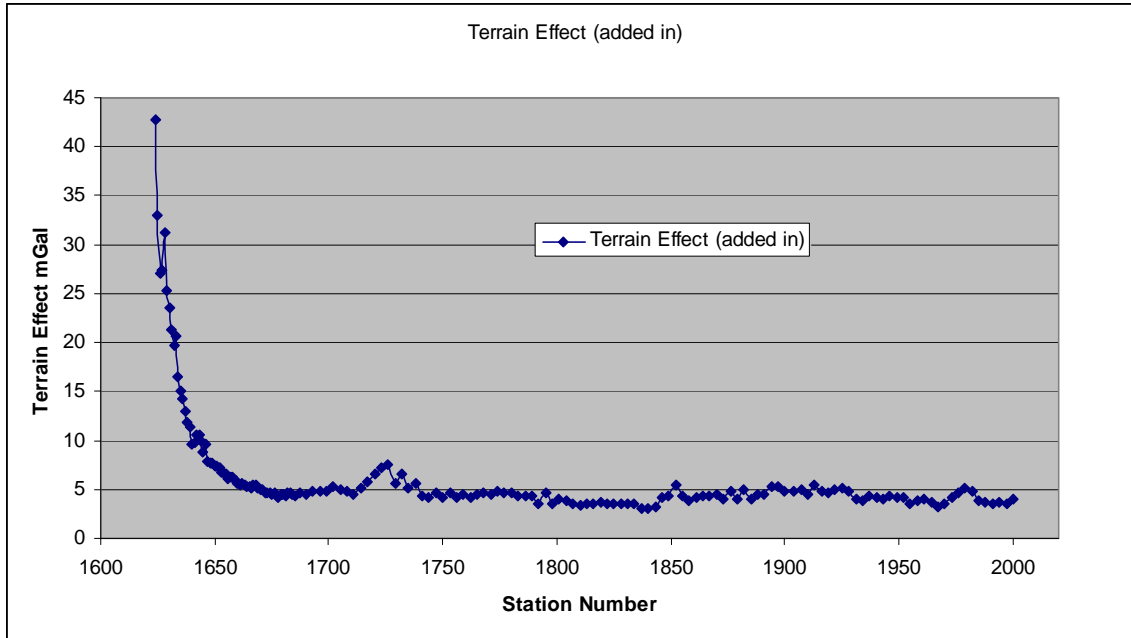
Figure 7C:  The terrain effect is essential for the western edge of the line when the elevation increases and the points are closer to the high mountains.
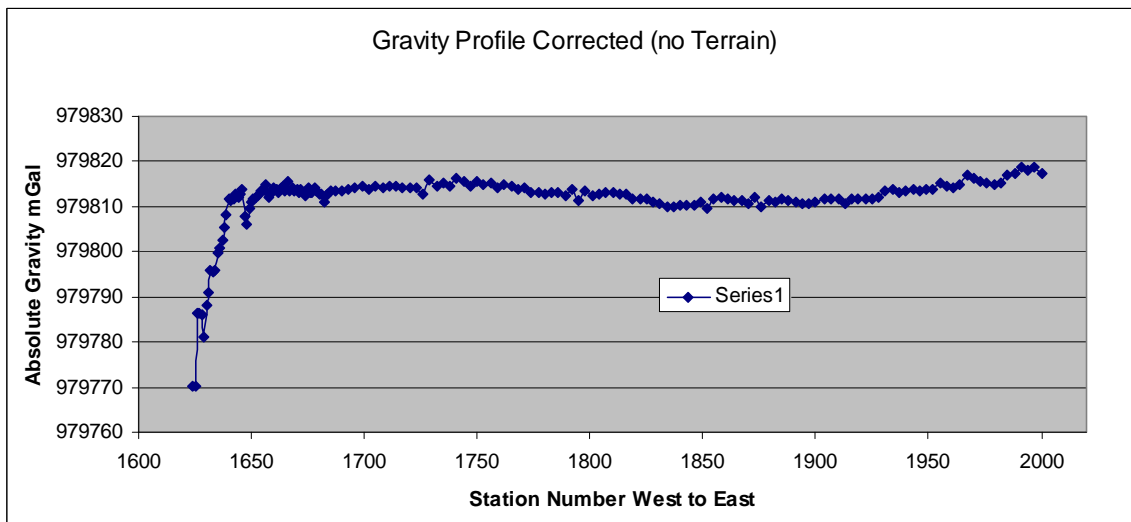


Figure 8C:  Final corrected gravity profile before the terrain correction is applied.. Notice that the western edge is significantly under corrected without the terrain correction.  The dip seen on the western edge is artificial.
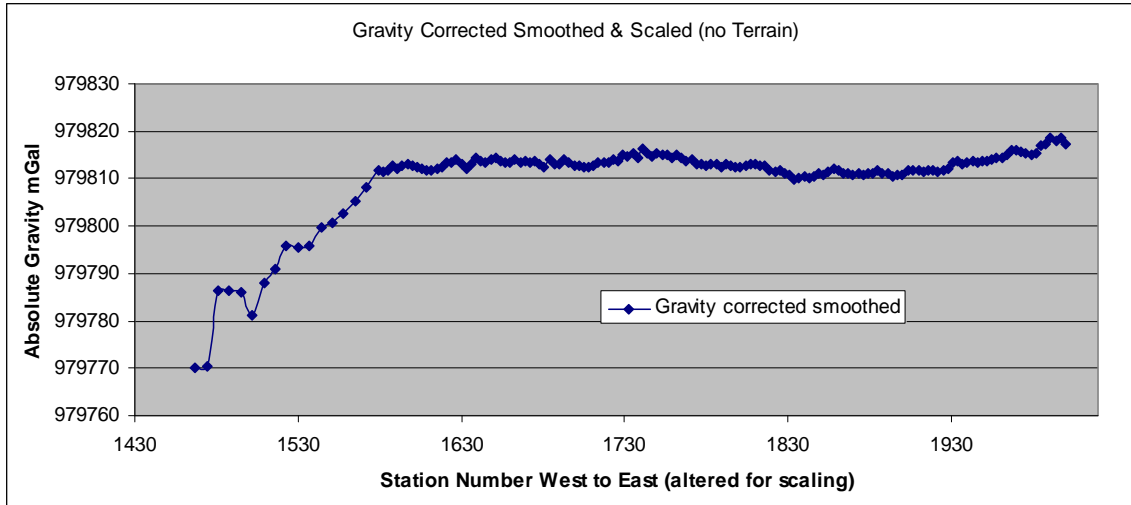
Figure 9C:  Gravity profile that has been smoothed to correct for error in elevation data.
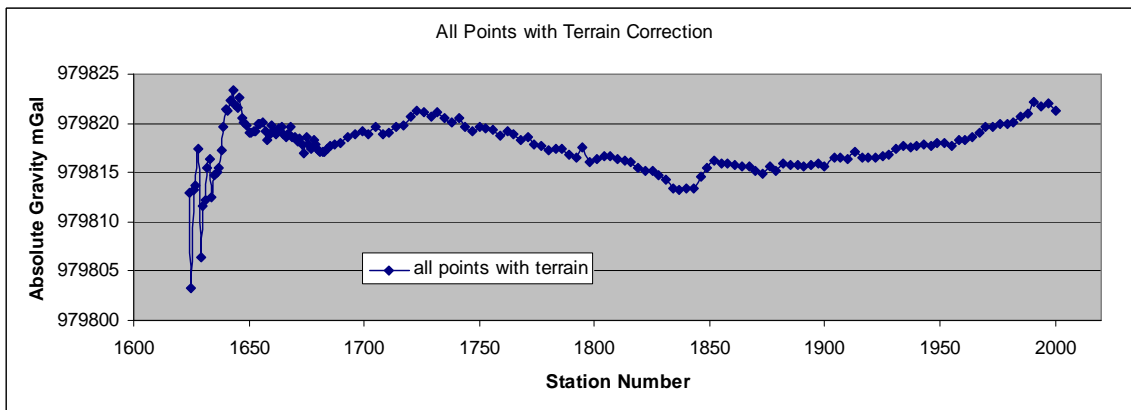
Figure 10C:  Terrain correction applied to the smoothed data.  Notice that the western edge is still slightly under corrected due to limitations discussed in the error analysis section.
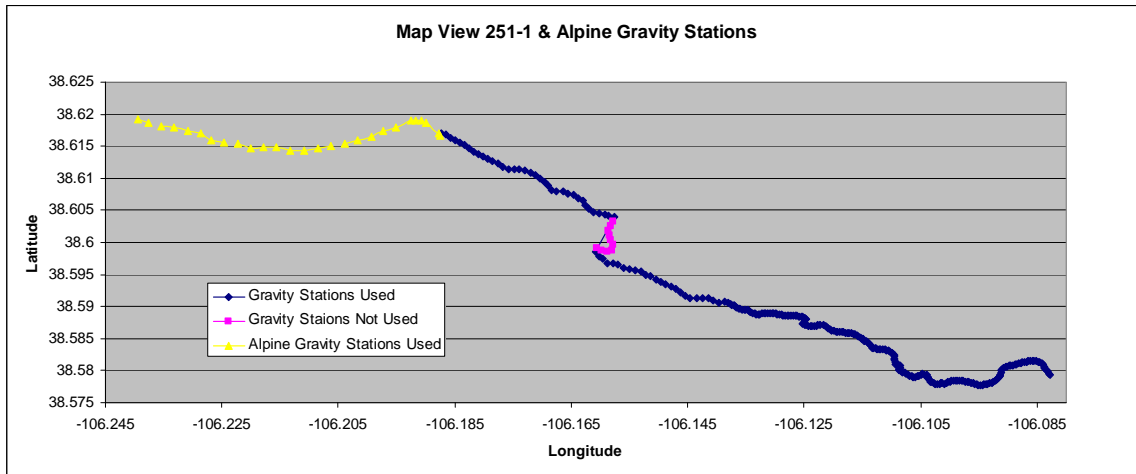
Figure 11C:  Spatial plot of the gravity line showing the points in pink that were removed to create a straighter profile.

## Appendix D: DC Pseudo Sections
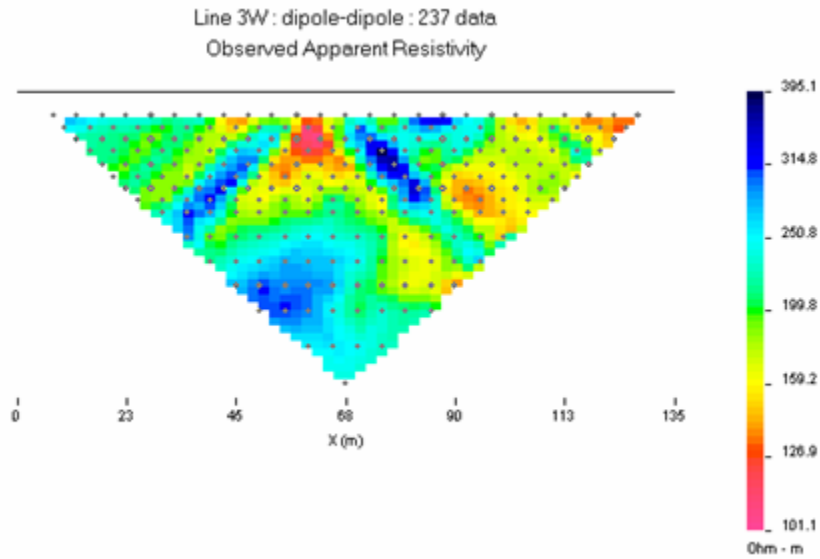


Figure 5.B.6: A pseudo section for Line 3W; N to S, 5m spacing.
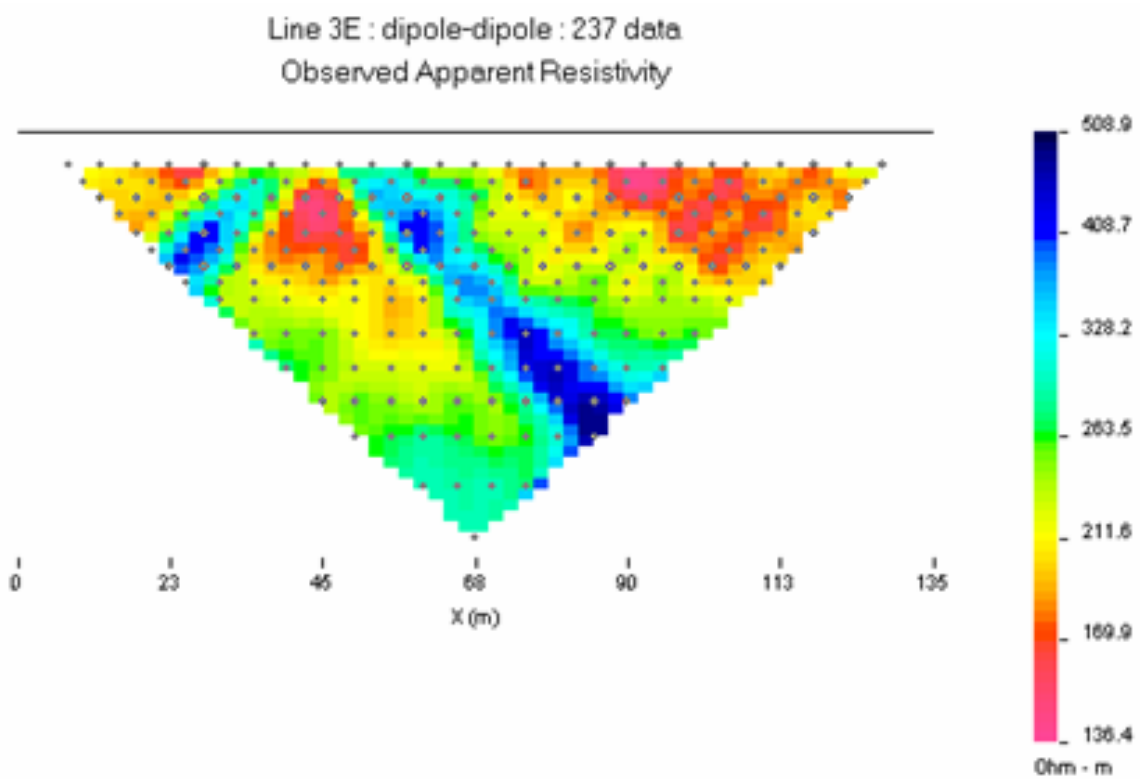


Figure 5.B.7:  A pseudo section for Line 3E; N to S, 5m spacing
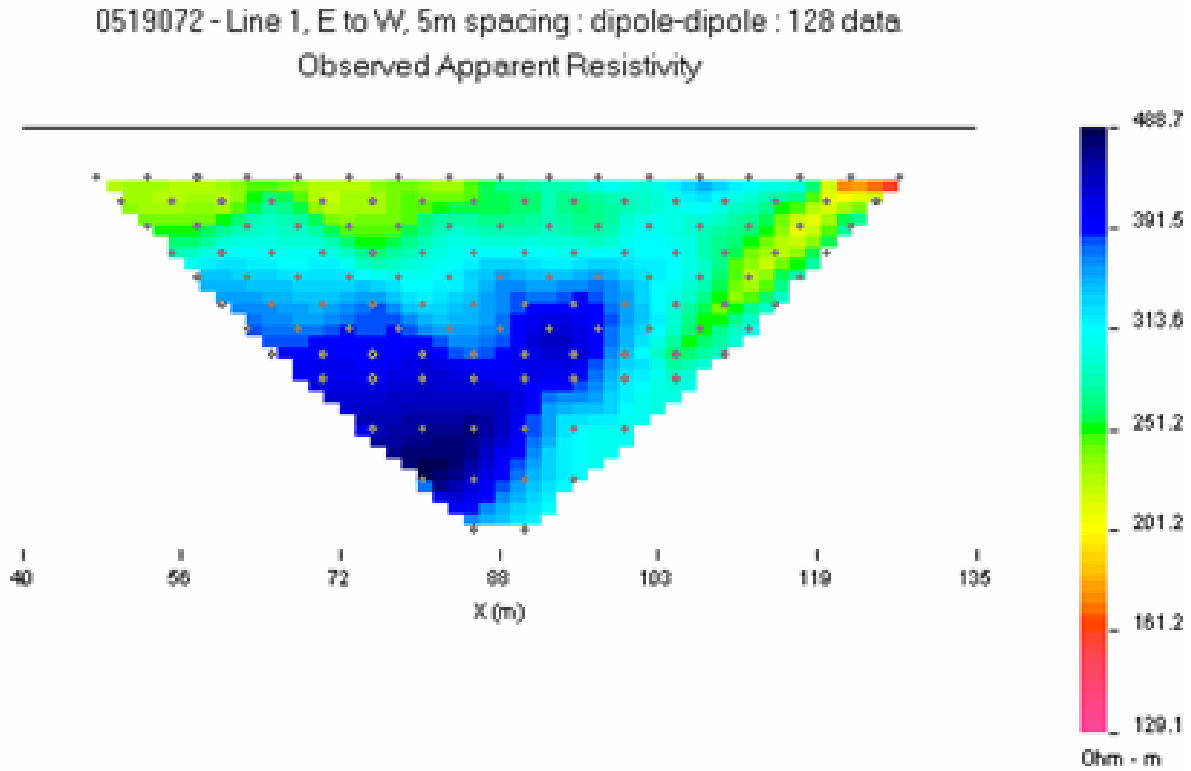
Figure 5B.8:  A pseudo section for Line 1;E to W, 5m spacing.
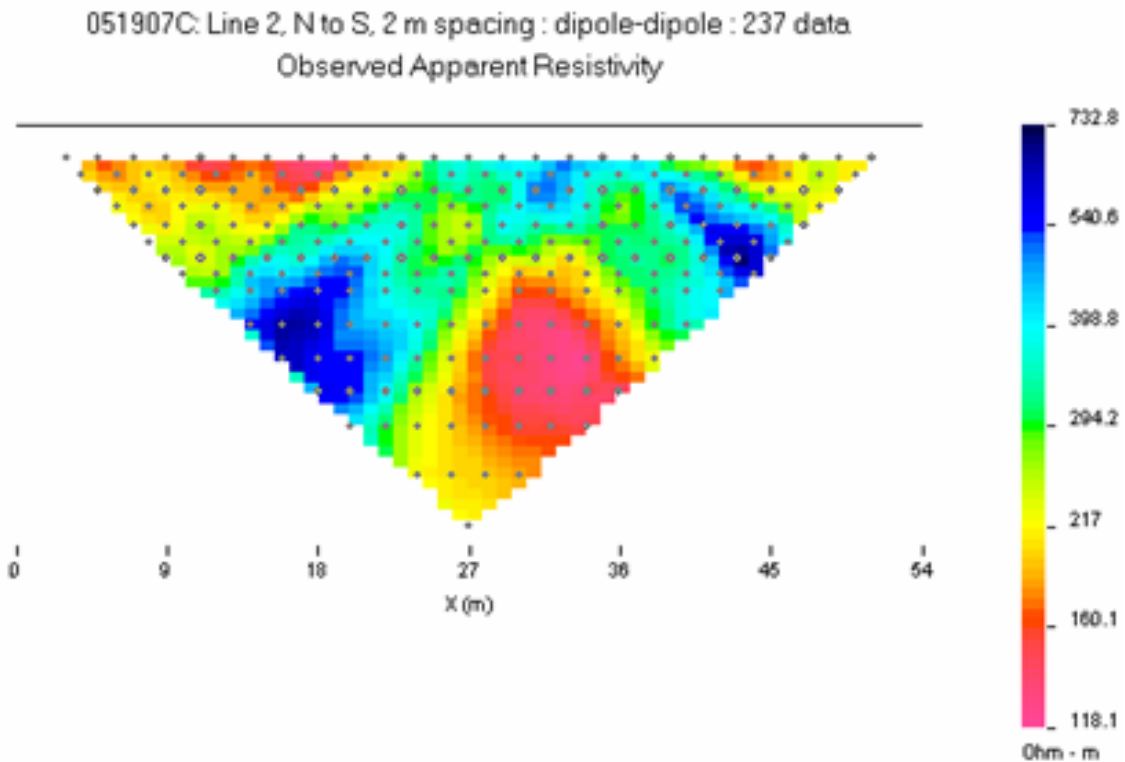
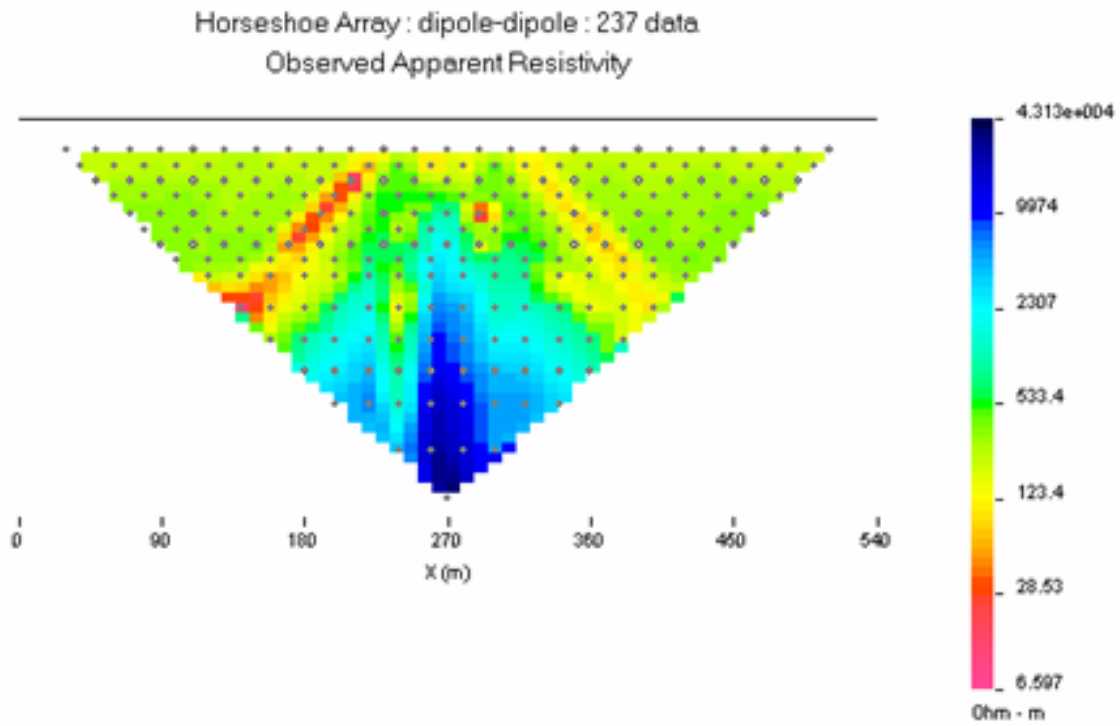Figure 5B.9:  A pseudo section for Line 2; N to S, 2m spacing.

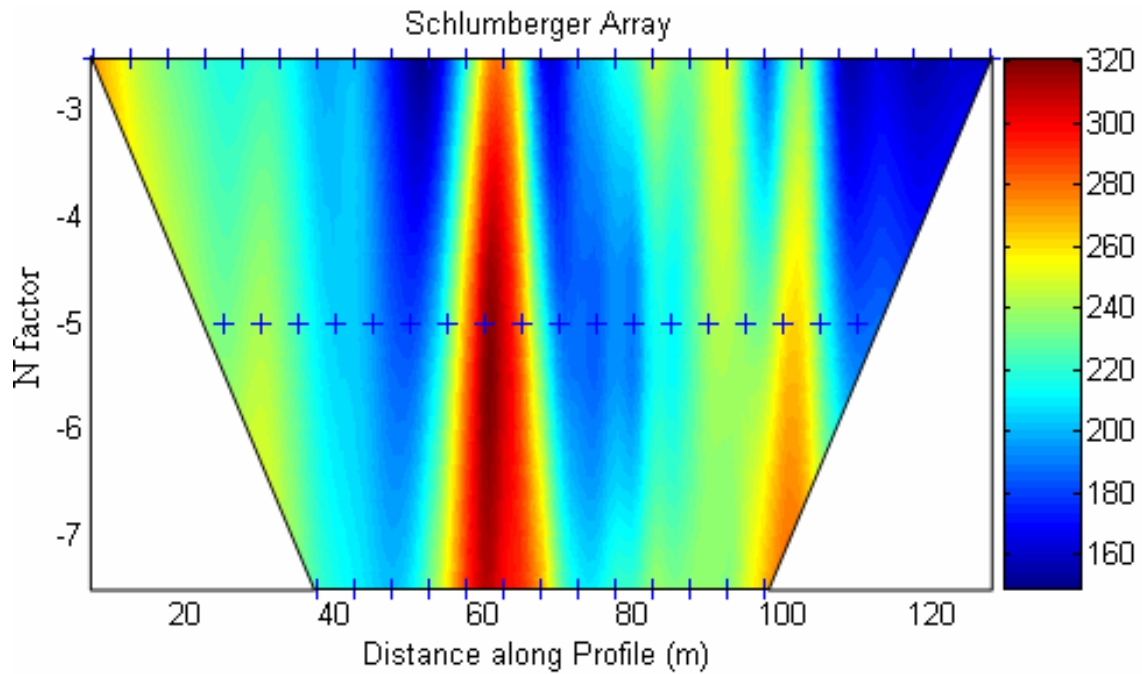Figure 5B.10:  A pseudo section for the horseshoe array.



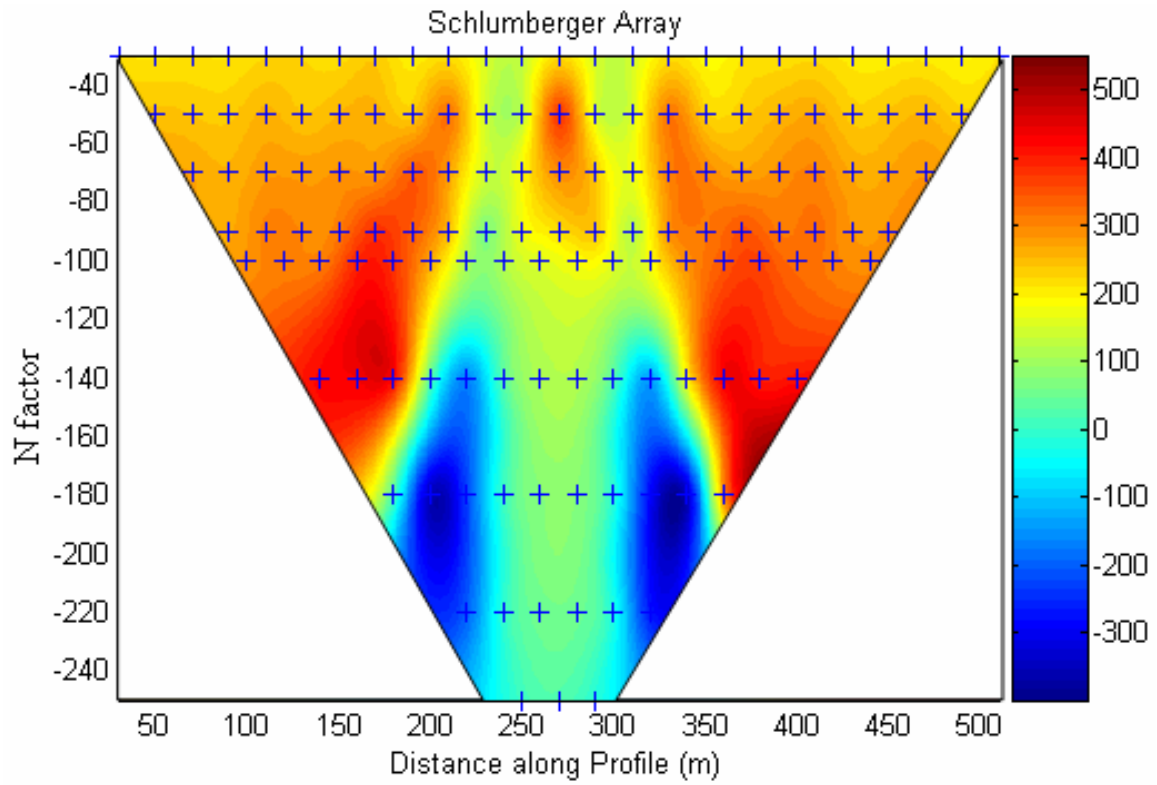Figure 5B.11:  A pseudo section for the Line 3W; S to N, 5m spacing. (Schlumberger)

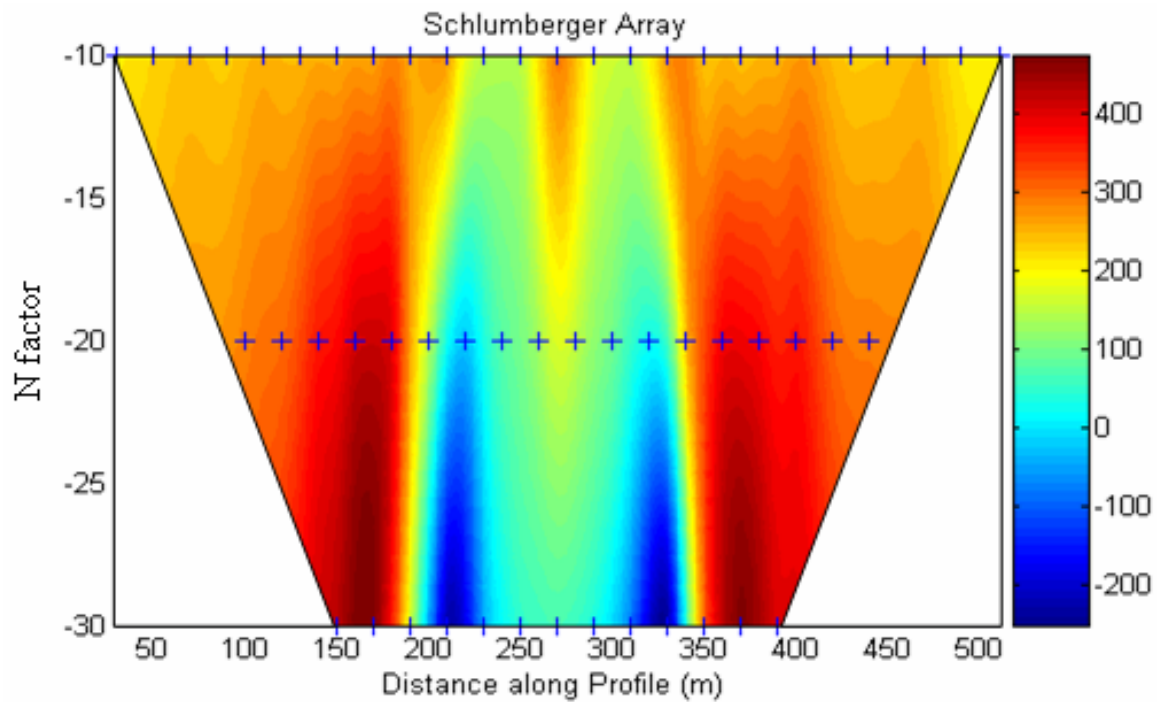Figure 5.B.12:  A pseudo section for t the horseshoe array. (Inverse Schlumberger)



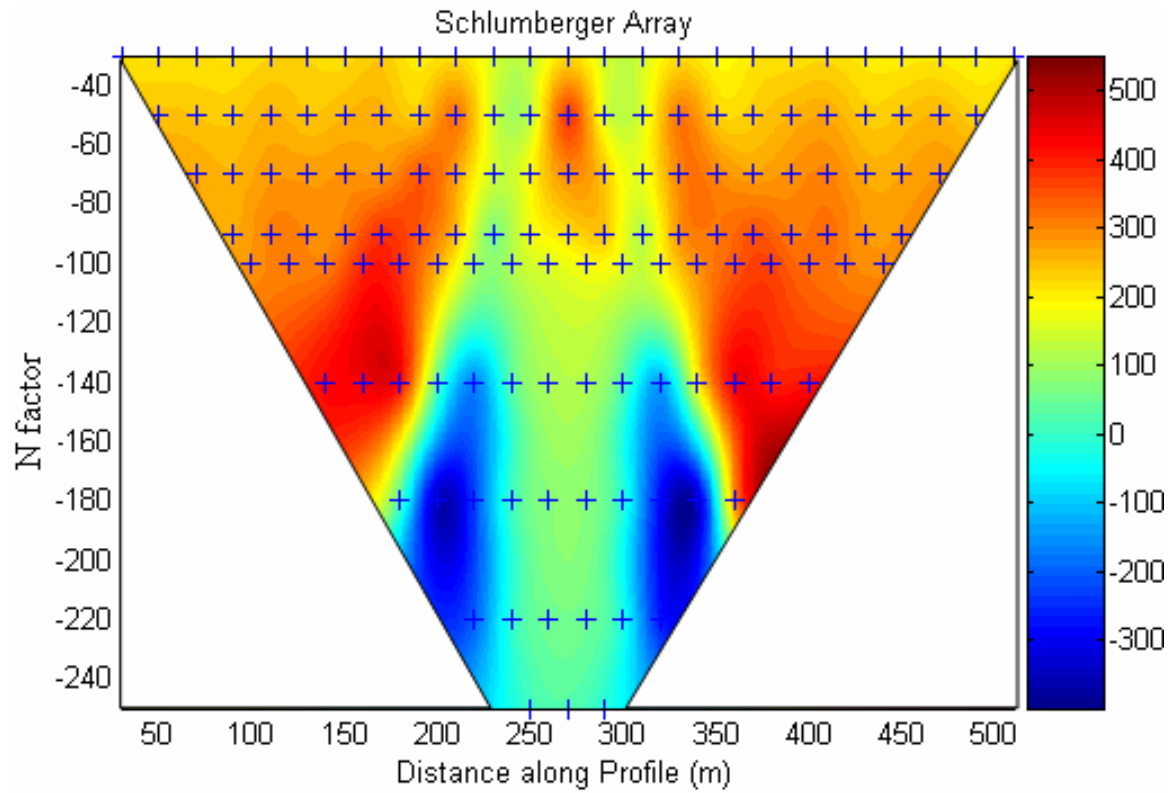Figure 5.B.13:  pseudo section for t the horseshoe array. (Schlumberger)

Figure 5.B.14:  A pseudo section for t the horseshoe array. (Inverse Schlumberger)
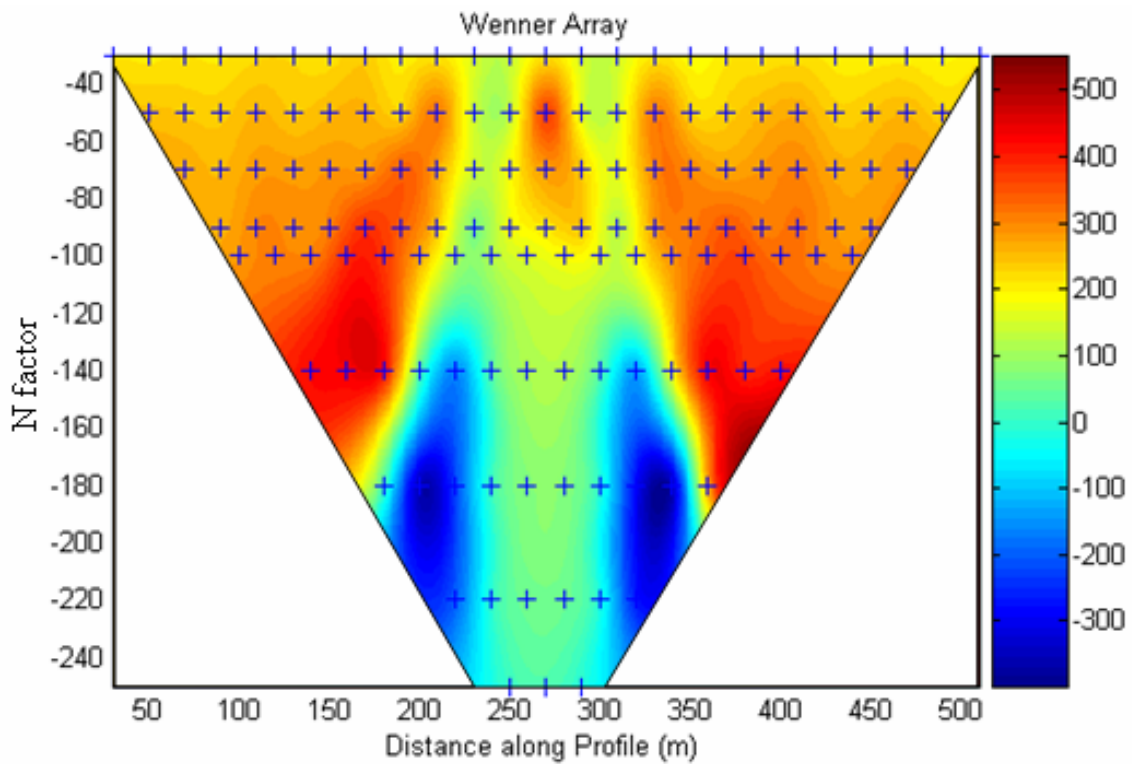


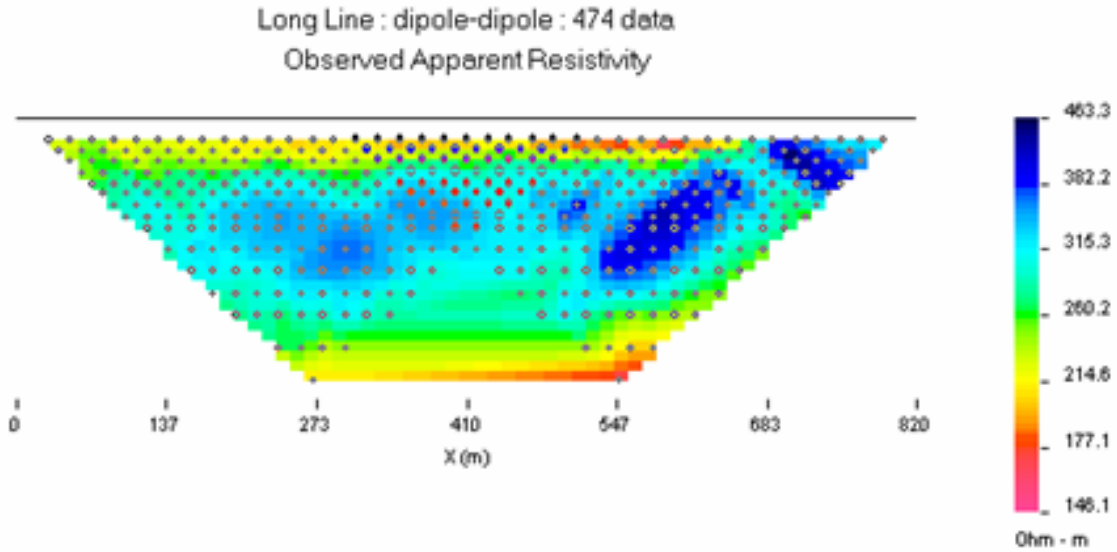Figure 5.B.15:  A pseudo section for t the horseshoe array. (Wenner)

Figure 5.B.16:  A pseudo section for the Long Line; West to East 20m electrode spacing.
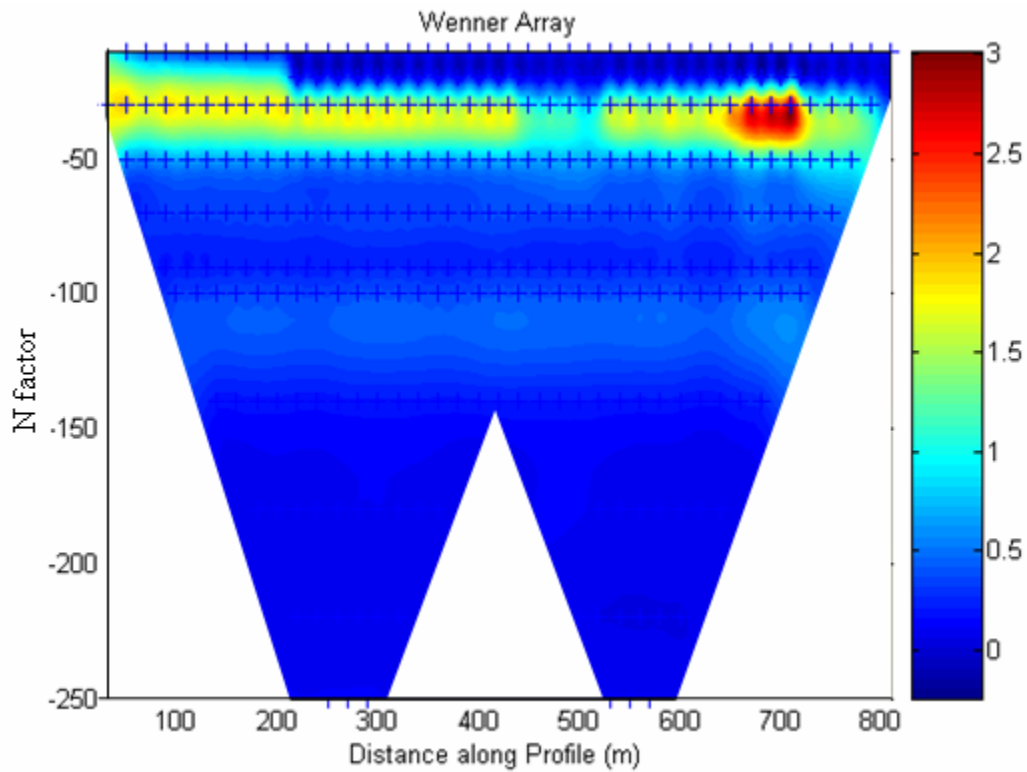


Figure 5.B.17:  A pseudo section for the Long Line; W to E line, 20 m spacing (Wenner)

# Appendix E: VSP Seismic UNIX Flows

Vertical Seismic Profiling

The equation used for VSP is a simple one: $h^2 = v_0^2 t^2 - d^2$, where h is offset, d is receiver depth, t is travel time from the source to the receiver, and $v_0$ is the material velocity. Velocity is the unknown. The units of h and d are meters; the units of t are seconds; and the units of $v_0$ are meters per second.

The computer codes to combine all of the shot records for a depth are as follows:

To see the vertical component of the waves:

```
#!/bin/sh

# concatenating all shotrecords:
cat 10m_vertical.txt 15m_vertical.txt 20m_vertical.txt 25m_vertical.txt 30m_vertical.txt
35m_vertical.txt 40m_vertical.txt 45m_vertical.txt 50m_vertical.txt 55m_vertical.txt
60m_vertical.txt |\
# convert all ascii data to a binary file:
a2b n1=1 | suaddhead ns=10240 |\
# set the time sampling interval:
sushw  key=dt a=100 |\
# set the shot and receiver locations:
sushw key=sx,gx a=5,10 b=5,0 c=0,5 i=10,10 j=10,10 |\
# data.su
# window entire su file by key word:
suwind key=gx min=$1 max=$1 tmax=0.25|\
suop op=avg |\
# normalize each trace:
suop op=norm|\
sufilter f=1,10,25,50,100 amps=0,1,1,1,0|\
#supswigp key=sx label1="time (s)" label2="offset (m)" perc=98 > $1m_plot.ps
suxwigb key=sx label1="time (s)" label2="offset (m)" title="receiver at $1 m"
suxpicker key=sx
```

To see the shear component of the waves:

```
#!/bin/sh

# concatenating all shotrecords:
cat 10m_radial.txt 15m_radial.txt 20m_radial.txt 25m_radial.txt 30m_radial.txt 35m_radial.txt
40m_radial.txt 45m_radial.txt 50m_radial.txt 55m_radial.txt 60m_radial.txt |\
# convert all ascii data to a binary file:
a2b n1=1 | suaddhead ns=10240 |\
# set the time sampling interval:
```

```
sushw  key=dt a=100 |\
# set the shot and receiver locations:
sushw key=sx,gx a=5,10 b=5,0 c=0,5 i=10,10 j=10,10 |\
# data.su
# window entire su file by key word:
suwind key=gx min=$1 max=$1 tmax=0.25|\
suop op=avg |\
# normalize each trace:
#suop op=norm|\
sufilter f=1,10,25,50,100 amps=0,1,1,1,0|\
#supswigp key=sx label1="time (s)" label2="offset (m)" > $1m_sh_plot.ps
suxwigb key=sx label1="time (s)" label2="offset (m)" perc=97
#suxpicker key=sx
```

To see the transverse component of the waves:

```
#!/bin/sh

# concatenating all shotrecords:
cat 10m_transversal.txt 15m_transversal.txt 20m_transversal.txt 25m_transversal.txt
30m_transversal.txt 35m_transversal.txt 40m_transversal.txt 45m_transversal.txt
50m_transversal.txt 55m_transversal.txt 60m_transversal.txt |\
# convert all ascii data to a binary file:
a2b n1=1 | suaddhead ns=10240 |\
# set the time sampling interval:
sushw  key=dt a=100 |\
# set the shot and receiver locations:
sushw key=sx,gx a=5,10 b=5,0 c=0,5 i=10,10 j=10,10 |\
# data.su
# window entire su file by key word:
suwind key=gx min=$1 max=$1 tmax=0.25|\
suop op=avg |\
# normalize each trace:
#suop op=norm|\
sufilter f=1,10,25,50,100 amps=0,1,1,1,0|\
#pswigp key=sx label1="time (s)" label2="offset (m)" > $1m_plot.ps
suxwigb key=sx label1="time (s)" label2="offset (m)" perc=97
#suxpicker key=sx
```

These codes were run in Seismic Unix.

The following Matlab code was made to make the figures that show the fit of the data at each depth.

```
clear all
close all
```

```
% little script to determine the average velocity up to a receiver at depth
% from a walkaway VSP.

% array of picked depths:
depth = [10 25 35 40 45 50 55 60];

for i = 1:length(depth)
    % reading the picks (created in SU) from a stick:
    x= dlmread(strcat(num2str(depth(i)),'m.txt'),' ')
    % fittin y = ax + b:
    [brob, stats] = robustfit(x(:,1).^2,x(:,2).^2)
    %[broblin = robustfit(x(:,1),x(:,2))

    % move out velocity is:
    v(i) = round(sqrt(brob(2)));
    %  standard deviation on velocity is:
    s(i) = round(stats.s);
    %brob(1) = -d^2 and brob(2) = v0^2

    figure
    % plotting the data:
    plot(x(:,1).^2,x(:,2).^2,'r+')
    hold on
    % plotting the fit in the same figure:
    plot(x(:,1).^2,brob(2)*x(:,1).^2+brob(1),'k')
    legend('data',strcat('Vp = ',num2str(v(i)),' \pm ',num2str(s(i)),' m/s'),'Location','Northwest')
    title(strcat('vertical geophone at ',num2str(depth(i)),'m Depth'))

end


%figure
%plot(x(:,1),broblin(2)*x(:,1)+broblin(1),'k')
%hold on
%plot(x(:,1),x(:,2),'r+')
%legend('fit','data') [3]
```

# References

## *Introduction*

[1]     Kammerer, J.C.  (Last Modified:  September 1, 2005).  "Largest Rivers in the       United States".  USGS.  [ONLINE].  Available:      http://pubs.usgs.gov/of/1987/ofr87-242. [Accessed: May 31, 2007].

[2]     Center for Gravity, Electrical, and Magnetic Studies.  (Last Modified:  2006).      "Upper Arkansas River Valley".  Colorado School of Mines.  [ONLINE].   Available: http://www.geophysics.mines.edu/cgem/projects/arkansas.html.
        [Accessed:  May 31, 2007}.


## *Geology Introduction:*

[1] Watts, K.R., 2005, 1994, Tectonic setting of the axial basins of the northern and central Rio Grande rift, in Keller, G.R., and Cather, S. M., eds., Basins of the Rio Grande Rift: Structure, Stratigraphy, and Tectonic Setting: Boulder, Colorado, Geological Society of America Special Paper 291, p. 6.

[2] Raynolds, R. G,  PhD, Denver Museum of Nature & Science

[3] Emslie, M. A., 1991, Structural Fabrics and Hydrothermal Alterations Along the West Flank of the Rio Grande Rift at Chalk Cliffs, Central Sawatch Range, Central Colorado: M.S. thesis, Colorado School of Mines.

[4] Scott, G. R., 1975, Reconnaissance Geologic Map of the Buena Vista Quadrangle, Chaffee and Park Counties, Colorado, United States Geological Survey, Department of the Interior.


## *Surveying*

[1]     Multiple Authors.  (Last Modified:  2007).  "What is GPS?".  Trimble:  GPS
        Tutorial.  [ONLINE].  Available:  http://www.trimble.com/gps/whatgps.shtml.
        [Accessed June 7, 2007].

[2]     Multiple Authors.  (Last Modified:  May 28, 2007).  "GARMIN eTrex Vista Cx".
        TRAMsoft GmbH.  [ONLINE].  http://www.tramsoft.ch/gps/garmin_etrex-vista-
        color_en.html.  [Accessed June 7, 2007].

[3]     Greenwood, John A.  (1995). "Experiences With An Active Target Total Station   For Precise Angle Measurement".  Fermi National Accelerator Laboratory.     [ONLINE].  Available:      http://www.slac.stanford.edu/econf/C971013/papers/032.PDF.
        [Accessed June 7, 2007].

[4]     Dempsey, Caitlin.  (Last Modified:  2007).  "What is GIS?".  GIS Lounge.
        [ONLINE].  Available:  http://gislounge.com/library/introgis.shtml.
        [Accessed:  June 1, 2007].
[5]     United States Geological Survey.  (Last Modified:  February 22, 2007).     "Geographic Information Systems".          USGS.  [ONLINE].  Available:
        http://erg.usgs.gov/isb/pubs/gis_poster/#what.  [Accessed:  June 1, 2007].

## *Gravity*

Chapin, David A. May 1996. The Theory of the Bouguer Gravity Anomaly: A Tutorial.  The Leading Edge.

## *DC Resistivity*

[1]     Sheriff, Robert E. Sheriff, 2002. Encyclopedic Dictionary of Applied Geophysics, fourth edition.
[2]     Won, Ij, 2005. Apparent Conductivity (or Resistivity) Revisited.
http://www.geophex.com (Accessed June 8th, 2007).

[3]     MicroGeo, 2006. Electrical Resistivity Techniques: Dipole-Dipole Profiling.
www.microgeo.com (Accessed June 8th, 2007).

[4]     Geophysics Field Camp, 2007. Arkansas River Valley & Dam Site Evaluation.
Geophysics Department; Colorado School of Mines. Golden, Colorado 80401.

## *Electromagnetics*

[1]     North Carolina Department of Environmental and Natural Resources: Division of Water Resources, "Time Domain ElectroMagnetic Geophysics," *North Carolina Division of Water Resources*, Nov. 16, 2004.  [ONLINE].  Available:
        http://www.ncwater.org/Education_and_Technical_Assistance/Ground_Water/TDEM/.
[Accessed: Jun. 4, 2007].

## VSP

[1] http://www.slb.com/content/services/seismic/borehole/vsp.asp Accessed May 30, 2007.

 [2] Crouch, Thomas M., Doug Cain, P. O. Abbott, Robert D. Penley, R. Theodore Hurr, 1984, "Water Resources Appraisal of the Upper Arkansas River Basin from Leadville to Pueblo, Colorado," United States Geological Survey, 10-13.

[3] Van Wijk, Kasper, 2007, Computer code and personal Contact.

## Integration

Romani, J. and Stoltzman, B., 2006, Characterization of the upper Arkansas river valley (part II): Senior Design, Colorado School of Mines